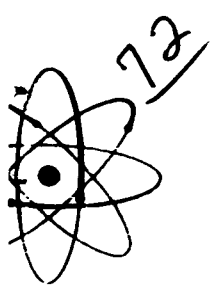

NP- 12194
Report Number

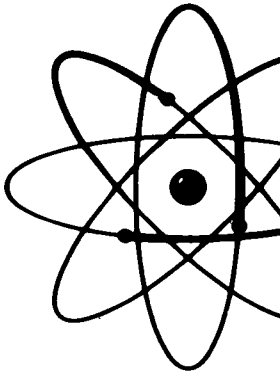

NO OTS

United States Atomic Energy Commission
Division of Technical Information

OTI-131(May 1962)

USAEC Division of Technical Information Extension, Oak Ridge, Tennessee

April 20, 1962

Semiannual Technical Report No. 2

VELA-UNIFORM

DYNAMIC PROPERTIES OF ROCKS

Prepared for:

ELECTRONIC SYSTEMS DIVISION
AIR FORCE SYSTEMS COMMAND
LAURENCE G. HANSCOM FIELD
BEDFORD, MASSACHUSETTS

By *V. C. Gregson* *D. R. Grine*
Poulter Laboratories

SRI Project No. PGU-3650

ARPA Order Number:	*180-61 Amendment 2) and 292-62*
Project Code Numbers:	*8100 (Task 2) and 8652*
Date of Contract:	*1 March 1961*
Name of Contractor:	*Stanford Research Institute*
Amount of Contract:	*$220,400*
Contract Number:	*AF 19(604)-8419*
Contract Expiration Date:	*15 August 1963*
Project Scientist:	*G. R. Fowles*
Phone Number:	*Davenport 6-6200, Ext. 3138*

Approved:

G. R. Fowles
G. R. FOWLES
PROJECT SUPERVISOR

Copy No. 50

CONTENTS

ILLUSTRATIONS

ILLUSTRATIONS

TABLES

I INTRODUCTION AND SUMMARY

Much interest and study is currently directed toward the dynamic properties of rocks. This interest is primarily the result of problems arising in the detection of nuclear explosions. Specifically, the pressure behavior of rocks controls the frequency spectrum and the amplitude of the resulting seismic signals from an explosion. The energy of a seismic signal is small compared to the energy of the explosion. The difference in energy between the explosion and the seismic signal is accounted for in the region near the explosion. The energy is left behind by the shock wave and exists as heat, increased surface area, and material flow.

At very high pressures any anisotropy of stress from material strength is conventionally neglected in comparison to the mean stress. The material is assumed fluid and hydrodynamic theory is applied. Propagation in this region is nonlinear. Energy from the shock is left in the medium as heat, surface energy, etc. This changes the shape of the shock wave as it travels. The material properties which influence shock propagation are the Rankine-Hugoniot curve and the adiabatic pressure-volume curves.

As the pressure of the shock from the explosion decays, there is a radius beyond which the efforts due to material strength can no longer be neglected. The shock front becomes unstable and breaks into two shock fronts, and this two-wave structure complicates the description and prediction of shock propagation in this intermediate region. Moreover, knowledge of more material properties is required for accurate predictions. The yield behavior under uniaxial, high strain-rate loading must be known in order to determine the maximum amplitude of elastic waves and to determine the pressure range within which a double shock wave occurs.

The shock wave will continue to decay until, at some radius, the strains are completely elastic. Studies in energy coupling of underground nuclear explosions show that it is important to be able to predict the radius and the critical maximum amplitude beyond which the subsequent propagation can be considered elastic. In the theory of coupling, which has been partially verified experimentally, these two quantities enter

directly and, in fact, constitute the major unknowns in computing the amplitude of seismic waves at large distances from an explosion

The goal of the present program is to measure some of the material properties under shock conditions in simple rocks and minerals. The pressure region of interest is the region in which the material strength of the rock affects the shock wave. The property that is measured is the Hugoniot equation of state. From measurements of this function, information is obtained about such aspects as phase transitions, elastic wave amplitudes and velocities, and pressure-volume relations above the elastic limit. The measurements in the program also permit a comparison of the behavior of single crystals with the polycrystalline rock.

The rock properties at these pressures are correlated insofar as possible with the properties that can be measured in their initial state. The initial state properties are porosity, grain size, preferential mineral alignment, and degree of cementation.

The minerals studied are quartz and calcite in both crystal and polycrystalline form. The polycrystalline rocks of quartz and calcite each include one porous and one non-porous rock.

Two-dimensional wedge experiments supply most of the data, plane-wave measurements provide checks at the lower pressures and give some values at higher pressures. Experiments were completed on:

Arkansas novaculite	30 to 200 kilobars
Sioux quartzite	10 to 230 kilobars
Eureka quartzite	45 to 60 kilobars
Coconino sandstone	2 to 130 kilobars
Yule marble	10 to 250 kilobars
Spergen limestone	1 to 200 kilobars
Quartz	230 kilobars
Calcite	20 to 130 kilobars

In summary, the results indicate ~~the following~~:

1. A two-wave front in the shock wave is recorded in each material. This is thought to be the result of failure at the elastic limit by either fracture or slip. A three-wave structure is sometimes recorded in the carbonates. The additional front is probably due to a phase transition.

2. There is a difference between the Hugoniots of single crystals and polycrystalline rocks. Compared to the single crystals, there is a decrease in peak stress and velocity in the first wave of the polycrystalline rocks. This is greatest for the porous rocks and least for polycrystalline rocks with no porosity. The peak stress and velocity of the first wave depends strongly on porosity but it has not been demonstrated which parameters controlling porosity (e.g., cementation, grain size, sorting, etc.) are most important

II EXPERIMENTAL METHODS

Parts of the following pages are quoted from the Semiannual Technical Report of October 20, 1961.

The principles of experimental methods for determining Hugoniot equations of state, utilizing explosively induced shock waves, have been reviewed in detail by Rice, *et al.*[1] These methods are based on the Rankine Hugoniot jump conditions expressing conservation of mass, momentum, and energy across a shock front. These may be written:

$$\frac{V_1}{V_0} = 1 - \frac{u_1 - u_0}{U_1 - u_0} \qquad \text{(mass)}$$

$$\sigma_1 - \sigma_0 = \rho_0 (U_1 - u_0)(u_1 - u_0) \qquad \text{(momentum)} \qquad (1)$$

$$E_1 - E_0 = \frac{(\sigma_1 + \sigma_0)}{2} (V_0 - V_1) \qquad \text{(energy)}$$

where $V(= 1/\rho)$ is specific volume, u is mass velocity, U is shock velocity, σ is compressive stress normal to the shock front, and E is specific internal energy. All wave and particle velocities used in this report refer to laboratory coordinates. Subscripts "0" refer to the state ahead of the shock front, and subscripts "1" to the state immediately behind the front.

Considering the initial state known, there remain five unknown quantities and three relations. Hence, measurement of any two allows the remaining quantities to be computed. In the experiments to be described both the shock wave velocity and the free-surface velocity produced upon reflection of the shock from a free boundary are measured. These, together with a relation between free-surface velocity and particle velocity prior to reflection, are sufficient to determine the stress-density-energy state behind the shock front. A series of measurements with different shock intensities thus determine the Hugoniot equation of state, or locus of states attainable through a single shock transition.

The particle velocity prior to reflection is, to an adequate approximation, one half the free-surface velocity. This approximation is based on the condition that entropy changes are small,[2] it works well for metals, crystals, and rocks with no porosity. It does not work past the elastic limit in the porous rocks, because the work expended in closing the pore space is largely irreversible and th involves large entropy changes. In that case a more devious procedure is required to establish the particle velocity, it will be described in Section IIIB.

It should be noted that while this procedure establishes the Hugoniot equation of state, no experimental information concerning the components of stress parallel to the shock front is obtained. These lateral stresses are related to the observed stress, normal to the front, through the effective Poisson's ratio, and must exist to maintain the macroscopic strain uniaxial as is required by symmetry. In isotropic materials the net strain is normal to the shock front, in anisotropic materials it may be inclined to the front but is still uniaxial.

It can be generally stated that, in any given solid, a range of final shock stresses exists for which a single shock front is unstable. This is due to violation of the sufficient condition for shock stability [1]

$$\frac{\partial^2 \sigma_x}{\partial V^2} \geq 0 \quad , \tag{2}$$

where σ_x is the component of stress normal to the shock front. It is easily shown that this condition is violated in a solid for stresses in the vicinity of the yield stress appropriate to the case of one-dimensional strain. (It may also be violated elsewhere if phase transitions occur.) Thus, for a range of shock stresses, a single front breaks up into a double front. The first of these travels with elastic velocity (dilational velocity in isotropic materials) and has a stress amplitude such that the difference between the principal stresses behind the front is just equal to the yield strength. The stress amplitude of this wave in the direction normal to the wave front is termed the Hugoniot elastic limit.

This elastic forerunner is followed by a slower shock front in which the effective rigidity modulus is reduced (or even zero) and which carries the material to the final state. The velocity of the second front increases with stress and for sufficiently high stresses this front will overtake the elastic front. Under these conditions a single front is again stable.

The above relationships are depicted qualitatively in Fig. 1. In this diagram the Hugoniot equation of state is represented by the curve AEFD. Point E is the Hugoniot elastic limit and is the amplitude of the first wave when a double wave exists. From Eq. (1) it is evident that shock velocity is given by: ($u_0 = 0$)

$$U_1 = V_0\left(\frac{P_1 - P_0}{V_0 - V_1}\right)^{1/2} \tag{1}$$

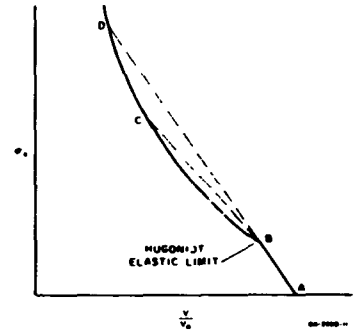

FIG. 1 HUGONIOT EQUATION OF STATE OF A SOLID IN THE VICINITY OF THE YIELD POINT

Hence, shock velocity is proportional to the square root of the negative slope of the straight line joining the initial and final states. This relation allows the range of stresses for which single shock fronts are unstable to be easily determined. Thus, Point D is the critical stress for which the second front just overtakes the first. For a final state C the shock consists of two fronts, of which the velocity of the first is related to the slope AB, and the velocity of the second to the slope BC.

In the above model, the slope of the elastic forerunner in the Hugoniot plane is constant. It is usually observed however, that the slope of the elastic forerunner in the Hugoniot plane is not constant but that the locus of states has some positive curvature. This is believed to be a result of the large principal stresses and the accompanying deviations from Hooke's law.

The terminology of the various pressure fronts resulting from shock instability is sometimes misleading. The first pressure front is usually called the elastic wave or similar designation. The second pressure front may represent the plastic wave, or a particular phase transition. Because of the uncertainty in separating phase transitions from yield transitions, the pressure fronts will be designated in the numerical order in which they are recorded, e.g., first wave, second wave.

Determining Hugoniot data from observations on a multiple wave system requires that each wave front be observed separately. The following methods were developed during the present project to satisfy this requirement. These methods use inclined mirror and optical lever recording techniques[3,6] which depend upon changes in reflectivity or turning of a mirror surface.

The arrangements described below are suitable for different purposes, the basic principles and measurements are the same in each application.

The plane-wave pellet arrangement is best used on non-porous materials and is the only one of the methods that can be used on single crystals at the present time. Shock velocities in crystals are more simply expressed along the principal crystallographic directions and in order to profit from this simplicity, the direction of shock propagation and measurement must be along the principal axes. This restriction does not permit wedge methods to be used.

The plane-wave beveled pellet arrangement differs from the plane-wave pellet arrangement in that an additional face is used. This allows a measurement of the shock velocity to be made on the wedge surface, and an impedance-match solution, that does not use the free-surface assumption, can be computed. Measurements and computations made in the plane-wave pellet arrangement are also made on the beveled pellet. The beveled pellet is useful for experiments with porous materials, where the free-surface assumption does not hold, or in instances where it is desired to check the free-surface assumption.

The plane-wave wedge experiments use only the wedge part of the beveled pellet and are useful for measurements in porous rocks for the above reason, and for measurement of shock attenuation.

The two-dimensional wedge experiment is used when feasible because it gives the state of the material at many pressures in one experiment, rather than only one pressure as in the plane-wave experiments.

A. PELLET METHOD

The pellet method is used for all crystals and nonporous solids. A sample of the material is cemented to a backing plate, and a plane shock wave is driven through the backing plate and into the pellet. The experiment is designed to determine shock wave and particle velocity.

Shock wave velocity is measured by observing the transit time of the shock wave through a known thickness of sample. Particle velocity is determined by measuring the free surface velocity produced upon interaction of the shock wave with a free boundary and converting to particle velocity as discussed above.

An explosive assembly,* which produces a plane detonation wave, is cemented to one surface of the backing plate; specimen and mirrors are cemented to the other surface (Fig. 2). The backing plate is usually ½ inch thick and large enough to cover the explosive lens. The materials most commonly used for the backing plates are aluminum, lucite, and laminates of mild steel and lucite. The two surfaces of the plates are cut parallel, lapped, and sometimes polished. The mirrors are made from lucite and aluminized on one side. Dimensions of the specimens are 1 to 1½ inches square and ¼ to ⅛ inch thick.

The mirrors are placed so that the aluminized surfaces are against the backing plate and cemented around the edges; precautions are taken so that no cement is between the aluminized surface and the plate. Figure 3 shows the arrangement.

Figure 4 is a simplified diagram of the interaction of the assembly with a plane shock wave. The diagram does not illustrate the interactions of shock waves with edges or the reflected waves after a surface is reached. The shock front, S_1, in the backing plate, generated by the explosive lens, travels with a velocity U_1. Mirrors at A, C, G, along with the aluminized lower surface of the specimen (if the specimen is transparent) record the arrival of the shock wave at the upper surface of the backing plate. This is recorded as a change in the intensity of reflected light when the shock wave destroys the aluminized surface of the mirrors. The planarity of the shock wave can be observed in this manner and corrections made in the data if there is a "tilt" to the shock wave. The reflection of the shock wave at the surface of the backing plate results in the surface traveling at a velocity u_{f_1}. The moving surface turns the inclined mirror and the point of collision is recorded by a change in the intensity of reflected light. The edge of Mirror B touching the backing plate also records the arrival of the shock wave at the surface. The mirror angle is adjusted so that the apparent velocity of the point of collision is supersonic. This

* Manufactured by Mason and Hanger, Inc., Amarillo, Texas.

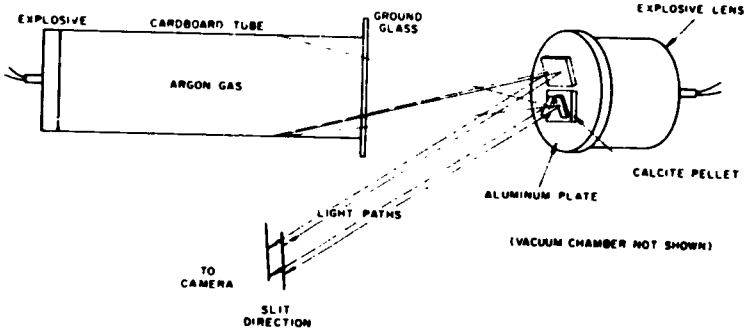

FIG. 2 DIAGRAM OF EXPERIMENTAL SETUP

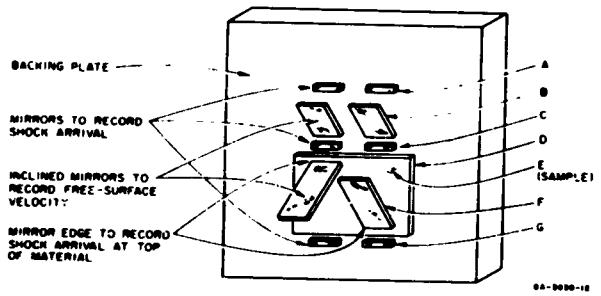

FIG. 3 DIAGRAM OF EXPERIMENTAL ASSEMBLY

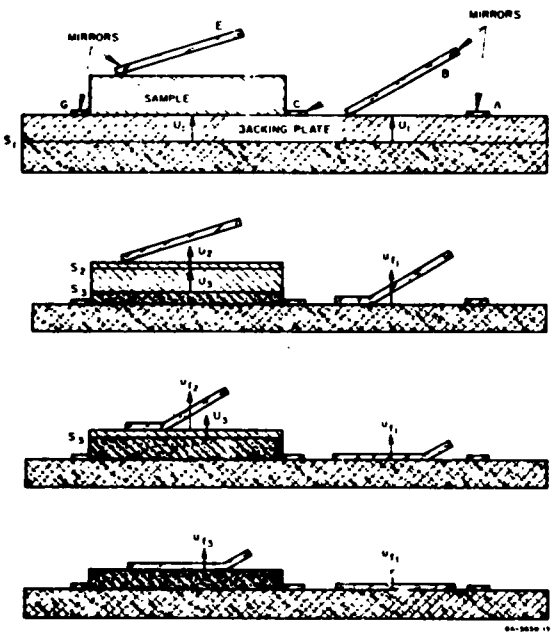

FIG. 4 SIMPLIFIED DIAGRAM OF THE ASSEMBLY UNDERGOING SHOCK LOADING

insures that no signal due to the collision can influence either the specimen or the mirror ahead of the point of collision.

The shock wave traveling in the backing plate reaches the boundary between the plate and specimen and interacts to transmit a shock wave of different pressure into the specimen. The shock wave in the specimen may be unstable and form a double shock, S_2 and S_3, indicating a phase change or failure at the elastic limit. The two shock waves S_2 and S_3, in the sample travel with velocities U_2 and U_3. The reflection of the shock wave with velocity U_2 at the surface of the sample accelerates the surface to velocity u_{f2}, which is much slower than the shock wave velocity, then the shock wave, S_3 with velocity U_3, overtakes the free surface and further accelerates it to velocity u_{f3}.

Initially, the inclined mirror on the sample is turned by the surface traveling with velocity u_{f2}, and if the angle between mirror and pellet surface is α, the point of intersection of mirror and pellet surface travels along the mirror with apparent velocity $U_{a_1} = u_{f2} \sin \alpha$. When the second shock accelerates the free surface to velocity u_{f3}, the apparent velocity, U_{a_2}, is increased to $u_{f3}/\sin \alpha$. These apparent velocities are recorded with a streak camera as described below. The edge of the inclined mirror that touches the sample also records the arrival of the shock wave at the upper surface of the specimen.

When possible, two separate systems of mirrors are used. This permits two independent measurements to be made, providing a check on the results. Further, the mirrors on the upper surface are inclined at different angles to provide optimum resolution for different parts of the free surface motion

An argon explosive light source is used to illuminate the mirrors during the experiment. Argon gas, which becomes strongly luminescent when shock loaded, is contained in a cardboard or wooden box with an explosive pad at one end and a glass cover at the other. The glass cover may be etched to diffuse the light or it may contain grid lines and various filters. The argon is allowed to flow through the box to minimize dilution by air; the duration of light is about 50 microseconds.

Figure 2 illustrates the basic experimental setup. The light source is properly timed to illuminate the specimen and mirrors during the interval of the experiment. The mirrors are oriented so as to direct light from the edges of the light source toward the camera, and they

are turned into the light source by the arrival of the shock wave. This results in a change in the intensity of the light reflected by the mirrors

Changes in light intensity are recorded by a streak camera which uses an air turbine to rotate, at 2000 rps, a mirror past a strip of 35-mm film arranged circumferentially in the camera. A 0.1-mm slit of light from the shot assembly is swept along the film to produce a one-dimensional time plot of the light and dark events contained in the field of view of the slit. The writing speed of the rotating mirror is 3.8 mm/μsec and time resolutions of 0.01 μsec are possible.

When two sets of mirrors are used on the specimen, a slit across each set sweeps along the film to give a double exposure of the events. It is still possible to separate the events from each mirror provided proper exposure is made.

Figure 5 is a streak camera photograph from a Z-cut calcite experiment Differences in light intensity demarcate the records from the two slits.

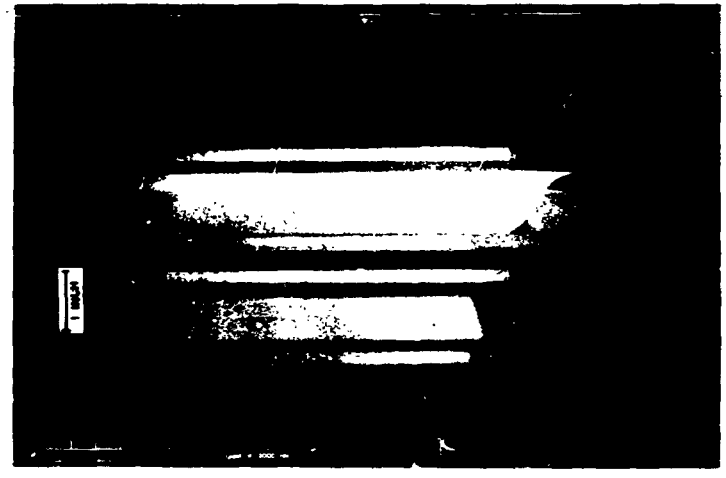

FIG. 5 STREAK CAMERA PHOTOGRAPH FOR A Z-CUT CALCITE CRYSTAL

The photograph has been retouched at L to D to H to show slight changes in intensity more clearly

At each slit differences in light intensity record the arrival of the shock wave. Figure 6 is a diagram of the information contained on the photograph. At slit 1, the arrival of the shock wave at the surface of the driver plate is recorded by A, B, C, D, H. The slope of the trace at B records the free-surface velocity of the driver plate. The distance between D and E (time interval t_0 to t_1) records the transit time of the shock wave in the calcite. E records the arrival of the shock wave at the upper surface of the calcite. The slope from E to E_1 records the free-surface velocity of the first wave in calcite; the slope from E_1 to E_2 provides a measure of the free-surface velocity of the second wave. Similar points are indicated for the other slit.

The data, which is obtained from the interpretation of the film, are angles of the inclined mirror traces and indications of the successive shock arrival at the interfaces. These data will be used in computing the necessary parameters of Eqs. 1. The computation described below is taken from a report by Fowles.[3]

The free-surface velocities, u_f, were computed by means of the relation:

$$u_f = \frac{\tan \alpha}{MF \tan \gamma} \qquad (4)$$

where α is the angle of the inclined mirror with respect to the quartz free surface, γ is (approximately) the angle of the trace on the film with respect to the space axis, M is the magnification or ratio of distance on the film to the corresponding distance on the shot, and F is the writing speed of the camera. This relation can be verified by reference to Fig. 7 which shows the correspondence of distances on the film to times and distances at the shot.

The velocities deduced from this relation require small corrections because of tilt in the incident shock, designated by θ in Fig 7, and because of small errors in alignment within the camera. The alignment error results from lack of precise orthogonality between the slit direction and sweep direction. The departure from orthogonality is designated by δ.

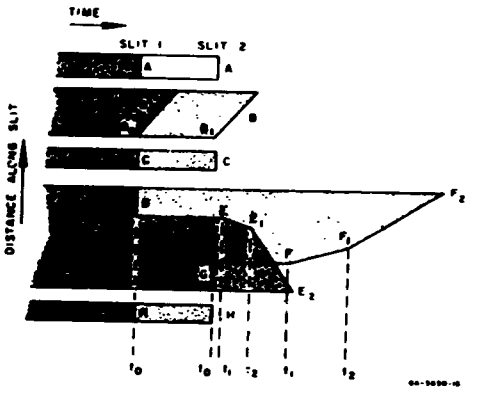

FIG. 6 DIAGRAM OF THE STREAK CAMERA PHOTOGRAPH

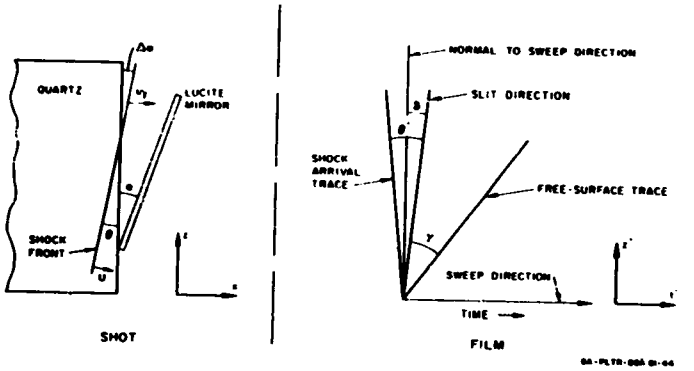

FIG. 7 CORRESPONDENCE OF TIMES AND DISTANCE AT SHOT TO DISTANCES ON STREAK RECORD

The correction to α due to shock tilt is given by:

$$\Delta\alpha \simeq \frac{\tan\alpha}{\tan\gamma}\theta' \qquad (5)$$

where θ' is the angle of shock tilt as measured on the film, and α is the mirror angle.

The correction to γ due to a nonzero value of δ is:

$$\tan\gamma = \tan\gamma' \sec\delta(1 - \tan\gamma'\delta) \qquad (6)$$

where γ' is the angle of trace with respect to the slit direction.

The procedure was, therefore, to determine γ from measured values of γ' and δ by Eq. (6), to compute $\Delta\alpha$ by Eq. (5), and finally, to compute u_f by Eq. (4) with $\alpha = \alpha_0 + \Delta\alpha$, where α_0 is the original mirror angle. In practice, the corrections to Eq. (4) resulting from replacement of α_0 by α, and γ' by γ were quite small.

The velocity of the first shock is computed immediately from the observed travel time, $(t_1 - t_0)$, and the known pellet thickness. An "average" velocity for the second shock is computed from the observed travel time, $(t_2 - t_0)$, and the effective pellet thickness, adjusted for the displacement of the specimen free surface prior to arrival of the second shock. Thus, to a first approximation the second shock velocity, U_2, is given by:

$$U_2 = \frac{d + u_{f_1}(t_2 - t_1)}{t_2 - t_0} \qquad (7)$$

where d is pellet thickness, u_{f_1} is the free-surface velocity due to the first shock, and t = (distance on film)/(writing speed).

The experimental precision, based on assembly tolerances, camera resolution, and film reading errors is estimated to be ±1% in shock velocity and ±5% in free-surface velocity. Most of the error in free-surface velocity is due to uncertainty in the reading on the film of angle γ. This error is estimated to be less than ±1°.

An impedance match solution may be used to check the results. This solution is described in the following section.

B. BEVELED PELLET METHOD

The Beveled Pellet Method differs from the method above by using an inclined surface as well as the surface that is horizontal to the backing plate. From the inclined surface, additional values of shock velocity are measured and used in an impedance match solution to provide check on the previous results. This type of experiment is suitable for porous or other materials in which the validity of using the free-surface approximation is questioned.

A schematic diagram of the experimental arrangement is given in Fig. 8. The explosively driven plane wave moves through the backing plate and into the beveled rock pellet. The mirrors and the polished backing plate are illuminated by the light from an argon light source similar to that described above. The only difference is that a grid of clear lines spaced 2 mm apart in a background of 0.6 photographic density is placed on the face of the argon tube. The shot is viewed through the slit of a streak camera so that the grid image appears as a series of light and dark spots. The image is swept along the film, producing parallel lines such as those at the left of Fig. 9. If a reflecting surface changes to a diffuse reflector, the images disappear. The wave arrival at the backing plate, visible in the regions A, and the arrival of the free surface of the backing plate at the tilted mirrors at B are visible in Fig. 9 for this reason. If reflectivity changes, light intensity changes. The mirror along the beveled pellet edge at C and the tilted mirror on the pellet at D both drop sharply in reflectivity to signal respectively the wave arrival and the arrival of the moving free surface of the pellet. A third effect by which arrivals could be noted is the displacement of images produced by any rotation of a reflecting surface.

Camera writing speed and image magnification are measured so that Fig. 9 may be used as a time-distance plot. Apparent velocities are obtained from the slopes of the streak camera traces. The average shock velocity, U, is obtained by dividing the pellet thickness by the transit time, indicated by the arrival at the backing plate and the point at which the smear from the large tilted mirror at D begins to cut off. Another value of U is obtained from the apparent wave velocity U_{app} along the mirror on the beveled part of the pellet at C in Fig. 9.

$$U = U_{app} \tan\theta \qquad (8)$$

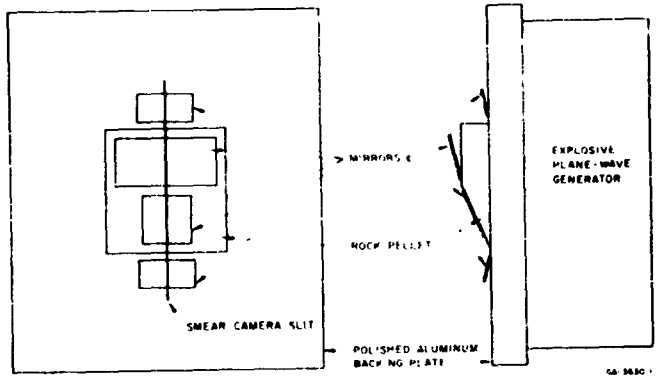

FIG. 8 SCHEMATIC OF BEVELED PELLET EXPERIMENT

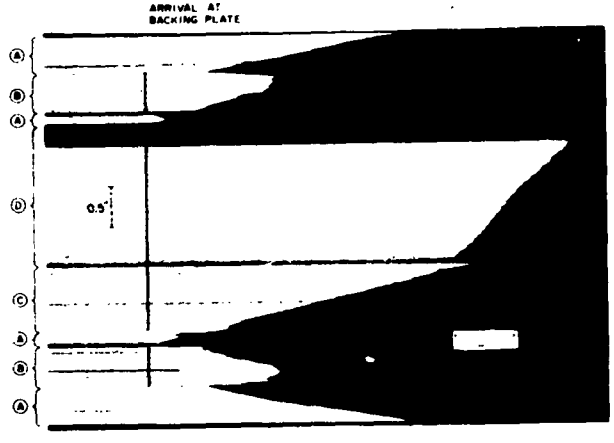

FIG 9 BEVELED PELLET RECORD – SANDSTONE (Shot No. 7861)

where θ is the measured angle of pellet bevel. These two velocity determinations differed by 0.2 percent on the shot of Fig. 9. The free-surface velocities of the aluminum backing plate and of the pellet were determined from the apparent velocities of the appropriate traces and from the measured angles α of the tilted mirrors by means of the formula, $U_f = U_{app} \tan \alpha$. This is the same as in the Pellet Method.

The impedance-match solution for the stress-particle velocity state in the specimen is obtained by the method shown in Fig. 10. The curve OA is the previously determined locus of points which can be attained by passing a shock through the backing plate of 2024 aluminum.[16] The point A represents the state behind the shock which is incident on the aluminum free surface and on the pellet.

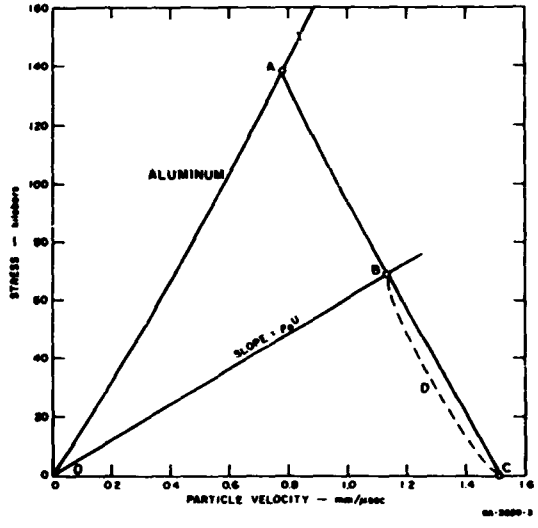

FIG. 10 GRAPHICAL INTERPRETATION OF BEVELED PELLET RECORD (Shot No. 7861)

The particle velocity, u, is obtained from the measured free-surface velocity, u_{fs}, of the aluminum plate by using the relation $u = (1/2)u_{fs}$. A reflected wave is generated when the shock reaches the interface between the aluminum backing plate and the pellet. The states which can be attained by the reflected wave can be calculated from the known properties of aluminum;[4] they are very close to AB, a mirror image of the curve OA. Since normal stress and particle velocity must be continuous across the interface, the state in the sample must lie on AB. From the equation for conservation of momentum, $\sigma = \rho_0 U u$, the state in the specimen must also be on a straight line with a slope $(\sigma/u) = \rho_0 U$. The intersection of this line with AB determines B, the state in the pellet. The associated compression and specific energy may be calculated from the equations for conservation of mass and energy across the shock front.

The free-surface velocity of the pellet in the example of Fig. 10 was 1.51 mm/μsec. This value gives a point at C on the locus of states attainable by a reflected rarefaction wave in the rock. Because of the porosity, the free-surface approximation was very poor for this sandstone; free-surface velocity was only 1.34 times particle velocity. If the rarefaction wave reflected from the free surface of the rock pellet is regarded as a sharp-fronted wave with velocity, $-U_r$, it adds a particle velocity, $u_r = u_{fs} - u$. The stress drop across the wave front is

$$\sigma_r = \rho(U_r + u)u_r \quad . \tag{9}$$

The free-surface boundary condition of zero stress forces the stress drop across the reflected wave to be equal in magnitude to the stress rise, σ, across the incident wave, and opposite in sign; therefore $\rho(U_r + u)u_r = -\sigma$. The velocity of the reflected wave relative to the particles it is moving into is then,

$$(U_r + u) = \frac{\sigma}{\rho u_r} \quad . \tag{10}$$

This quantity is just $1/\rho$ times the negative slope of the chord BC in Fig. 10. It equals 5.81 mm/μsec, almost twice the 3.06 mm/μsec velocity of the incident wave. The velocity of 5.81 mm/μsec is close to the velocity in crystal quartz so that it appears that the original porosity has negligible effect on the velocity of the reflected wave.

C. PLANE-WAVE WEDGE METHOD

A wedge of the sample is placed on the backing plate instead of the beveled pellet and the experiment is assembled in a similar manner. The only solution is obtained by the impedance-match method. Two different metals were used as mirrors on each shot so that a check could be obtained by having two different impedance-match solutions.

A schematic diagram of the plane-wave wedge arrangement is shown in Fig. 11. The explosively driven plane wave moves from the backing plate into the small wedges of rock and aluminum. The shot is illuminated by an argon light source, on the face of which a grid of clear lines spaced $\frac{1}{4}$ inch apart on an opaque background is placed. The shot is viewed through two slits by the streak camera. The sets of grid lines for the two slits are offset from one another by $\frac{1}{8}$ inch so that the traces from one slit do not overlap the traces from the other slit. In addition, the shot is photographed in color with a colored filter over one slit so that traces on the resulting smear record can be followed even should they cross

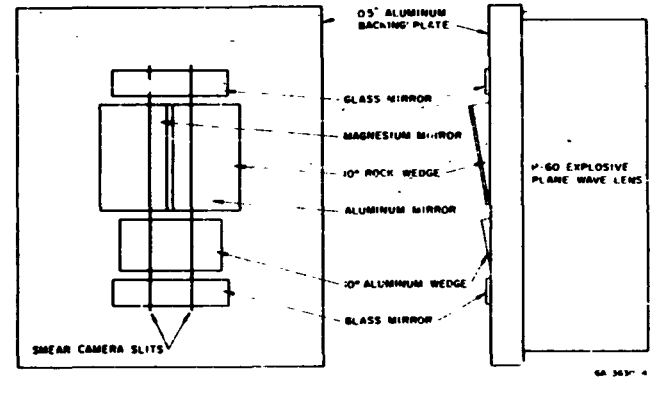

FIG. 11 SCHEMATIC OF PLANE-WAVE WEDGE EXPERIMENT

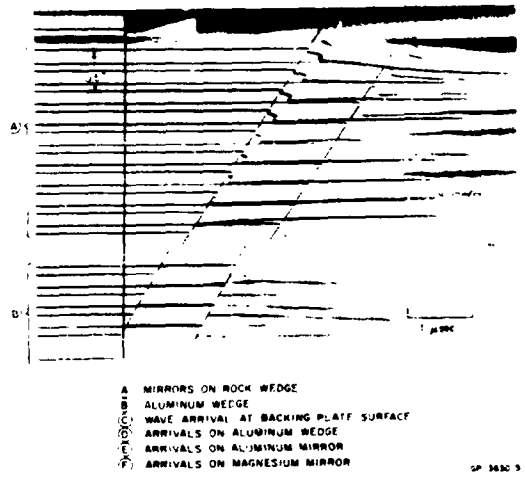

FIG 12 PLANE-WAVE WEDGE RECORD OF SIOUX QUARTZITE

The reflecting surfaces of the aluminum wedge and of the two mirrors on the rock pellet turn upon arrival of the wave. Images of the light source grid are displaced as shown in the record of Fig. 12.

The wave velocities in the aluminum wedge and rock are calculated as in the beveled pellet method. The normal component of free-surface velocity, u_n, is obtained from the magnitude, a, of the displacements of the images of the light source grid, $u_n = (a/2d)U_{app}$ where d is the normal distance of the grid from the shot and U_{app} is the apparent velocity determined as before by the slope of the trace. Details of this optical lever technique are given by Fowles.[6]

The wave arrivals and displacements on the aluminum wedge at D give wave velocity and free-surface velocity in the backing plate. Use of the free-surface approximation gives the stress-particle velocity point at D in the graphical solution of Fig. 13. The fact that this point agrees

with the previously determined $\sigma - u$ curve of aluminum provides a check on the calculations and measurements.

The wave arrivals at the mirrors on the rock show a two wave system in the rock pellet with the first wave indicated by the dashed lines at E and F in Fig. 12. The $\sigma - u$ state of the first wave cannot be determined by the usual impedance-match solution of Fig. 10. From the apparent velocities of arrivals, velocities of the first and second waves were calculated as $C_1 = 5.58$ and $C_2 = 4.96$ km/sec. The free-surface approximation is used to obtain particle velocities in the aluminum and magnesium mirrors on the rock pellet, giving points A and B on the known $\sigma - u$ loci of these metals shown in Fig. 13. A lies on the locus of states attainable

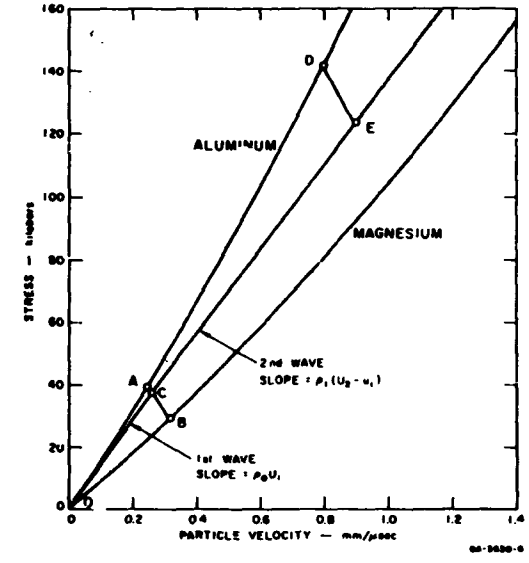

FIG. 13 GRAPHICAL INTERPRETATION OF PLANE-WAVE WEDGE EXPERIMENT

by reflected shocks in the rock and B lies on the locus of reflected rarefections. Since A and B are close to one another, the straight line AB is a good approximation to the cross curve of reflected wave states of the rock Hugoniot. The intersection at C of AB with the line from the origin of slope $\rho_0 U_1$ determines the state behind the first wave in the Sioux quartzite pellet of Figs. 10 and 11.

The state behind the second wave on the other hand, can be determined from an ordinary impedance-match solution. Thus, state E is determined by the intersection of the locus of reflected rarefactions from the state D of the aluminum backing plate with the line of slope $\rho_1(U_2 - u_1)$ passing through the state C of the first wave. This solution for the second wave at E should also be obtained in the same manner as for the first wave, the intersection of the line connecting the states behind the second waves in the aluminum and magnesium mirrors with the line of slope $\rho_1(U_2 - u_1)$. The agreement between the two solutions provides a check on the results.

The slope of the line connecting the states on the aluminum and magnesium mirrors leads to an approximate value for sound speed behind the shock front for reasons given in the discussion of the beveled pellet method.

D TWO-DIMENSIONAL WEDGE EXPERIMENT

The two-dimensional wedge geometry of Fig. 14 has two advantages over the plane-wave arrangements described above. Each shot yields data for a range of stress instead of just one point, and low stresses can be more easily reached in the wedge than in the plane-wave experiments. The wedge geometry was first used by Katz, *et al.*[5]

As shown in Fig. 14, a detonation front progresses in an explosive slab with constant velocity, U_D, inducing a shock wave in the specimen. The shock decays as it progresses into the wedge so that a range of stresses will be observed at the wedge face. When the detonation wave has traveled far enough, the shock wave will be steady in time, i.e., the point of intersection of the shock with any horizontal plane will travel with an apparent velocity equal to detonation velocity. Under these conditions it is apparent from the figure that shock velocity, U_s, at any point, is given by:

$$U_s = U_D \sin\alpha - U_{app} \sin\gamma \qquad (11)$$

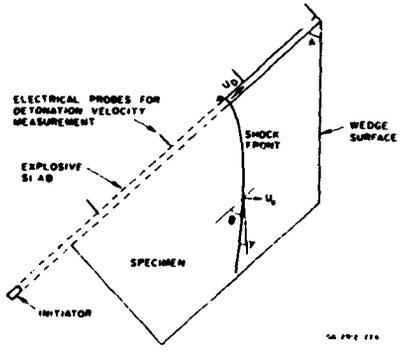

FIG. 14 SIDE VIEW OF TWO DIMENSIONAL WEDGE EXPERIMENT

where U_D is detonation velocity and U_{app} is the apparent velocity with which the shock intersects a plane parallel to the wedge face.

Moreover, since

$$\alpha + \gamma = A \quad , \qquad (12)$$

$$\sin\alpha = \frac{U_{app}}{U_D} \sin(A - \alpha) \qquad (13)$$

from which

$$\cot\alpha = \cot A + \frac{U_D}{U_{app} \sin A} \quad , \qquad (14)$$

thus, when U_{app}, U_D, and A are measured, U_s can be calculated at any point on the wedge surface. U_{app} is obtained from the streak camera record of the arrival of the wave at the wedge surface. At the same time, the component of free-surface velocity normal to the wedge face is measured by the method described below.

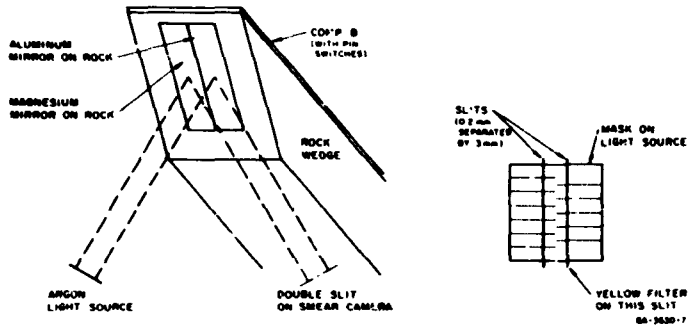

FIG. 15 SCHEMATIC OF TWO MIRROR WEDGE EXPERIMENT

Two mirrors are placed on the wedge face as shown in Fig. 15. The normal component of free-surface velocity at each point covered by a grid line is obtained by the optical lever arm technique described in the preceding section. The free-surface velocity approximation is then used to obtain particle velocity for each mirror as a function of depth in the wedge. At any depth, particle velocity is read from plots of the mirror data. The particle velocity in the rock at that depth is graphically obtained in the same way as point C in Fig. 13. The process can be repeated for multiple wave systems by applying the jump conditions across each wave front in turn.

The two-dimensional method was used to generate most of the data on the polycrystalline rocks. The two plane-wave arrangements are easier to interpret and are used to spot-check the results of the two-dimensional method. Appendix C contains further details about the reduction of data from the two-dimensional wedge experiments.

III RESULTS

Values of shock parameters obtained from shock wave experiments on quartz, calcite, and the related rocks are listed in Tables III, IV, V, VI. Table I lists the experiments on each rock and Table II lists pertinent information on each rock. Diagrams of the states of stress-particle velocity and stress-volume for the various materials are shown in Figs. 16-19, 22-25.

A. QUARTZ

Table III records all of the data on quartz measured at SRI. The measurements on quartz were made by Fowles,[6] with the exception of Shot 8504.

Figure 16 displays all the known shock wave data on quartz. Agreement between Fowles'[3] and Wackerle's[4] measurements is generally good. The scale in Fig. 16 is expanded in Fig. 17 and displays the shock wave data on quartz up to 250 kilobars. Agreement between Fowles' and Wackerle's measurements is more apparent. The only disagreement in data is for the second wave in Z-cut quartz. Data by Fowles lie about 25 kilobars above data by Wackerle. Shot 8504 was designed on this project to specifically measure the shock parameters of the second wave in Z-cut quartz. The result agrees with data by Fowles.

B QUARTZ ROCKS

Table IV and part of Table VI lists the values obtained from shock wave experiments; significant data on stress-particle velocity and stress-volume relations are displayed graphically in Figs. 18 and 19 respectively.

Comparisons are made of the data from rocks that differ in only a few of the initial state parameters so that any differences in shock wave data can then be attributed to variations in these initial parameters. The reader is referred to Table II or Appendix A and D for information on the differences and similarities of each rock, and the parameters that affect porosity.

Table I

SUMMARY OF EXPERIMENTS

MATERIAL	SHOT NO.	GEOMETRY	PRESSURE RANGE (Kilobars)	PRECURSORS (Kilobars)	NOTES
Quartz	8504	Plane-wave pellet	230 to 230	170	Z-cut pellet
Arkansas Novaculite	8230	Plane-wave beveled-pellet	82 to 89	82	
	8270	Plane-wave beveled-pellet	97 to 125	97	
	8272	Plane-wave beveled-pellet	198		
	8273	Two-dimensional wedge	21 to 41		
	8299	Two-dimensional wedge	38 to 62		
	8300	Two-dimensional wedge	38 to 79		
Sioux Quartzite	7095	Plane-wave wedge	231		
	7468	Two-dimensional wedge	10 to 102		
Eureka Quartzite	7990	Two-dimensional wedge	45 to 60	36	
Coconino Sandstone	7715	Plane-wave pellet	133		Parallel to bedding
	7716	Plane-wave pellet	--		Perpendicular to bedding
	7889	Plane-wave wedge	146		
	7951	Plane-wave beveled-pellet	89		
	7963	Plane-wave wedge	67		
	8151	Plane-wave beveled-pellet	98		
	8164	Plane-wave wedge	171		
	8119	Two-dimensional wedge	38	5	
	8162	Two-dimensional wedge	7 to 91	5	
	8269	Two-dimensional wedge	40 to 58	3	
	8270	Two-dimensional wedge	44 to 59		
	8862	Two-dimensional X-ray	2 to 40		
Calcite	8460	Plane-wave pellet	29 to 92	29	Cleavage-cut Calcite
	8461	Plane-wave pellet	22 to 84	22	Cleavage-cut Calcite
	8506	Plane-wave pellet	86		Z-cut Calcite (results are
	8506	Plane-wave pellet	133		Z-cut Calcite (poor
Yule Marble	7705	Plane-wave wedge	176		Poor results
	7706	Plane-wave wedge	--		Poor results
	8280	Plane-wave beveled-pellet	120	12	
	8281	Plane-wave beveled-pellet	81		
	8317	Plane-wave wedge	253		
	7997	Two-dimensional wedge	30 to 120	12, 16, 24	Unoriented
	8279	Two-dimensional wedge	38 to 120	4, 9, 22	
	8318	Two-dimensional wedge	10 to 132	15	
Spergen Limestone	8079	Plane-wave beveled-pellet	98		
	8080	Plane-wave beveled-pellet	201		
	8081	Plane-wave wedge	91	2	
	8150	Plane-wave beveled-pellet	62		
	8165	Plane-wave beveled-pellet	221		
	8171	Plane-wave beveled-pellet	86		
	8110	Two-dimensional wedge	29 to 39	17	
	8162	Two-dimensional wedge	5 to 72	2	
	8252	Two-dimensional wedge	64 to 135		Precursor not readable at magnification
	8268	Two-dimensional wedge	1 to 6	3	

Table II

SUMMARY OF ROCK INFORMATION

NAME	GRAIN SIZE (mm)	CEMENT	POROSITY (%)	DENSITY (g/cc)	COMMENTS
QUARTZ ROCKS					
Arkansas Novaculite	0.01	None observed	~0.2 if no H_2O	2.649	Pure α-qtz. and no orientation observed. Some banding.
Eureka Quartzite	0.1-0.2	None observed	<1	2.58	98% qtz.; relic bedding but diffuse and slight.
Sioux Quartzite	0.6	Qtz. overgrowth	<1	2.636	99% qtz.; hematite dust between grain and overgrowth. (No orientation study made.)
Coconino Sandstone	0.117	Weak to moderate silica overgrowth (20%)	15-25	2.26	97% qtz.; laminated grain orientation ∥ to bedding and "diffuse"
CARBONATE ROCKS					
Yule Marble	0.2-0.4	None	<1	2.69	Increase in twins by shock. Preferred orientation of grains.
Spergen Limestone	0.3-0.4	0.2-0.3	15.1	2.30	Not oriented fossiliferous

Table III

SUMMARY OF EXPERIMENTAL DATA FOR QUARTZ[6] AND CALCITE

SHOT NO.	EXPLOSIVE	ORIENTATION	PELLET THICKNESS (cm)	ARRIVAL TIMES		FREE-SURFACE VELOCITIES		FIRST SHOCK				SECOND SHOCK			
				$t_1 - t_0$ (μs)	$t_2 - t_0$ (μs)	U_{f_1} (cm/μs)	U_{f_2} (cm/μs)	Shock Velocity U_1 (cm/μs)	Particle Velocity u_1 (cm/μs)	Stress σ_1 (kb)	V_1/V_0	Shock Velocity U_2 (cm/μs)	Particle Velocity u_2 (cm/μs)	Stress σ_2 (kb)	V_2/V_0
QUARTZ*															
5648	P-40 lens	X(- to +)	6.378	1.057	1.296	0.692	1.62	6.03	0.346	55.5	0.9426	5.05	0.810	117.0	0.8495
		X(- to +)	6.388	1.075	1.308	0.807	1.62	5.94	0.403	63.7	0.9320	5.03	0.810	117.4	0.8500
5907	P-40 lens	X(+ to -)	6.388	1.079	1.320	0.836	1.52	5.92	0.416	65.7	0.9294	4.99	0.758	110.1	0.8603
		Z	6.383	0.876		1.02		7.28	0.508	98.4	0.9302		not observed		
5880	P-40 lens	X(+ to -)	6.391	1.078	1.322	0.754	(1.66)	5.93	0.377	59.4	0.9364	4.97	(0.828)	118.1	0.8444
5921	P-40 lens + 1° Comp B	X(+ to -)	6.388	1.079	1.146	(0.786)	2.630	5.91	0.393	(61.8)	(0.9335)	5.61	1.315	198.8	0.7686
		Y	6.347	1.020	1.146	0.994	2.56	6.22	0.497	82.2	0.9201	5.66	1.281	199.0	0.7803
5920	P-40 lens + 1° Comp B	X(- to +)	6.391	1.069	1.139	(0.687)	2.63	5.98	0.344	(54.6)	(0.9426)	5.65	1.315	199.9	0.7702
		Z	6.388	0.876		1.40		7.28	0.698	135.1	0.9041		not observed		
6009	P-40 lens	Y	6.358	1.058	1.363	0.819	1.43	6.01	0.410	65.2	0.9320	4.85	0.713	103.7	0.8684
		Z	6.388	0.893		1.12		7.15	0.560	106.6	0.9215		not observed		
5997	P-40 lens + 2° Comp B	Y	6.369	1.011	1.158	1.01	3.00	6.29	0.515	86.2	0.9140	5.62	1.50	231.9	0.7411
		Z	6.386	0.871	1.201	1.40	(2.63)	7.33	0.700	136.1	0.9046	5.70	(1.32)	(227.2)	(0.7924)
7363	P-40 lens	Z	6.599	0.914	1.024	1.04	1.58	7.22	0.520	99.8	0.9280	4.14	0.79	127.4	0.8598
		Z	3.396	0.469	0.958	1.09	1.65	7.24	0.545	104.8	0.9247	4.10	0.82	133.4	0.8519
7394	P-40 lens + 1° Comp B	Z	6.607	0.899	1.336	1.27	2.32	7.35	0.635	123.6	0.9139	5.36	1.16	195.8	0.8124
		Z	3.411	0.462	0.681	1.51	2.47	7.38	0.751	147.6	0.8981	5.49	1.23	215.3	0.8066
7395	P-40 lens	Y	6.601	1.088	1.448	0.836	1.60	6.07	0.418	67.7	0.9308	4.77	0.880	114.9	0.8495
		Y	3.399	0.562	0.745	0.862	1.58	6.05	0.413	69.3	0.9287	4.77	0.790	113.9	0.8519
8504	P-40 lens + 2° Comp B	Z	6.601	0.913	1.252	1.38	2.68	7.22	0.689	132.4	0.9048	5.64	1.34	227.5	0.7857
CALCITE															
8460	P-40 lens + Al driver	Cleavage	9.190	1.321	1.889	0.302	1.272	6.955	0.151	28.5	0.9783	4.96	0.636	91.7	0.8796
8461	P-40 lens + lucite driver	Cleavage	9.246	1.297	2.063	0.227	1.233	7.126	0.114	22.0	0.9841	4.61	0.616	84.2	0.8739
8506	P-40 lens + Al driver	Z	10.980		2.272		1.383		not observed			4.85	0.651	85.7	0.8659
			10.980		2.286		2.032		not observed			4.82	1.016	132.7	0.7890

* Data except Shot 8504 from Reference 6.

( ) points in parentheses are less reliable.

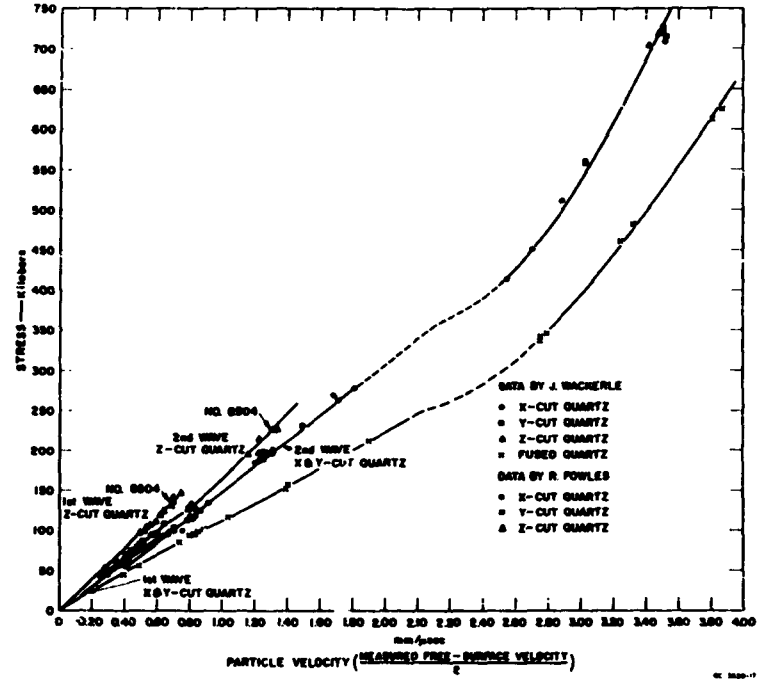

FIG. 16 STRESS vs. PARTICLE VELOCITY FOR QUARTZ

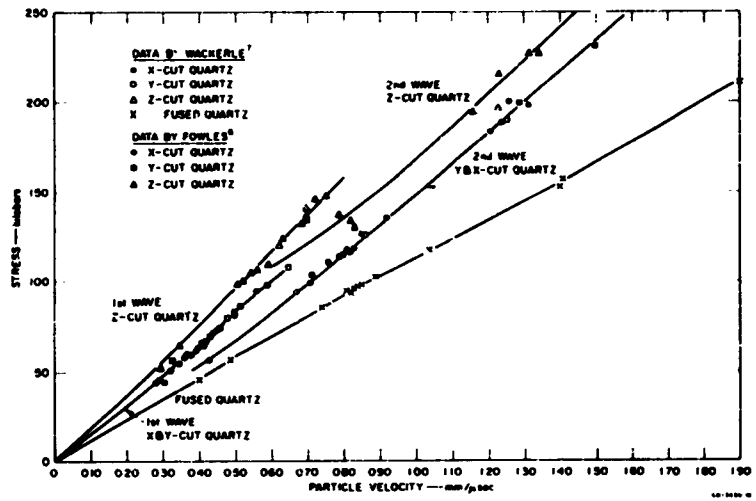

FIG. 17 STRESS vs. PARTICLE VELOCITY FOR QUARTZ

Table IV

SUMMARY OF DATA FOR QUARTZ ROCKS, TWO-DIMENSIONAL WEDGE EXPERIMENTS

ROCK PARAMETERS							SHOCK PARAMETERS								
Rock	Shot No.	Specimen Dimensions	Dynamic Velocity (mm/μs)	Explosive Type	Explosive Thickness (in.)	Specimen Density (g/cc)	Depth in Rock (in.)	Shock Angle α (deg)	Shock Velocity U (mm/μs)	Particle Velocity u (mm/μs)	Ratio ρ_0/ρ	Stress σ (kb)	Volume (cc/g)	Mirror	Notes
Arkansas Novaculite	8275	A= 40.9° a= 1.0" b= 2.0" c= 8.0"	7.396	Sheet EL506D	0.026	2.649	0.360 0.421 0.477 0.544 0.601 0.642 0.688 0.636 0.731 0.781 0.827 0.928 0.940	54.6 54.5 54.5 54.3 54.3 54.2 54.1 54.1 54.0 53.9 53.9 53.8 53.7 53.7	6.032 6.028 6.026 6.011 6.006 6.003 5.996 5.992 5.989 5.981 5.977 5.974 5.966 5.965	(0.236) 0.257 0.220 0.196 0.204 0.153 0.159 0.160 0.147 0.135	(0.960) 0.957 0.963 0.967 0.965 0.974 0.973 0.973 0.975 0.977	(37.583) 41.039 35.090 30.987 32.468 24.303 25.318 25.376 23.267 21.383	(0.362) 0.361 0.363 0.365 0.364 0.367 0.367 0.367 0.368 0.369	Auto Auto Auto Auto Auto Auto Auto Auto Auto Auto	First wave
Arkansas Novaculite	8299	A= 40.6° a= 1.0" b= 2.0" c= 8.0"	7.375	Sheet EL506D	0.100	2.642	0.097 0.189 0.236 0.280 0.374 0.418 0.464 0.555 0.601 0.644 0.740 0.787 0.832 0.869	56.1 56.0 56.0 55.9 55.8 55.8 55.8 55.7 55.7 55.6 55.6 55.5 55.5 55.4	6.123 6.117 6.115 6.112 6.106 6.104 6.101 6.096 6.098 6.091 6.085 6.082 6.080 6.077	0.378 0.360 0.368 0.336 0.328 0.306 0.301 0.282 0.275 0.256 0.253 0.250 0.234	0.938 0.941 0.942 0.944 0.946 0.949 0.950 0.953 0.954 0.957 0.958 0.958 0.961	61.216 58.194 56.360 54.362 52.615 49.690 48.609 45.564 44.356 41.223 40.733 40.321 37.664	0.355 0.356 0.356 0.357 0.358 0.359 0.360 0.361 0.361 0.362 0.363 0.363 0.364	A1 A1 A1 A1 A1 A1 A1 A1 A1 A1 A1 A1 A1	First wave
Arkansas Novaculite	8309	A= 30.7° a= 1.0" b= 2.0" c= 8.0"	7.908	Comp B	0.25	2.642	0.107 0.143 0.177 0.249 0.285 0.321 0.398 0.433 0.473 0.546 0.584 0.621 0.695 0.735 0.769 0.845 0.871 0.886	52.0 52.0 51.9 51.8 51.7 51.7 51.5 51.5 51.4 51.3 51.3 51.2 51.1 51.0 51.0 50.8 50.8 50.8	6.235 6.230 6.225 6.215 6.210 6.205 6.195 6.190 6.185 6.175 6.170 6.165 6.155 6.149 6.145 6.134 6.131 6.129	0.479 0.476 0.449 0.428 0.411 0.409 0.412 0.386 0.400 0.384 0.381 0.375 0.370 0.383 0.364 0.360 0.281 0.135	0.923 0.923 0.927 0.931 0.933 0.934 0.933 0.937 0.935 0.937 0.938 0.939 0.939 0.937 0.940 0.941 0.954 0.977	78.921 78.477 73.941 70.334 67.451 66.999 67.449 53.214 65.462 62.662 62.205 61.288 60.278 62.274 59.098 58.451 45.618 21.883	0.349 0.349 0.351 0.352 0.353 0.353 0.353 0.355 0.354 0.355 0.355 0.355 0.355 0.355 0.356 0.356 0.361 0.370	A1 A1 A1 A1 A1 A1 A1 A1 A1 A1 A1 A1 A1 A1 A1 A1 A1 A1	First wave

( ) points in parentheses are less reliable.

Table IV Continued

ROCK PARAMETERS							SHOCK PARAMETERS								
Rock	Shot No.	Specimen Dimensions	Determination Velocity (mm/μs)	Explosive Type	Explosive Thickness (in.)	Specimen Density (g/cc)	Depth in Rock (in.)	Shock Angle α (deg)	Shock Velocity U (mm/μs)	Particle Velocity u (mm/μs)	Ratio ρ_0/ρ	Stress σ (kb)	Volume (cc/g)	Mirror	Notes
Sioux Quartzite	7468	A = 39 deg a = 2.3" b = 4.1" c = 9.5"	7.920	Comp B	0.50	2.640	0.338	-0.1	5.716	0.264	0.953	39.985	0.361	Al	First wave, ramps ignored
							0.472	45.9	5.695	0.235	0.958	35.340	0.363	Al	
							0.625	45.7	5.671	0.240	0.956	37.250	0.362	Al	
							0.761	45.5	5.649	0.233	0.952	31.809	0.364	Al	
							0.911	45.2	5.626	0.244	0.956	36.252	0.362	Al	
							1.060	45.0	5.605	0.223	0.953	33.060	0.364	Al	
							1.183	44.8	5.584	0.175	0.968	25.884	0.367	Al	
							1.331	44.6	5.561	0.206	0.962	30.369	0.364	Al	
							1.445	44.3	5.541	0.168	0.969	24.622	0.367	Al	
							1.609	44.1	5.520	0.134	0.975	19.642	0.369	Al	
							1.742	43.9	5.499	0.106	0.980	15.408	0.371	Al	
							1.883	43.7	5.477	0.066	0.987	9.650	0.374	Al	
							0.295	38.6	4.951	0.741	0.856	102.025	0.324	Al	Second wave, ramps ignored
							0.423	38.0	4.881	0.615	0.880	83.969	0.333	Al	
							0.536	37.5	4.829	0.787	0.843	106.620	0.319	Al	
							0.666	36.9	4.759	0.703	0.858	92.973	0.325	Al	
							0.798	36.4	4.705	0.799	0.837	104.634	0.317	Al	
							0.976	35.6	4.629	0.588	0.897	67.470	0.340	Al	
							1.136	35.0	4.566	0.342	0.931	45.787	0.353	Al	
							1.215	34.7	4.536	0.495	0.898	66.373	0.340	Al	
							1.385	34.0	4.469	0.380	0.939	39.956	0.356	Al	
							1.494	33.5	4.375	0.231	0.952	31.026	0.361	Al	
							1.587	33.1	4.329	0.246	0.948	31.418	0.359	Al	
							1.721	32.5	4.265	0.250	0.944	30.284	0.358	Al	
Eureka Quartzite	7498	A = 60 deg a = 2.8" b = 5.0" c = 9.5"	7.936	Comp B	0.25	2.640	0.638	43.6	5.477					Al	First wave, Light into test first part of record
							0.793	45.0	5.616	0.253	0.954	37.606	0.361	Al	
							0.870	44.2	5.539	0.383	0.930	56.061	0.352	Al	
							0.976	45.3	5.648	0.319	0.943	47.680	0.357	Al	
							1.088	44.6	5.577	0.248	0.[illegible]	36.587	0.362	Al	
							1.110	45.6	5.671	0.222	0.[illegible]	33.270	0.364	Al	
							1.185	45.1	5.625	0.277	0.[illegible]	41.273	0.360	Al	
							1.255	45.8	5.696	0.174	0.969	26.209	0.367	Al	
							1.315	45.5	5.660	0.164	0.970	24.573	0.367	Al	
							1.439	46.2	5.729	(0.222)	(0.961)	(33.673)	0.364	Al	
							1.512	46.0	5.715	0.265	0.953	40.108	0.361	Al	
							1.647	46.6	5.766	0.318	0.944	48.489	0.358	Al	
							1.666	46.5	5.758	0.228	0.960	34.816	0.364	Al	
							1.792	46.8	5.791	0.277	0.952	42.468	0.361	Al	
							1.926	47.1	5.816	0.212	0.963	32.662	0.365	Al	
							(0.000)	(34.6)	(4.515)						Second wave
							(0.989)	(35.9)	(4.661)	(0.410)	(0.923)	(58.553)	(0.350)		
							(1.075)	(37.7)	(4.856)	(0.313)	(0.941)	(44.891)	(0.356)		

( ) points in parentheses are less reliable.

Table IV Continued

ROCK PARAMETERS							SHOCK PARAMETERS								
Rock	Shot No.	Specimen Dimensions	Detonation Velocity (mm/μs)	Explosive Type	Explosive Thickness (in.)	Specimen Density (g/cc)	Depth in Rock (in.)	Shock Angle α (deg)	Shock Velocity U (mm/μs)	Particle Velocity u (mm/μs)	Ratio ρ_0/ρ	Stress σ (kb)	Volume (cc/g)	Mirror	Notes
Coconino Sandstone	8119	A = 35.1° a = 2.3° b = 4.9° c = 9.9°	7.800	Comp B	0.25	1.992	0.759	23.6	3.124	0.068	0.978	4.236	0.491	Al	First wave.
							0.926	23.6	3.126	0.022	0.991	1.748	0.497	Al	
							0.986	24.7	3.271	0.023	0.989	2.162	0.496	Al/Ar	Precursor arrived with small amplitude, values may be poor
							1.068	23.6	3.127	0.020	0.994	1.872	0.497	Al	
							1.124	24.8	3.273	0.038	0.988	2.336	0.496	Al/Ar	
							1.179	23.6	3.129	0.077	0.975	4.815	0.190	Al	
							1.294	24.8	3.275					Al/Ar	
							1.341	23.6	3.130	0.051	0.983	3.203	0.493	Al	
							1.376	24.8	3.276	0.075	0.976	4.949	0.490	Al/Ar	
							1.489	23.6	3.132	0.041	0.986	2.615	0.495	Al	
							1.522	24.8	3.278	0.066	0.979	4.336	0.491	Al/Ar	
							1.573	23.6	3.133	0.129	0.958	8.096	0.481	Al	
							1.674	24.8	3.280	0.056	0.982	3.691	0.493	Al/Ar	
							1.708	23.7	3.135	0.050	0.983	3.162	0.493	Al	
							1.816	24.8	3.282	0.055	0.982	3.653	0.493	Al/Ar	
							1.911	23.7	3.137	0.046	0.985	2.929	0.494	Al	
							1.989	24.9	3.285	0.024	0.992	1.627	0.498	Al/Ar	
							2.089	23.7	3.138	0.084	0.973	5.268	0.488	Al	
							1.189	24.8	1.995	(0.466)	(0.773)	(19.535)	(0.389)	Al	Second wave
Coconino Sandstone	8143	A = 20.0° a = 2.0° b = 4.2° c = 11.5°	7.910	Comp B	0.25	2.010	0.278	25.2	3.378	0.016	0.995	1.162	0.495	Al	First wave.
							0.365	24.8	3.328	0.026	0.991	1.792	0.493	Al	Precursor arrived with small amplitude, values may be poor
							0.413	23.6	3.146	0.017	0.994	1.108	0.495	Al/Ar	
							0.465	24.5	3.283	0.008	0.997	0.579	0.496	Al	
							0.498	23.5	3.156	0.008	0.998	1.810	0.493	Al/Ar	
							0.540	24.1	3.231	0.106	0.967	6.987	0.481	Al	
							0.583	23.6	3.167	0.020	0.998	1.959	0.493	Al/Ar	
							0.614	23.8	3.192	0.010	0.996	0.650	0.496	Al	
							0.663	23.6	3.177	0.011	0.996	0.740	0.496	Al/Ar	
							0.698	23.4	3.148	0.028	0.990	1.825	0.493	Al	
							0.868	23.8	3.199	0.142	0.955	9.166	0.475	Al/Ar	
							0.871	22.7	3.062	0.087	0.971	5.377	0.483	Al	
							0.913	23.9	3.208	0.014	0.995	0.953	0.495	Al/Ar	
							1.016	24.0	3.220	0.152	0.952	9.870	0.474	Al	
							1.038	22.1	2.982	0.138	0.953	8.300	0.474	Al	
							1.121	21.8	2.964	0.168	0.942	9.966	0.469	Al	
							1.189	24.2	3.242	0.171	0.947	11.177	0.471	Al/Ar	
							1.250	24.2	3.256	0.026	0.991	1.700	0.493	Al/Ar	
							1.288	21.2	2.870	0.176	0.938	10.160	0.467	Al	
							0.388	18.6	2.534	(1.789)	(0.294)	(91.229)	(0.146)	Al	Second wave
							0.443	17.9	2.435	(0.695)	(0.716)	(34.390)	(0.356)	Al/Ar	
							0.463	18.0	2.446	(1.726)	(0.297)	(85.711)	(0.148)	Al	
							0.506	17.1	2.333	0.745	0.682	35.369	0.339	Ar	

( ) points in parentheses are less reliable

Table IV Concluded

ROCK PARAMETERS							SHOCK PARAMETERS							
Rock	Shot No.	Specimen Dimensions	Detonation Velocity (mm/μs)	Explosive Type	Explosive Thickness (in.)	Specimen Density (g/cc)	Depth in Rock (in.)	Shock Angle α (deg)	Shock Velocity U (mm/μs)	Particle Velocity u (mm/μs)	Ratio ρ_0/ρ	Stress σ (kb)	Volume (cc g)	Mirror	Notes
Coconino Sandstone	8163 (cont.)	A = 20.0° a = 2.0° b = 5.0° c = 11.5°	7.910	Comp B	0.25	2.010	0.546 0.595 0.615 0.652 0.706 0.753 0.774 0.829 0.875 1.001 1.139 1.232	16.8 16.0 16.2 15.4 15.3 15.1 14.9 13.9 13.9 13.5 12.8 11.7	2.293 2.189 2.208 2.105 2.087 2.071 2.044 1.906 1.907 1.850 1.753 1.611	0.803 0.436 0.900 0.508 0.532 (0.674) 0.931 (0.364) 0.592 0.557 (0.650) (0.207)	0.650 0.801 0.594 0.758 0.745 (0.692) 0.552 (0.811) 0.896 0.720 (0.656) (0.870)	37.198 19.415 40.349 21.528 22.339 (30.745) 39.560 (14.292) 11.215 23.425 (26.247) (6.737)	0.323 0.398 0.296 0.377 0.371 (0.344) 0.275 (0.403) 0.421 0.358 (0.326) (0.433)	Al Mg Al Mg Al Mg Al Mg Al Al Al Al	Second wave
Coconino Sandstone	8269	A = 20.0° a = 2.1° b = 5.0° c = 11.2°	7.099	Sheet (2.50#)	0.060	2.021	0.003 0.029 0.076 0.116 0.173 0.201 0.248 0.271 0.347 0.428 0.488 0.023 0.037 0.077 0.089	27.7 11.0 27.2 28.3 26.6 26.5 26.1 25.0 25.5 25.0 26.7 8.6 8.7 17.8 16.1	3.305 3.060 3.250 3.296 3.180 3.169 3.127 3.001 3.060 3.007 2.909 1.067 1.078 2.171 1.978	0.088 0.001 0.020 0.064 0.032 0.027 0.085 0.090 0.258 0.303 0.437 0.784	0.997 0.999 0.994 0.985 0.989 0.991 0.972 0.970 0.768 0.733 0.437 0.508	0.667 6.102 0.1393 2.881 2.111 1.765 5.318 5.502 6.488 7.916 54.352 39.587	0.491 0.492 0.489 0.485 0.487 0.488 0.479 0.478 0.378 0.361 0.215 0.251	Mg Al Mg Al Mg Al Al Al Mg Mg Al Al	First wave Second wave
Coconino Sandstone	8278	A = 17.0° a = 2.1° b = 5.1° c = 11.4°	8.072	Comp B	1.00	2.067	0.341 0.418 0.473 0.559 0.612 0.689 0.767 0.828 0.897 0.971 1.049	27.2 26.6 26.2 25.5 25.2 24.6 24.1 23.7 23.4 22.9 22.6	3.695 3.[illegible] 3.[illegible] 3.486 3.4[illegible] 3.370 3.304 3.254 3.207 3.143 3.106	(1.170) (1.315) (1.041) (1.378) (1.017) (1.217) (1.417) (1.255) (0.978) (1.228) (0.718)	(0.683) (0.63[illegible]) (0.708) (0.606) (0.704) (0.638) (0.571) (0.614) (0.694) (0.577) (0.748)	(89.371) (98.437) (76.753) (99.365) (72.355) (84.881) (96.816) (84.460) (64.704) (86.291) (46.150)	(0.330) (0.307) (0.342) (0.292) (0.340) (0.308) (0.276) (0.297) (0.335) (0.279) (0.371)	Al Al Al Al Al Al Al Al Al Al Al	Second wave
Coconino Sandstone	8262 (X ray)		7.4	Sheet (2.50#)	0.200	2.000	0.240 0.517 0.770	19.6 15.7 12.5	2.483 2.082 1.601	0.796 0.266 0.066	0.679 0.867 0.959	39.5 10.6 2.1	0.340 0.434 0.480		

( ) points in parentheses are less reliable

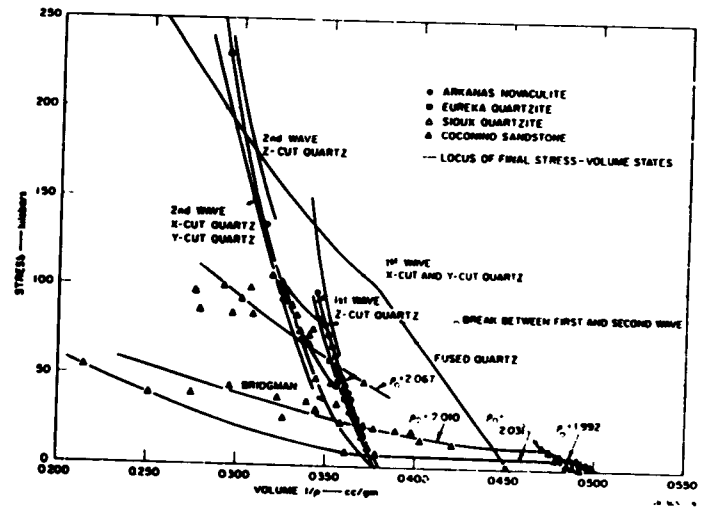

FIG. 18 HUGONIOTS FOR QUARTZ AND QUARTZ ROCKS

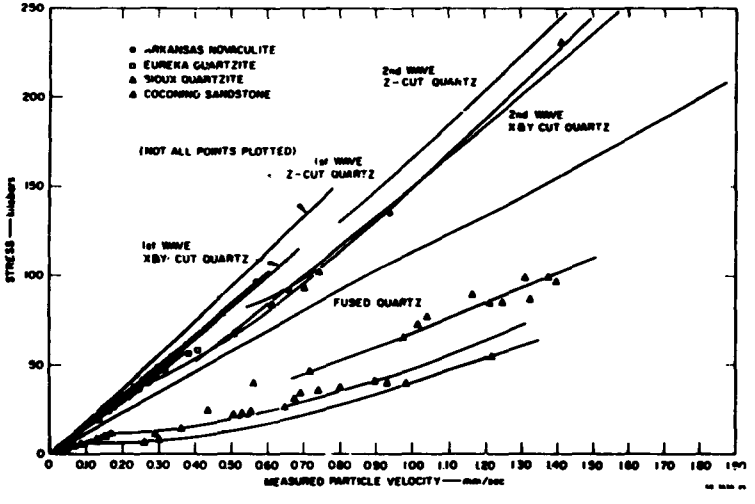

FIG. 19 STRESS vs. PARTICLE VELOCITY FOR QUARTZ ROCKS

From the data shown in Figs. 18 and 19 and from the observed differences and similarities of the rocks, the following conclusions are drawn:

1. In the main, Hugoniot data for the quartzites and novaculites agree with the single crystal data. That is, the velocities for the first waves agree and the velocity for the second wave lies between the velocities for the *X*, *Y*-cut and *Z*-cut quartz. The data for the sandstone scatters widely. This scatter occurs in the state of the second wave. Data from the first wave is more consistent but the peak stress and velocity is much less than in the single crystal.

2. The break in the stress-particle velocity graphs of the Arkansas novaculite, Sioux and Eureka quartzite, and Coconino sandstone indicates a transition from elastic to nonelastic behavior of the rock and not a phase transition. This is indicated by the wide range in transition pressures for the various rock types, although they are mineralogically the same. This is also shown by the agreement of the first wave velocities of the quartzites, and especially the novaculite, with those of the *X*-cut and *Y*-cut first-waves in crystal quartz.

No dynamic phase transitions in crystal quartz are reported at the temperatures and pressures obtained in these experiments. When a sample of novaculite, shocked to 100 kb, was recovered from one of our experiments and examined petrographically, no indication of a phase change was found in the inter-granular structure. However, coesite and stishovite are recorded in meteor craters and this indicates the possibility of finding them in the shock wave experiments at higher pressures. The break at about 400 kb in Wackerle's data is suggested by him to be a phase change to stishovite.

3. Porosity plays a major role in determining the velocity with which the first wave propagates, Fig. 20. Compare the propagation velocity of the first wave for novaculite, which has no porosity, with first wave velocity of other rocks (Table IV). The quartzites have less than 1 percent porosity and a first wave velocity slightly less than that of the novaculite; while the Coconino sandstone, with a porosity of about 23 percent, has a first wave velocity much less than the above rocks.

4. The peak stress amplitude of the first wave is dependent upon the porosity. Figure 21 shows that the peak stress is quite sensitive

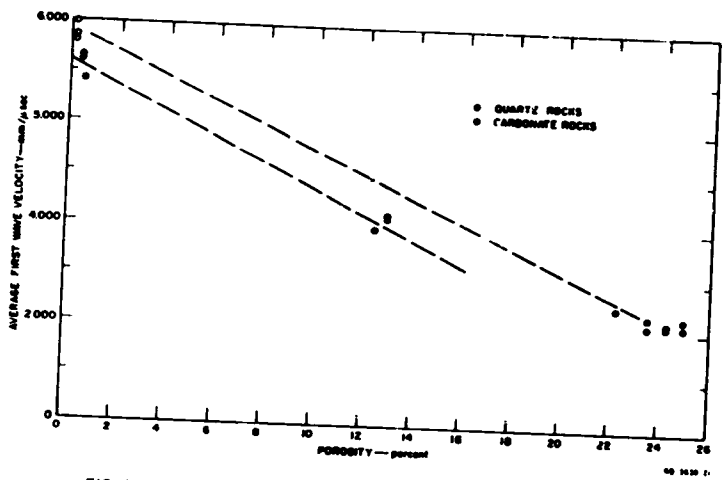

FIG. 20 AVERAGE FIRST WAVE VELOCITY vs. POROSITY FOR QUARTZ AND CARBONATE ROCKS

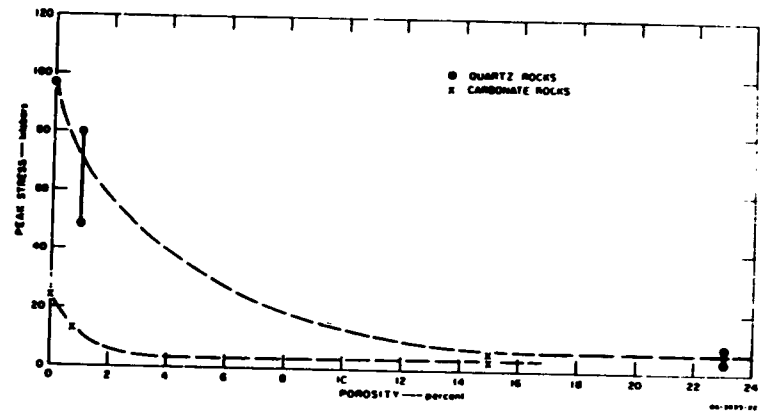

FIG. 21 PEAK STRESS OF FIRST WAVE vs. POROSITY FOR QUARTZ AND CARBONATE ROCKS

to porosity for the first few percent. It is possible that one of the parameters that controls porosity (e.g., cementation) plays a major role in the relationship. The secondary quartz overgrowths on the grains in the Sioux quartzite would influence the peak stress of the first wave if this were the case; unfortunately, the exact peak stress of the first wave from the Eureka quartzite is not available for comparison so that the proper importance of cementation can not be evaluated. It is expected that static compression tests will give a measure of the cementation effect.

Until more information is available, the peak stress amplitude will be assumed to be a function of porosity only.

5. The grain size of the rock has little influence on the shock wave parameters. There is no correlation of peak stress or first wave velocity with grain size. Besides which, for well sorted sand grains, the porosity does not depend upon grain size. The grain size may determine the rise time of the shock wave but no data are available to support the idea.

C CALCITE

All the data obtained at SRI are recorded in Table III. The Plane-Wave Pellet Method was used in the experiments; others were performed but errors in the assemblies have devaluated the results. Further experiments are in progress. Figures 22, 23, and 24 include tentative graphs of the data for cleavage-cut calcite. It is uncertain whether the break between the two waves, 30 kb is a phase transition or an elastic to plastic transition. Adadurov, *et al.*,[8] have determined phase transitions in marble at 16, 21.5, 30 kb by static methods but, except for the transition at 30 kb which is in question, these transitions have not been detected by our dynamic measurements.

The second wave data in calcite lie to the right of the marble results. However, the scatter in the polycrystalline data is so large that it is difficult to say whether or not this effect is significant. Further work is required to clarify this point.

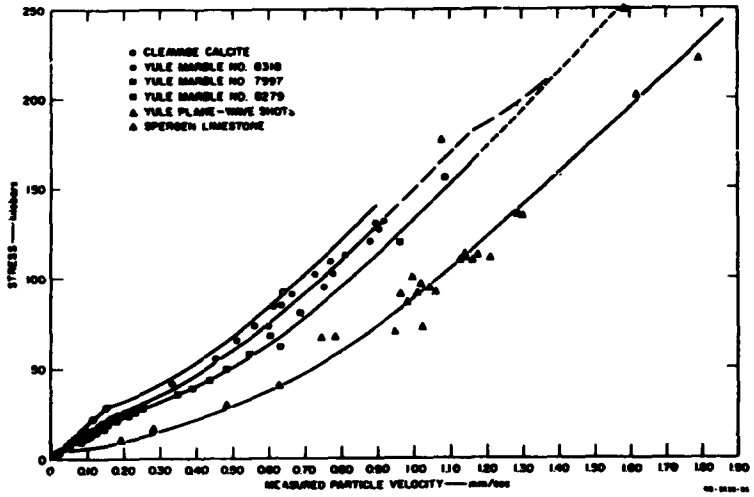

FIG. 22 STRESS vs. PARTICLE VELOCITY FOR CALCITE AND CARBONATE ROCKS

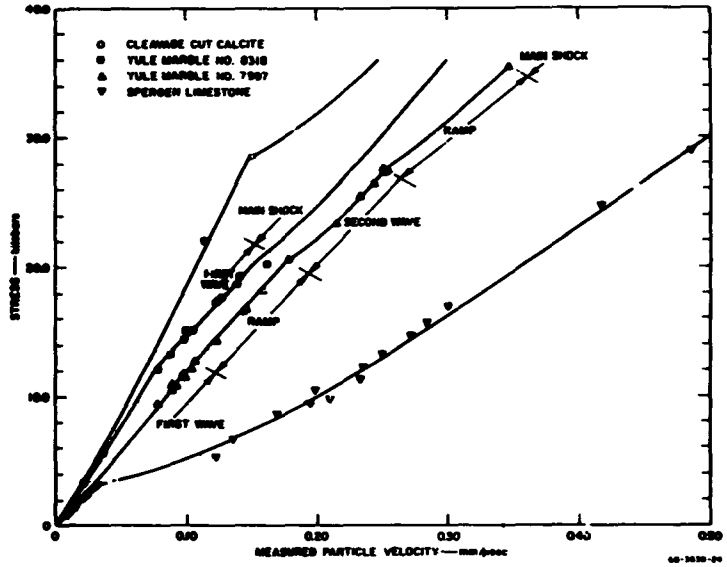

FIG. 23 STRESS vs. PARTICLE VELOCITY FOR CALCITE AND CARBONATE ROCKS

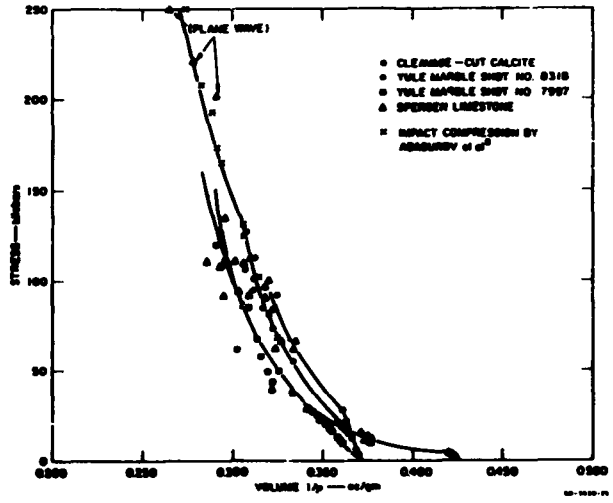

FIG. 24 HUGONIOT FOR CALCITE AND CARBONATE ROCKS

D. CARBONATE ROCKS

Table V and part of Table VI summarizes all the data for the carbonate rocks. Figures 22, 23, and 24 show plots of stress-particle velocity and stress-volume for Yule marble and Spergen Limestone. Using the above data together with the differences and similarities of the rocks, the following conclusions are drawn:

1. For the carbonate rocks, agreement is poor among the Hugoniot data, Fig. 24. There are differences in the data between rock types as well as differences between the two-dimensional experiments and the plane-wave experiment on each rock. The general behavior is the same as in the quartz rocks, however. The velocities of the first waves in the carbonates is less than calcite; with the more porous rock having the lowest first wave velocity.

Table V

SUMMARY OF DATA FOR CARBONATE ROCKS, TWO-DIMENSIONAL WEDGE EXPERIMENTS

ROCK PARAMETERS							SHOCK PARAMETERS								
Rock	Shot No.	Specimen Dimensions	Determination Velocity (cm/μs)	Explosive Type	Explosive Thickness (in.)	Specimen Density (g/cc)	Depth in Rock (in.)	Shock Angle α (deg)	Shock Velocity U (cm/μs)	Particle Velocity u (cm/μs)	Ratio ρ_0/ρ	Stress σ (kb)	Volume (cc/g)	Mirror	Notes
Tule Marble	8318	A = 28.0° a = 2.5° b = 5.1° c = 9.1°	7.974	Comp B	1.0	2.693	0.164	47.2	(5.856)	(0.820)	(0.996)	(3.381)	(0.370)	Al	First wave, range ignored
							0.228	49.8	(6.086)	(0.884)	(0.999)	(0.886)	(0.371)	Al	
							0.288	46.3	(5.774)	(0.836)	(0.995)	(5.616)	(0.369)	Al	
							0.351	47.8	(5.913)	(0.826)	(0.995)	(4.266)	(0.370)	Al	
							0.414	45.7	5.692	0.878	0.986	12.875	0.366	Al	
							0.486	46.5	5.791	0.888	0.986	12.487	0.366	Al	
							0.552	46.7	5.616	0.887	0.984	13.225	0.365	Al	
							0.608	45.4	5.687	0.886	0.984	13.254	0.365	Al	
							0.649	44.0	5.542	0.100	0.983	15.034	0.364	Al	
							0.721	44.6	5.584	0.093	0.983	14.086	0.365	Al	
							0.766	43.3	5.470	0.105	0.981	15.071	0.364	Al	
							0.860	43.4	5.482	0.112	0.979	16 675	0.364	Al	
							0.878	42.6	5.408	0.099	0.981	16.684	0.364	Al	
							0.950	42.5	5.398	0.102	0.980	16.965	0.364	Al	
							0.996	41.9	5.329	0.108	0.980	15.191	0.364	Al	
							1.071	41.5	5.291	0.126	0.976	18.044	0.363	Al	
							1.114	41.2	5.258	0.122	0.976	17.394	0.362	Al	
							1.181	40.7	5.202	0.119	0.976	16.887	0.362	Al	
							1.229	40.6	5.190	0.124	0.975	17.430	0.362	Al	
							1.300	39.8	5.108	0.137	0.972	18.863	0.361	Al	
							1.345	39.9	5.123	0.127	0.975	17.689	0.362	Al	
							1.412	39.8	5.022	0.134	0.973	18.219	0.361	Al	
							1.463	39.3	5.057	0.141	0.971	19.287	0.361	Al	
							1.533	38.2	4.932	0.161	0.967	21.513	0.359	Al	
							1.581	38.7	4.998	0.142	0.967	21.082	0.359	Al	
							1.646	37.4	4.868	0.165	0.965	21.624	0.358	Al	
							1.693	38.1	4.929	0.140	0.971	18.677	0.360	Al	
							1.738	36.7	4.769	0.138	0.971	17.754	0.361	Al	
							1.806	37.6	4.868	0.135	0.972	17.734	0.361	Al	
							1.856	36.1	4.699	0.973	0.984	9.264	0.365	Al	
							0.350	42.3	(5.369)	(0.895)	(0.833)	(129.731)	(0.309)	Al	Second wave
							0.467	41.5	(5.289)	(0.915)	(0.827)	(130.146)	(0.340)	Al	
							0.545	40.9	5.238	(0.778)	(0.853)	(108.887)	(0.317)	Al	
							0.578	41.0	5.232	0.896	0.829	127.163	0.308	Al	
							0.698	40.2	5.153	0.902	0.825	126.260	0.306	Al	
							0.773	40.0	5.129	(0.727)	(0.859)	(101.592)	(0.319)	Al	
							0.787	39.6	5.088	0.813	0.841	112.444	0.312	Al	
							0.906	38.8	5.002	0.880	0.825	119.366	0.306	Al	
							0.986	38.9	5.010	(0.663)	(0.869)	(90.752)	(0.323)	Al	

( ) points in parentheses are less reliable

Table V *Continued*

ROCK PARAMETERS							SHOCK PARAMETERS								
Rock	Shot No.	Specimen Dimensions	Determination Velocity (cm/μs)	Explosive Type	Explosive Thickness (in.)	Specimen Density (g/cc)	Depth in Rock (in.)	Shock Angle α /deg)	Shock Velocity U (cm/μs)	Particle Velocity u (cm/μs)	Ratio ρ_0/ρ	Stress σ (kb)	Volume (cc/g)	Mirror	Notes
Yule Marble	8318 (Cont)	A = 28.0° a = 2.5° b = 5.1° c = 9.1°	7.974	Comp B	1.0	2.693	1.013	38.1	4.924	0.878	0.823	117.571	0.306	Al	Second wave.
							1.125	37.4	4.848	0.880	0.819	116.201	0.304	Al	
							1.203	37.7	4.879	(0.632)	(0.872)	(84.369)	(0.324)	Mg	
							1.225	36.9	4.788	0.775	0.840	101.363	0.312	Al	
							1.341	36.2	4.712	0.827	0.824	106.434	0.307	Al	
							1.413	36.5	4.754	(0.562)	(0.883)	(73.227)	(0.328)	Mg	
							1.445	35.6	4.644	0.767	0.836	97.442	0.310	Al	
							1.557	35.0	4.579	0.752	0.838	94.337	0.311	Al	
							1.612	35.5	4.635	(0.513)	(0.891)	(65.254)	(0.331)	Mg	
							1.666	34.5	4.520	0.679	0.852	84.502	0.316	Al	
							1.765	33.8	4.447	0.598	0.868	75.319	0.322	Al	
							1.862	33.3	4.384	0.452	0.899	55.125	0.334	Al	
							1.887	32.6	4.307	0.087	0.979	10.159	0.364	Al	
Yule Marble	8279	A = 40.0° a = 3.1° b = 5.1° c = 8.1°	7.348	Comp B	0.25	2.697	0.215	56.5	6.130	0.058	0.990	9.722	0.367	Al	First wave.
							0.371	55.8	6.082	0.061	0.989	10.157	0.367	Al	
							0.524	55.7	6.076	0.063	0.989	10.346	0.367	Al	Light source failed two more
							0.678	54.5	5.989	0.066	0.988	10.734	0.366	Al	
							0.835	53.9	5.941	0.069	0.988	11.060	0.366	Al	
							0.989	53.3	5.893	0.073	0.987	11.711	0.366	Al	
							1.136	52.7	5.849	0.067	0.988	10.657	0.366	Al	
							1.288	52.1	5.802	0.069	0.987	10.915	0.365	Al	
							1.443	51.5	5.755	0.072	0.987	11.306	0.366	Al	
							1.589	51.0	5.711	0.066	0.988	10.262	0.366	Al	
							1.661	52.8	5.857	0.057	0.990	9.030	0.367	Mg	
							1.734	50.4	5.667	0.058	0.989	8.892	0.367	Al	
							1.807	51.9	5.783	0.058	0.989	9.102	0.367	Mg	
							1.884	49.9	5.622	0.059	0.989	9.013	0.367	Al	
							1.958	50.9	5.707	0.062	0.989	9.653	0.367	Mg	
							2.038	49.3	5.576	0.061	0.989	9.178	0.367	Al	
							2.103	50.0	5.634	0.052	0.990	8.023	0.367	Mg	
							2.190	48.8	5.531	0.058	0.989	8.643	0.367	Al	
							2.268	49.2	5.562	0.049	0.991	7.640	0.367	Mg	
							2.332	48.3	5.489	0.051	0.990	7.685	0.367	Al	
							2.397	48.3	5.489	0.049	0.991	7.293	0.367	Mg	
							2.459	47.8	5.451	(0.012)	(0.997)	(1.825)	0.370	Al	
							0.078	30.1	3.685	(0.187)	(0.955)	(22.416)	0.354	Al	Second wave
							0.236	30.5	3.729	(0.156)	(0.953)	(23.655)	0.353	Al	
							0.438	31.0	3.786	(0.154)	(0.965)	(19.574)	0.358	Al	

( ) points in parentheses are less reliable.

Table V *Continued*

ROCK PARAMETERS							SHOCK PARAMETERS								
Rock	Shot No.	Specimen Dimensions	Detonation Velocity (mm/μs)	Explosive Type	Explosive Thickness (in.)	Specimen Density (g/cc)	Depth in Rock (in.)	Shock Angle α (deg)	Shock Velocity U (mm/μs)	Particle Velocity u (mm/μs)	Ratio σ_0/ρ	Stress σ (kb)	Volume (cc/g)	Mirror	Notes
Yule Marble	7997	A = 61.75° a = 2.8° b = 4.9° c = 10.1°	7.874	Comp B	0.25	2.720	1.352	32.5	4.240	9.098	0.976	11.419	0.359	Al	First wave (Ramps made into steps)
							1.359	33.1	4.305	0.140	0.967	16.484	0.356	Al	
							1.509	32.8	4.266	0.104	0.975	12.163	0.359	Al	
							1.540	33.4	4.335	0.110	0.974	12.988	0.358	Al	
							1.670	33.0	4.295	0.099	0.976	11.597	0.359	Al	
							1.716	33.5	4.362	0.099	0.977	11.786	0.359	Al	
							1.843	33.3	4.323	0.092	0.978	10.848	0.359	Al	
							1.876	33.0	4.288	0.101	0.976	12.116	0.359	Al	
							2.008	33.5	4.352	0.088	0.979	10.435	0.360	Al	
							2.037	34.0	4.414	0.102	0.976	12.357	0.359	Al	
							2.139	33.7	4.378	0.098	0.977	11.684	0.360	Al	
							2.199	34.3	4.448	0.102	0.976	12.351	0.359	Al	
							2.323	34.5	4.467	0.106	0.975	12.767	0.359	Al	
							2.362	34.5	4.467	0.096	0.978	11.681	0.360	Al	
							2.494	34.3	4.438	0.078	0.982	9.488	0.361	Al	
							2.515	34.7	4.493	0.110	0.975	13.453	0.359	Al	
							2.647	34.5	4.465	0.109	0.980	10 840	0.360	Al	
							1.476	24.9	3.869	0.147	0.965	16.858	0.355	Al	Ramp
							1.626	29.7	3.910	0.154	0.963	17.634	0.354	Al	
							1.634	30.6	4.008	0.159	0.961	18.175	0.353	Al	
							1.803	30.4	3.992	0.146	0.965	16.688	0.355	Al	
							1.827	30.2	3.964	0.118	0.972	13.980	0.357	Al	
							1.963	30.3	3.977	0.146	0.965	16.713	0.355	Al	
							1.999	30.6	4.011	0.109	0.973	13.091	0.359	Al	
							2.124	30.1	3.950	0.145	0.966	16.533	0.355	Al	
							2.158	31.0	4.055	0.112	0.974	13.506	0.358	Al	
							2.265	30.0	3.944	0.178	0.957	20.436	0.352	Al	
							2.456	29.9	3.929	0.123	0.970	14.300	0.357	Al	
							1.374	27.5	3.645	0.199	0.950	21.997	0.349	Al	Second wave
							1.520	27.5	3.643	0.208	0.948	22.784	0.349	Al	
							1.574	27.6	3.657	0.252	0.936	27.317	0.344	Al	
							1.694	27.6	3.654	0.198	0.950	21.843	0.349	Al	
							1.734	27.6	3.648	0.244	0.938	26.365	0.345	Al	
							1.879	27.6	3.658	0.180	0.955	20.121	0.351	Al	
							1.882	27.5	3.637	0.254	0.935	27.354	0.344	Al	
							2.069	27.6	3.658	0.173	0.957	19.524	0.352	Al	
							2.080	27.4	3.627	0.233	0.941	25.382	0.346	Al	
							2.216	27.7	3.664	0.178	0.955	19.842	0.351	Al	
							2.222	27.3	3.611	0.251	0.937	27.546	0.345	Al	
							2.370	27.7	3.665	0.187	0.954	21.174	0.351	Al	
							2.384	27.2	3.605	0.215	0.945	23.283	0.347	Al	

( ) points in parentheses are less reliable.

Table V Continued

ROCK PARAMETERS							SHOCK PARAMETERS								
Rock	Shot No.	Specimen Dimensions	Detonation Velocity (mm/μs)	Explosive Type	Explosive Thickness (in.)	Specimen Density (g/cc)	Depth in Rock (in.)	Shock Angle α (deg)	Shock Velocity U (mm/μs)	Particle Velocity u (mm/μs)	Ratio $\rho_0 U / \sigma$	Stress σ (kb)	Volume (cc/g)	Mirror	Notes
Yule Marble	7997 (Cont)	A = 41.75° a = 2.8° b = 4.9° c = 10.1°	7.874	Comp B	0.25	2.720	1.317	23.5	3.143	0.143	0.962	15.173	0.354	Al	Hump
							1.477	23.9	3.190	0.146	0.962	15.770	0.354	Al	
							1.543	24.0	3.206	0.347	0.906	35.468	0.333	Al	
							0.548	35.4	4.562	0.960	0.789	1'3.253	0.280	Al	Third wave main shock
							0.709	33.2	4.319	0.684	0.841	80.465	0.309	Al	
							0.847	31.6	4.128	0.603	0.853	67.725	0.314	Al	
							0.982	29.3	3.862	0.453	0.885	49.239	0.325	Mir	
							1.022	29.4	3.866	0.547	0.857	57.689	0.316	Al	
							1.136	27.4	3.625	0.358	0.906	37.618	0.333	Mir	
							1.202	27.7	3.662	0.481	0.870	49.042	0.320	Al	
							1.379	25.9	3.451	0.630	0.823	61.851	0.303	Al	
							1.383	25.3	3.373	0.266	0.930	28.225	0.342	Mir	
							1.509	24.0	3.207	0.238	0.930	25.277	0.345	Mir	
							1.591	24.4	3.264	0.436	0.870	43.242	0.323	Al	
							1.685	23.9	3.088	0.390	0.890	38.579	0.327	Al	
Spergen Limestone	8118	A = 35.1° a = 3.0° b = 5.3° c = 11.8°	7.940	Comp B	0.25	2.396	0.977	19.2	2.612	0.318	0.877	19.952	0.408	Mir	First wave
							1.201	17.6	2.408	0.232	0.903	13.419	0.377	Mir	
							1.461	15.0	2.066	0.209	0.898	10.323	0.375	Al	
							1.552	14.5	1.997	0.492	0.753	23.544	0.315	Al	
							0.729	20.5	2.791	0.577	0.793	38.572	0.331	Al	Second wave
							0.962	18.2	2.488	0.435	0.824	25.844	0.344	Al	
							1.284	16.2	2.213	0.344	0.844	18.313	0.352	Al	
							1.364	14.8	2.038	0.580	0.711	28 906	0.297	Al	
							0.698	20.3	2.754	(1.095)	(0.589)	(70.346)	(0.246)	Al	Third wave
							0.944	18.3	2.505	(0.938)	(0.612)	(54.689)	(0.256)	Al	
							1.198	16.7	2.287	(1.448)	(0.543)	(79.038)	(0.143)	Al	
Spergen Limestone	8162	A = 28.0° a = 3.0° b = 5.1° c = 11.9°	7.850	Comp B	0.25	2.360	0.218	32.1	4.177	(0.029)	(0.992)	(2.920)	(0.420)	Mir	First wave
							0.333	32.1	4.176	(0.022)	(0.994)	(2.191)	(0.421)	Mir	
							0.399	32.4	4.214	(0.024)	(0.994)	(2.455)	(0.421)	Al	
							0.446	32.1	4.176	(0.012)	(0.997)	(1.218)	(0.422)	Mir	
							0.514	32.4	4.217	(0.021)	(0.994)	(2.138)	(0.421)	Al	
							0.560	32.1	4.176	(0.014)	(0.996)	(1.468)	(0.422)	Mir	
							0.638	32.5	4.220	(0.024)	(0.994)	(2.432)	(0.421)	Al	
							0.675	32.1	4.175	(0.009)	(0.997)	(0.975)	(0.422)	Mir	
							0.744	32.5	4.224	(0.021)	(0.994)	(2.118)	(0.421)	Al	
							0.793	32.1	4.175	(0.022)	(0.994)	(2.195)	(0.421)	Mir	
							0.857	32.5	4.227	(0.015)	(0.996)	(1.506)	(0.422)	Al	
							0.905	32.1	4.175	(0.009)	(0.997)	(0.976)	(0.422)	Mir	
							0.974	32.6	4.230	(0.018)	(0.995)	(1.799)	(0.422)	Al	

( ) points in parentheses are less reliable.

Table V *Continued*

ROCK PARAMETERS							SHOCK PARAMETERS								
Rock	Shot No.	Specimen Dimensions	Detonation Velocity (mm/μs)	Explosive Type	Explosive Thickness (in.)	Specimen Density (g/cc)	Depth in Rock (in.)	Shock Angle α (deg)	Shock Velocity U (mm/μs)	Particle Velocity u (mm/μs)	Ratio ρ_0/ρ	Stress σ (kb)	Volume (cc/g)	Mirror	Notes
Spergen Limestone	8142 (Cont.)	A = 20.0° a = 3.9° b = 5.1° c = 11.9°	7.880	Comp B	0.25	2.360	1.082	22.1	4.175	(0.682)	(0.984)	(2.196)	(0.421)	Mir	First wave
							1.088	22.6	4.234	(0.688)	(0.995)	(2.288)	(0.422)	Al	
							1.136	22.1	4.174	(0.687)	(0.985)	(1.789)	(0.421)	Mir	
							1.188	22.6	4.237	(0.688)	(0.991)	(0.886)	(0.422)	Al	
							1.251	22.1	4.174	(0.684)	(0.984)	(1.468)	(0.423)	Mir	
							1.317	22.7	4.241	(0.681)	(0.997)	(1.103)	(0.422)	Al	
							1.384	22.1	4.174	(0.682)	(0.997)	(1.288)	(0.423)	Mir	
							1.436	22.7	4.244	(0.687)	(0.998)	(1.766)	(0.422)	Al	
							1.479	22.1	4.174	(0.682)	(0.997)	(1.222)	(0.423)	Mir	
							1.540	22.7	4.247	(0.688)	(0.997)	(0.879)	(0.422)	Al	
							1.591	22.1	4.173	(0.682)	(0.997)	(1.222)	(0.423)	Mir	
							1.664	22.7	4.251	(0.684)	(0.998)	(1.458)	(0.422)	Al	
							1.708	22.1	4.173	(0.699)	(0.997)	(0.979)	(0.423)	Mir	
							1.739	22.6	4.234	(0.684)	(0.994)	(1.433)	(0.423)	Al	
							1.805	22.6	4.238	(0.682)	(0.992)	(1.189)	(0.424)	Al	
							0.461	22.9	3.864	(0.951)	(0.891)	(69.339)	(0.293)	Al	Second wave
							0.521	22.8	2.953	(1.886)	(0.653)	(72.897)	(0.277)	Al	
							0.597	20.2	2.717	0.570	0.791	37.853	0.335	Al	
							0.701	19.4	2.614	0.632	0.758	39.638	0.322	Al	
							0.788	19.2	2.589	0.587	0.886	38.732	0.342	Mir	
							0.888	18.2	2.484	0.417	0.888	36.797	0.353	Al	
							0.922	18.2	2.455	0.486	0.804	28.966	0.341	Al	
							1.079	17.1	2.389	0.388	0.572	16.940	0.369	Mir	
							1.088	16.8	2.281	0.304	0.836	15.128	0.371	Al	
							1.188	16.3	2.388	0.272	0.879	14.740	0.372	Mir	
							1.217	16.0	2.189	0.238	0.886	13.369	0.375	Al	
							1.365	15.2	2.078	0.215	0.889	12.388	0.377	Al	
							1.363	15.4	2.094	0.199	0.987	10.448	0.384	Mir	
							1.467	14.5	1.973	0.195	0.988	9.535	0.383	Al	
							1.475	14.8	2.011	0.169	0.918	8.670	0.389	Mir	
							1.513	14.0	1.906	0.221	0.881	11.246	0.373	Al	
							1.688	14.1	1.924	0.136	0.931	6.899	0.394	Mir	
							1.701	13.4	1.825	0.210	0.888	9.852	0.376	Al	
							1.739	13.5	1.839	0.123	0.932	5.379	0.395	Al	
Spergen Limestone	8252	A = 20.0° a = 2.9° b = 5.0° c = 11.8°	7.993	Comp B	1.00	2.381	0.102	33.2	4.381	1.292	0.705	134.816	0.296	Al	Precursor not readable at this magnification
							0.182	32.6	4.310	1.303	0.697	133.753	0.293	Al	
							0.241	32.1	4.259	1.107	0.739	112.353	0.310	Al	
							0.312	31.6	4.199	0.997	0.762	99.727	0.320	Al	
							0.388	31.0	4.123	1.113	0.730	109.380	0.306	Al	
							0.467	30.4	4.056	1.146	0.717	110.724	0.301	Al	
							0.568	29.9	3.992	1.176	0.705	111.837	0.296	Al	
							0.648	29.4	3.932	1.164	0.703	109.050	0.295	Al	
							0.727	28.9	3.873	1.168	0.698	107.806	0.293	Al	

( ) points in parentheses are less reliable.

Table V Concluded

ROCK PARAMETERS							SHOCK PARAMETERS								
Rock	Shot No.	Specimen Dimensions	Detonation Velocity (mm/µs)	Explosive		Specimen Density (g/cc)	Depth in Rock (in.)	Shock Angle α (deg)	Shock Velocity U (mm/µs)	Particle Velocity u (mm/µs)	Ratio ρ_0/ρ	Stress σ (kb)	Volume (cc/g)	Mirror	Notes
				Type	Thickness (in.)										
Spergen Limestone	8252 (Cont.)	A = 30.0° a = 2.9° b = 5.0° c = 11.8°	7.993	Comp B	1.00	2.381	0.811	28.4	3.812	1.214	0.481	110.280	0.306	Al	Precursor not readable at this magnification
							0.879	28.0	3.764	1.044	0.722	93.587	0.303	Al	
							0.937	27.7	3.724	0.747	0.799	64.296	0.335	Al	
							1.035	27.2	3.680	0.984	0.730	85.759	0.306	Al	
							1.122	26.7	3.602	1.062	0.704	91.167	0.296	Al	
							1.186	26.4	3.361	0.744	0.779	66.534	0.327	Al	
Spergen Limestone	8268	A = 27.0° a = 2.9° b = 5.0° c = 11.9°	7.235	Sheet (EL506D)	0.064	2.398	0.120	42.8	4.9[illegible]	0.061	0.989	6.085	0.412	Al	First wave
							0.130	36.5	4.311	0.021	0.995	2.211	0.415	Mg	
							0.2[illegible]	42.3	4.[illegible]	0.021	0.995	2.540	0.415	Al	
							0.257	36.7	4.339	0.029	0.993	3.079	0.414	Mg	
							0.314	41.5	4.[illegible]	0.025	0.994	2.093	0.414	Al	
							0.366	36.9	4.346	0.023	0.994	2.4[illegible]	0.415	Mg	
							0.4[illegible]	40.9	4.73[illegible]	0.021	0.995	2.497	0.415	Al	
							0.477	37.0	4.3[illegible]	0.026	0.994	2.737	0.415	Mg	
							0.534	40.2	4.672	0.029	0.993	3.361	0.414	Al	
							0.5[illegible]	37.2	4.3[illegible]	0.022	0.994	2.387	0.415	Mg	
							0.6[illegible]	39.5	4.6[illegible]	0.027	0.993	3.[illegible]72	0.414	Al	
							0.6[illegible]	37.4	4.396	0.0[illegible]	0.995	2.195	0.415	Mg	
							0.721	38.9	4.548	0.0[illegible]	0.993	3.135	0.414	Al	
							0.7[illegible]	37.6	4.414	0.022	0.994	2.4[illegible]	0.415	Mg	
							0.8[illegible]	38.3	4.[illegible]	0.029	0.993	3.178	0.414	Al	
							0.904	37.7	4.4[illegible]	0.0[illegible]	0.995	2.238	0.415	Mg	
							0.9[illegible]	37.8	4.426	0.017	0.995	3.[illegible]92	0.415	Al	
							1.0[illegible]	37.9	4.447	0.015	0.996	1.682	0.416	Mg	
							1.072	37.2	4.374	0.025	0.994	2.0[illegible]	0.415	Al	
							1.115	36.1	4.464	0.017	0.996	1.[illegible]	0.415	Mg	
							1.177	36.6	4.3[illegible]	0.023	0.994	2.461	0.414	Al	
							1.2[illegible]	38.2	4.[illegible]	0.021	0.995	2.201	0.415	Mg	
							1.2[illegible]	36.1	4.2[illegible]	0.021	0.995	2.172	0.415	Al	
							1.3[illegible]	38.4	4.[illegible]	0.019	0.995	2.157	0.415	Mg	
							1.3[illegible]	36.5	4.397	0.023	0.994	2.3[illegible]	0.415	Al	
							1.4[illegible]	38.0	4.517	0.017	0.996	1.876	0.415	Mg	
							1.4[illegible]	36.9	4.15[illegible]	0.0[illegible]	0.993	2.0[illegible]	0.414	Al	
							1.5[illegible]	38.[illegible]	4.[illegible]	0.0[illegible]	0.995	2.1[illegible]	0.415	Mg	
							1.6[illegible]	39.0	4.[illegible]	0.018	0.995	2.030	0.415	Al	
							1.74[illegible]	33.9	4.[illegible]	(0.061)	(0.984)	(5.9[illegible])	0.410	Mg	
							1.785	39.2	4.574	(0.035)	(0.992)	(3.040)	(0.414)	Mg	
							0.176	10.0	1.364	(0.074)	(0.966)	(4.175)	(0.380)	Mg	Second wave
							0.176	10.0	1.2[illegible]	(0.133)	(0.9[illegible])	(5.0[illegible])	(0.377)	Mg	
							0.2[illegible]	10.9	1.373	(0.104)	(0.9[illegible])	(5.4[illegible])	(0.3[illegible])	Al	
							0.270	7.1	0.[illegible]	(0.114)	(0.8[illegible])	(4.4[illegible])	(0.371)	Al	
							0.275	6.9	0.874	(0.150)	(0.851)	(5.812)	(0.355)	Al	

( ) points in parentheses are less reliable.

Table VI

SUMMARY OF DATA FOR PLANE WAVE SHOTS

ROCK	SHOT NO.	GEOMETRY	EXPLOSIVE P-60 *	ALUMINUM			ROCK							NOTES
				Free-Surface Velocity (mm/μs)	Shock Velocity (mm/μs)	Stress σ (kb)	Free-Surface Velocity (mm/μs)	Shock Velocity (mm/μs)	Particle Velocity (mm/μs)	Stress σ (kb)	Ratio (ρ_0/ρ)	Density (g/cc)	Volume (cc/g)	
Arkansas Novaculite	8238	Plane-wave beveled pellet	none	1.188	--	103	1.064†	5.88		82.6	0.9098	2.648	0.3435	ρ_1 = 2.91
	8270	Plane-wave beveled pellet	none	(1.685)	--	151	1.141	3.118	0.660	92	0.864	2.648	0.3262	
							(1.745)	6.480	0.5705	96.7	0.9109	2.648	0.3440	ρ_1 = 2.907 u_f doubtful
	8272	Plane-wave beveled pellet	2* Comp B	(2.672)	(6.923)	(265)	--	3.87	0.940	135	0.836	2.648	0.314	
								6.375	--	--	--	2.648	--	
								(4 70)	(1.56)	(214)	(0.492)	2.648	0.2612	Poor value
Sioux Quartzite	7695	Plane-wave wedge	none				2.40	6.20	1.415	231	0.772	2.64	0.292	Best record of precursor development
Cocconino Sandstone	8131	Plane-wave beveled pellet	none	1.178	--	102	--	>(2.96)	--	--	--	2.00	--	Lucite cutoff ragged
							1.381	2.793	0.875	48.5	0.6867	--	0.363	Information from beveled edge not used
	7842	Plane-wave wedge	none	(1.50)	--	(110)	1.405	3.11	1.09	67	0.652	1.97		
	7861	Plane-wave pellet	none	(1.54)		(118)	1.51	3.042	(0.75)	68.5	0.631	1.975		
	17715	Plane-wave pellet	1* T.N.T.	(2.52)	--	--	2.71	(3.85)	(1.74)	143	0.548	(2.00)	(0.274)	⊥ to bedding§
	7716	Plane-wave pellet	1* T.N.T.	(2.33)	--	--	(3.38)	(3.85)	(1.64)	125	0.574	--		∥ to bedding§
	7809	Plane-wave wedge	1* Comp B	2.56	(7.54)	--	(3.50)	4.26	1.75	146	0.589	1.96	0.300	Stops in aluminum low
	8164	Plane-wave wedge	2* Comp B	2.93	(7.45)	298	(3.99)	4.29	1.995	171	0.528	2.00	0.264	Only u_f used to obtain stress in driver
Yule Marble	8281	Plane-wave pellet	none	1.195	--	103	1.374	5.5-	0.6+	89+	0.987	2.695		Pellet 1 is ∥ to optic axis; pellet 2 is ⊥
							1.289	4.46	0.715	80.5		2.695	0.3123	Shock velocities equal but u_f different
	8280	Plane-wave beveled pellet	none	1.579	--	140	(1.6)	5.45	0.8+	118	0.9853	2.695	0.366	
							1.619	4.91	0.890	119	0.822	2.695	0.305	
	7785	Plane-wave wedge	1* Comp B	(2.89)	(6.64)	--	--	(5.52)	(1.17)	(176)	(0.788)	2.70	(0.292)	Wave tilt not observed
	7786	Plane-wave wedge	1* Comp B	--	(7.03)	--	--	(5.83)	(1.12)	(177)	(0.8081)	2.70	(0.299)	Wave tilt not observed. Displaced trace poor
	8317	Plane-wave wedge	2* Comp B	(2.870)	7.333	292	2.188	5.91	1.590	253	2.7307	2.695	0.2709	Two mirror system
Spargon Limestone	8150	Plane-wave beveled pellet	none	1.161	--	100	--	>4.7	--	--	--	--	--	Ragged Lucite cutoff
							1.294	3.38	0.789	62	0.7668	2.364	0.3241	
	8075	Plane-wave beveled pellet	none	1.51	--	--	--	--	--	--	--	--	--	Poor cutoff on inclined mirror
							1.46	3.94	0.965	90	0.755	2.372	0.318	
	8681	Plane-wave wedge	none	1.54	6.-	--	1.32	3.797	1.01	91	0.734	2.372	0.309	
	8271	Plane-wave beveled pellet	none	1.587	-	141	--	(4.42)	--	--	--	--	--	
							1.360	4.11	1.020	96.5	0.7517	2.364	0.3180	Beveled edge shows attenuation
	8079	Plane-wave pellet	none	1.51	--	136	1.46	3.94	0.965	90	0.755	2.372	0.318	
	8080	Plane-wave beveled pellet	1* Comp B	2.67	--	--	(2.20)	5.21	1.62	201	0.689	2.367	0.291	
							--	--	--	--	--	--	--	u_f poor
	8165	Plane-wave beveled pellet	2* Comp B	2.942	(7.704)	298	--	--	--	--	--	--	--	
							2.60	5.23	1.790	221	0.6575	2.364	0.2781	

* Inclined mirror measurement

( ) points in parentheses are less reliable

† Wedge measurement

§ Poor free-surface velocity on aluminum, curved wave arrival from T.N.T.

There is one area of agreement. Data from the two-dimensional shot, 8318, and plane-wave shots on marble and limestone agree with data by Adadurov, *et al.*[8] (Figs. 25 and 26).

2. There is evidence for both yield and phase transitions in the carbonates. All of the data records at least one break in the stress-particle velocity curve with two breaks occurring for one marble and one limestone experiment. The first break is recorded at 28 kilobars in calcite, 21 and 12 kilobars in marble, and 3 kilobars in limestone. This indicates that the first break is a yield transition that may sometimes be influenced by phase transitions. The second break occurs at

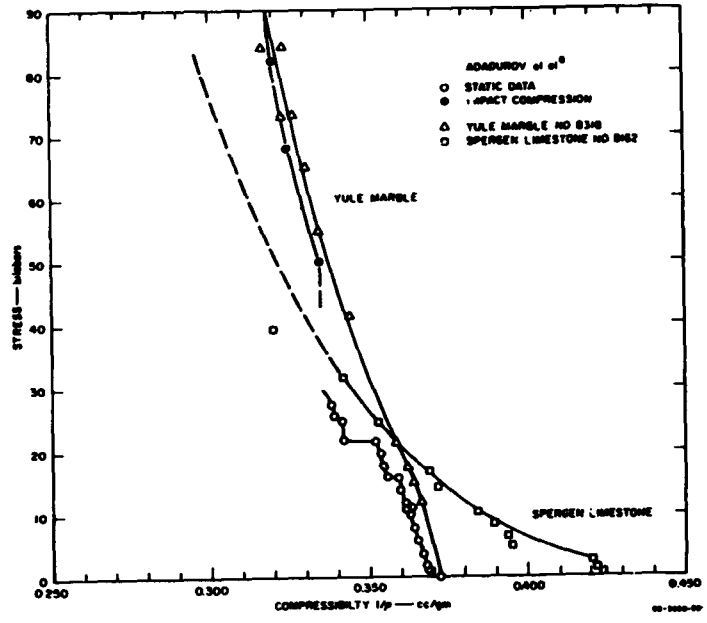

FIG. 25 HUGONIOT FOR CARBONATE ROCKS

about 30 kilobars (data from the limestone experiment is less reliable) and is probably a phase transition. The phase transition reported at 150 kilobars by Adadurov, *et al.*,[8] is also indicated in the above experiments by a break in the Hugoniot curve at about 150 kilobars.

Additional evidence for yield is found in some of the recovered samples of Yule marble. The stress produced in the sample was 100 kilobars or less and an examination of thin sections from the sample showed that the number of twin planes in the individual crystals doubled. This yield mechanism in calcite is not completely understood in detail but has been studied extensively by Turner, *et al.*[9,10]

3. Porosity plays a major role in determining the velocity with which the first wave propagates, Fig. 20. The propagation velocity of the first wave in the marble, porosity 0.75 percent, is greater than the velocity of the first wave in limestone, porosity 15 percent.

4. The peak stress amplitude of the first wave is dependent upon the porosity. Figure 21 shows that the peak stress is quite sensitive to porosity for the first few percent. It is possible that one of the parameters that controls porosity plays a major role in the relationship but it is uncertain which one. The porosity in the marble and limestone is primarily the result of chemical processes involved in metamorphism and diagenesis and has little relation to the original porosity of the rock. Relationships of porosity to other rock parameters in this situation are not understood as well as in the quartz rocks.

Until more information is available, the peak stress amplitude will be assumed to be a function of porosity only.

5. The grain size of the rock has little influence on the shock wave parameters. There is no correlation of the peak stress or first wave velocity with grain size. The grain size may determine the rise time of the shock wave but no data are available to support this idea.

A comparison between Shot 7997 and 8318 in Yule marble makes the discussion above somewhat uncertain. The problem is that 8318 is a shot in which the C-axis of the calcite grains were parallel to the ray path of the detonation front; Shot 7997 was not, but the exact orientation is not known. Since the sound velocity is slower along the C-axis in calcite, the first wave velocity in 8318 should be less than that in 7997. It is not, however, and the reason for the discrepancy is not understood. Shot 8279 covered such a small pressure range that it is neglected on some of the figures.

APPENDIX A

PETROGRAPHIC DESCRIPTIONS

APPENDIX A

PETROGRAPHIC DESCRIPTIONS

The following rocks were used in the experiments.

ARKANSAS NOVACULITE

Arkansas novaculite is a formation name for a novaculite-shale sequence of Devonian age and also a trade name. The formation is found in southwestern Arkansas and southeastern Oklahoma.

The Arkansas novaculite is a white to gray-white, microcrystalline quartz rock composed of 100 percent quartz grains. Sometimes differences in color and banding are present indicating a possible layering.

The average grain size is 0.01 mm in diameter with occasional grains 0.05 mm in diameter. The surfaces of the individual grains have a curved appearance characteristic of the novaculite-type rocks." A powder X-ray diffraction pattern was made (Fig. 26) from a sample of the rock and was identical with a pattern made from alpha-quartz. The orientation of the grains is assumed to be random. This has almost always been the case from X-ray diffraction analysis."

No porosity was observed in a thin section. The density of the novaculite is 2.649 g/cc. This also adds evidence that the rock is a pure quartz rock with at most a porosity of a few tenths of a percent if there is no water included in the rock. Some novaculite contains included water If so, the amount of water will determine the decrease in density from that of pure quartz, 2.653 g/cc. The rock is well cemented. No quartz overgrowths or pore filling was detected.

Some of the novaculite was recovered from one of the experiments in which pressures of less than 100 kilobars were generated. A study of the thin section shows no observable difference from material studied before the experiment.

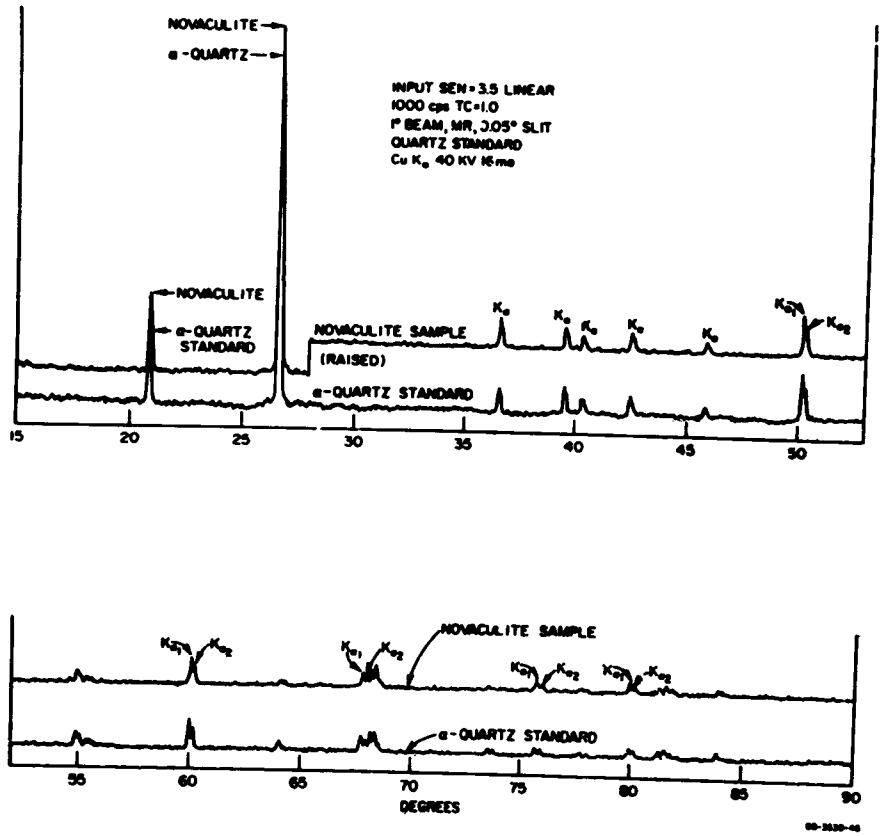

FIG. 26 X-RAY DIFFRACTION PATTERN OF ARKANSAS NOVACULITE

COCONINO SANDSTONE

This formation is in the Aubrey group and is Permian in age. The sandstone is found in northern Arizona, southern Utah, and southeastern Nevada.

The following description is taken from a personal communication from H. J. Moore[8] and agrees with the results from samples that were used in this series of experiments.

The Coconino sandstone "is a laminated, yellowish gray, weakly cemented, fine-grained sandstone composed of about 97 percent quartz, 3 percent feldspar" (microcline and orthoclase), "and a fraction of a percent of clay and heavy minerals."

"Average and modal grain size of the sandstone is between 0.117 and 0.149 mm in diameter; the grains," which are sub-rounded, "range from less than 0.062 to 0.71 mm across." Subparallel laminae 5.0 to 17.5 mm thick are separated by thin laminae 0.5 mm thick containing more than average amounts of silt and clay-sized grains. The bulk density, measured from rectangular-sawed blocks, is 2.26 g/cc;" but ranges to 2.06 g/cc; "the grain density is 2.67 g/cc, and the calculated porosity is 15 to 25 percent. The sandstone is only weakly to moderately-well cemented with silica, mainly in the form of quartz overgrowths on the sand grains." (About 20 percent of the quartz grains have the overgrowths. The individual overgrowth has a different optic orientation than the grain itself.) "Some laminae can be disaggregated with finger pressure. Unconfined crushing strengths measured perpendicular to the bedding of three 2.2 cm by 2.2 cm by 5 cm blocks under load applied in the long direction were 320 and 371 kg/cm^2 for water free specimens."

The plot of the c-axis of quartz grains (Fig. 27) shows that the axes are primarily parallel to the plane of the bedding and are grouped in either of two directions.

Using the classification of pure sandstones (Fig. 28) by Gilbert,[9] the Coconino sandstone can be considered as an "end member" and would be termed a quartz arenite.

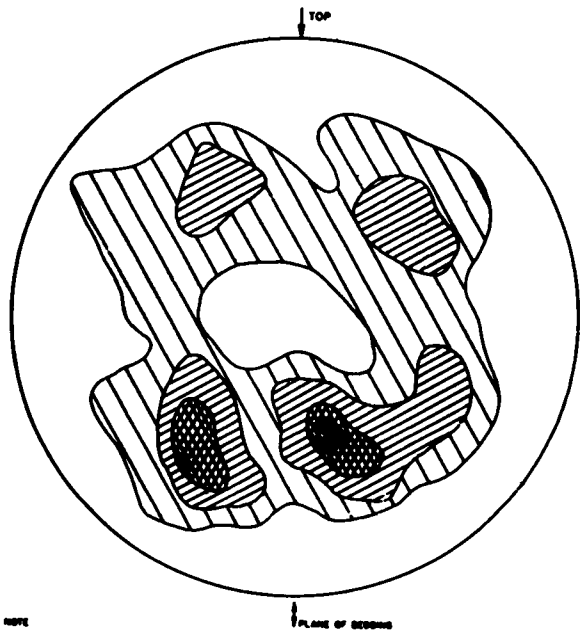

FIG. 27 FABRIC ORIENTATION OF COCONINO SANDSTONE

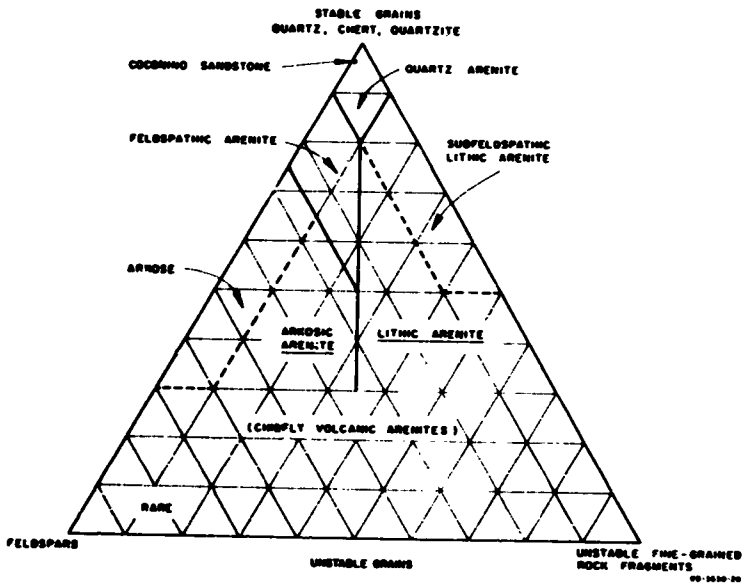

FIG. 28 CLASSIFICATION OF PURE SANDSTONES

EUREKA QUARTZITE

This formation is middle Ordovician in age and is found in northern Nevada, western Utah, and Inyo county, California.

The Eureka quartzite is a massive, white, fine grained, quartzite composed of about 98 percent quartz, and a percent or two of orthoclase feldspar.

The grain size ranges from 0.05 mm to 0.5 mm and the average grain size is 0.1 mm to 0.2 mm in diameter. The grains are sub-angular. The rock is strongly cemented by pore fillings and grain contacts. No secondary quartz overgrowths were present. The quartzite contains occasional fractures that are cemented with silica.

The porosity is less than 1 percent.

The plot of the c-axis of the quartz grains (Fig. 29) shows that the c-axes lie in two broad bands. This is probably a relic bedding rather than a result of any metamorphism. The degree of mineral alignment in the quartzite did not seem to affect the results of the experiments with the rock.

The quartzite can be considered an "end member" and would be called an orthoquartzite.

SPERGEN LIMESTONE

Indiana limestone or Indiana marble is the trade name for the Spergen limestone. This formation belongs to the Meramec group, is Missis ippian in age and is found in southern Indiana. The formation was called the Bedford limestone but is now termed the Spergen limestone by U.S. Geological Survey. The Indiana and Illinois Geological Surveys use the term Salem limestone.

The Spergen limestone is a gray, well cemented, microcoquina composed of about 60 percent fossil fragments, 20 percent bioclastic debris including carbonate detritus, 20 percent calcite and a percent or two of oolites. The fossil debris is composed primarily of bryozoan fragments together with complete tests of Foraminifera (Endothyra). Some brachiopod and crinoid fragments are also present.

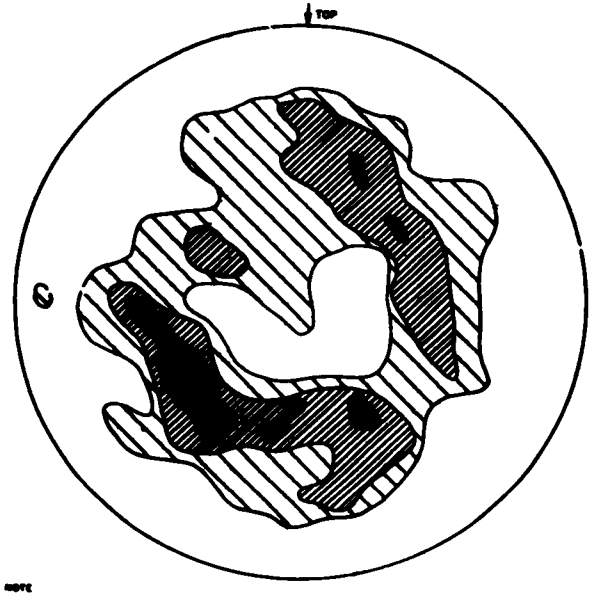

NOTE
PLOT OF 222 C-AXIS OF QUARTZ GRAINS IN THE EUREKA QUARTZITE
CONTOURS ARE 1 3, 2 7, 4 0 PERCENT PER ONE PERCENT AREA

FIG. 29 FABRIC ORIENTATION OF EUREKA QUARTZITE

The size of the sub-rounded fragments range from 0.1 mm to 0.7 mm with the average size being about 0.3 to 0.4 mm in diameter. The average grain size of the void filling calcite is 0.2 to 0.3 mm in diameter with an occasional grain as large as 1.0 mm in diameter.

The calcite grains tend to have a "sub-poikiloblastic" texture. Some of the bioclastic fragments, which are included in the grains of cementing calcite have the same optic orientation as the neighboring calcite grains.

The porosity is about 12 percent. The density ranges from 2.360 to 2.398 g/cc.

The plot of the c-axis of the calcite grains and fossil detritus shows that there is no marked anisotropy of the fabric (Fig. 30).

According to the classification by Pettijohn,[14] the rock would be an "end member" and called an encrinite or microcoquina (Fig. 31).

SIOUX QUARTZITE

The Sioux quartzite is Pre-Cambrian and is found in southeastern South Dakota, southwestern Minnesota, northwestern Iowa, and northeastern Nebraska.

The Sioux quartzite is a reddish, massive rock with no indication of bedding. The rock is composed of 99 percent quartz and less than one percent of clinozoisite and tourmaline. The clinozoisite and tourmaline are inclusions in the individual quartz grains. About 3 percent of the grains are composed of a fine-grained quartz.

The rounded grains range in size from 0.1 mm to 1.0 mm and the average size is 0.6 mm. The rounded grains have a quartz overgrowth. The rounded grains are outlined by a fine hematite dust between the grain and the overgrowth.

The porosity is less than 1 percent. The rock is strongly cemented by the quartz overgrowths.

The rock fabric was not studied.

The rock would be termed an orthoquartzite.

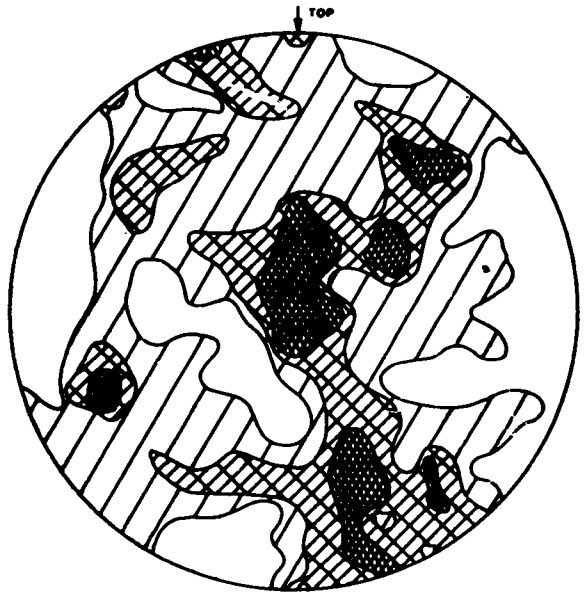

NOTE:
PLOT OF 216 C-AXIS OF CALCITE GRAINS IN THE SPERGEN LIMESTONE
NO DISTINCTION WAS MADE BETWEEN GRAINS OF CEMENT AND GRAINS OF FOSSIL DETRITUS
CONTOURS ARE 0.9, 1.8, 2.8 PERCENT PER ONE PERCENT AREA

FIG. 30 FABRIC ORIENTATION OF SPERGEN LIMESTONE

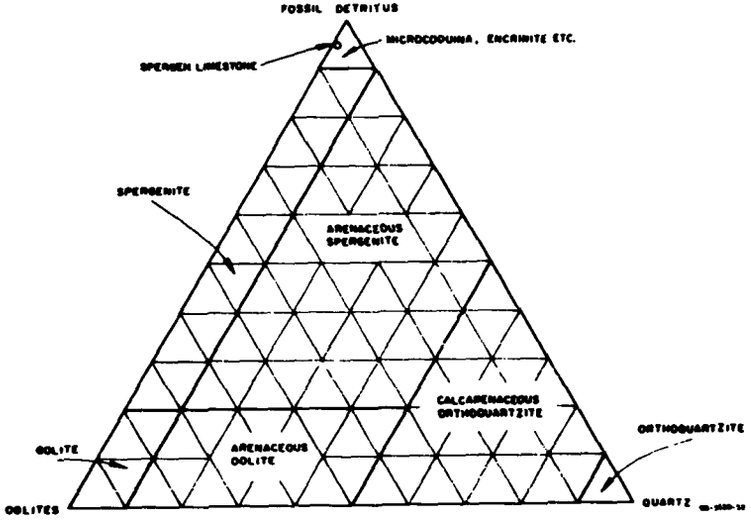

FIG. 31 CLASSIFICATION OF CALCARENITES

YULE MARBLE

The Yule marble is a trade name for the marble quarried from the metamorphosed Leadville limestone in Gunnison county, Colorado. The Leadville limestone is Mississippian in age.

The Yule marble is a massive, white, homogeneous marble that is composed of 100 percent calcite.

The average grain size of the marble is between 0.2 mm and 0.4 mm with an occasional grain as large as 1.5 mm in diameter (apparent grain size in the thin section depends upon orientation as the grains are platy).

The porosity is 0.75%. The c-axis of the calcite grains are grouped about the vertices of a triangle (Fig. 32) and the specimens used in the experiments were cut with respect to the orientation of the maximum concentration of the c-axis of the grains.

Some samples were recovered from an experiment in which the pieces probably were at shock pressures of less than 50 kilobars. A study of the thin sections shows that there is an increase in the number of twin lamellae and that the twin lamellae seem to be at a different spacing than before the experiment. The distance between the twin lamellae created from the shock pressure is much less than the distance between many of the lamellae in samples before the experiments. An approximate number of twins per grain before the experiment is about 3 with a range of 0 to 5. An approximate number of twins per grain after the experiment is about 7 with a range of 4 to 10.

All descriptions of the rocks were obtained by observing hand specimens and studying orientated thin sections under the petrographic microscope. The accuracy of the points used in constructing the equal area nets is 5 percent and occasional checks were made by repeating observations. The study of the mineral orientation of the rocks had a twofold purpose:

1. The presence and the degree of mineral orientation in the samples might affect the interpretation of the results.
2. Once the direction of mineral alignment is known, the specimens used in the experiments can be oriented to determine the effect of the mineral alignment.

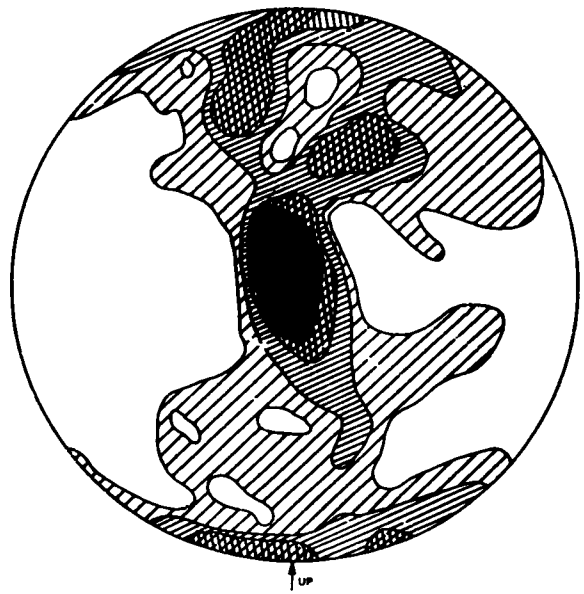

NOTE
PLOT OF 302 C-AXIS OF CALCITE GRAINS IN THE YULE MARBLE
CONTOURS ARE 1, 2, 3, 5 PERCENT PER ONE PERCENT AREA

FIG. 32 FABRIC ORIENTATION OF YULE MARBLE

APPENDIX B

SAMPLE TESTING AND PREPARATION

APPENDIX B

SAMPLE TESTING AND PREPARATION

BULK DENSITY

A sample from each rock was cut into a parallelpiped with a rotary diamond saw. The sample was then baked at 120°C until its weight reached a steady state. While dry, it was weighed and measured. The bulk density could then be computed to a precision of ±¼ percent. The main source of error was uncertainty in the sample volume caused by chipping of edges while sawing the rock.

COMPOSITION

The composition of Arkansas Novaculite was determined by X-ray diffraction. Optical examinations of thin sections were made of all rocks and fabric studies were made on all but the Sioux quartzite and Arkansas Novaculite. Yule marble and Spergen limestone were both more than 99 percent calcite. Arkansas novaculite, Sioux quartzite, and Eureka quartzite each contained more than 99 percent quartz and Coconino sandstone contained about 97 percent quartz. The observed impurities in the last three rocks were mostly feldspars.

CRYSTAL DENSITY

A volumetric density-determination of the average crystal density was made using the rock with the highest percentage of impurities, Coconino sandstone. Crystal density agreed with that of quartz within the expected experimental error of ±¼ percent. Average crystal densities of the other rocks should also be equal to the densities of their major constituents with this precision.

POROSITY

Porosity of all rocks were computed by the formula

$$\text{Porosity (\%)} = 100\,\frac{\rho_c - \rho_B}{\rho_c}$$

in which ρ_c is average crystal density and ρ_g is bulk density. Porosity of Coconino sandstone was also computed by comparing the weight of a water saturated sample of known volume with the weight of the same sample dried. The sample was saturated by evacuating air from its pores and submerging it in distilled water to which a wetting agent had been added. Then

$$\text{Porosity (\%)} = 100\,\frac{W - D}{V}$$

when W is wet weight in g, D is dry weight in g, and V is volume in cc. Porosity determined by this method was 23 percent, slightly less than the 26 percent value determined for the same sample by the crystal density method. A slight disagreement in this direction is expected since the water does not completely fill all pores.

The porosity of Coconino sandstone samples from two blocks averaged 25 percent. Porosity of Indiana limestone averaged 12 percent. Porosity of all other rocks was less than 1 percent.

WATER ABSORPTION

Dried samples of all rocks were allowed to stand in a room in which the humidity varied from 40 to 60 percent. These samples were weighed to 0.1 percent precision at intervals during the two days after drying. None of the rock samples changed weight sufficiently to indicate an appreciable absorption of water from the atmosphere. It is concluded that water absorption from the atmosphere probably did not affect the dried rocks used in the shock wave experiments.

SOUND VELOCITY

Transducer measurements of sound velocity were made on samples of each rock and on many of the pieces used in shock experiments. The apparatus has two ½-inch-diameter piezoelectric transducers mounted in 1-inch-diameter steel pistons in a press which will exert up to a 2250-lb force on the sample. Birch[15,16] observed that a unidirectional stress on a rock sample produced nearly the same effect on sound velocity, in the direction of the stress, as an equal hydrostatic stress. Dried rock samples were measured at the highest applied stress they could withstand so that the value of sound velocity would be nearer the value of precursor

velocity in shock experiments. Birch found that values of sound velocity of a rock at atmospheric pressure varied widely when measurements were made on different samples of the rock. This was also found to be true in our measurements. Velocity rose rapidly in most rocks as the first hundred atmospheres on different samples of a rock gave small scatter in sound velocities.

SAMPLE PREPARATION

Specimens used in shock experiments were sawed with a rotary diamond saw. The surfaces of the quartzites and novaculite which would be observed or would be attached to backing plates or to explosive slabs were then lapped. All rocks were then heated at 120°C until they were dry, i.e., until weight reached a steady state. The surfaces of the Yule marble and the porous rocks were ground, while dry, after they were heated.

All specimens were measured and weighed. Values of bulk density could be calculated to ±½ percent for large specimens. The same values were used for most of the small pellets which could not be measured within such small error.

CALCITE PREPARATION

The calcite specimens were cut from naturally occuring "Iceland spar" found in Chihuahua, Mexico. The pellets were usually about ¼ inch thick and about 1¼ inch on a side. Only crystals that were colorless, free from cleavage, partings and obvious defects were used. Four different orientations were cut. The designation of a particular cut means that the shock wave travels parallel to the designated crystallographic axis (Fig. 33). The cuts used were X, Y, Z, and cleavage. Thus a Z-cut crystal will be orientated such that the Z-crystallographic axis is perpendicular to the surface of the backing plate and the ray of the shock wavefront will travel parallel to the Z-crystallographic axis. A similar designation is used for the X and Y crystallographic directions. The designation of cleavage cut is used to indicate that the ray path of the shock wave traveled parallel to the $(01\bar{1}2)$ crystal plane.

The cleavage cut calcite was prepared by smoothing the proper faces of the calcite rhombehedron. The X, Y, and Z-cut calcite was prepared by orientating the rhombehedron by an analysis of the X-ray Laue pattern and cutting the proper thickness from the crystal. After the cuts were made

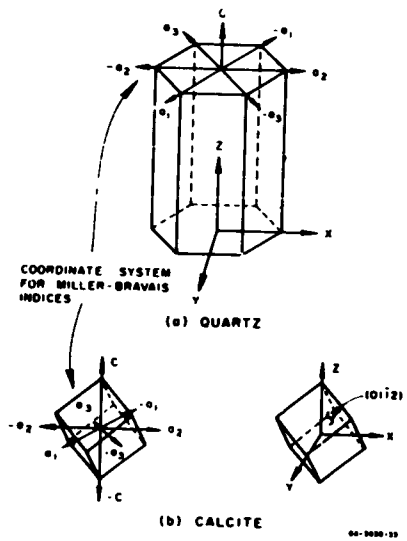

FIG. 33 COORDINATE SYSTEMS USED IN HEXAGONAL CRYSTALS

they were again checked by X-ray Laue patterns; and if necessary re finished until the orientation was within the proper tolerance.

TOLERANCES

The tolerances used in constructing the experiments are the following:

1. Crystal cuts within ±1 degree
2. Pellet surfaces plane within ±0.0002 inch
3. Backing plate within ±1.0 minute of arc.

APPENDIX C

PROGRAM FOR TWO-DIMENSIONAL WEDGE EXPERIMENTS

APPENDIX C

PROGRAM FOR TWO-DIMENSIONAL WEDGE EXPERIMENTS

Most of the experiments on this project used the wedge geometry and the optical lever arm recording method. Diagrams of experimental setups are shown in the previous section describing the experiments.

The detonation velocity is determined from a separate oscillographic record of the times at which the detonation front "connects" a series of electrical contacts.

The time and position coordinates of the wave-front arrival and position of the displaced trace are measured from the streak camera record. The measurements are made with a Vanguard Motion Analyser, Model 7½ W, which magnifies the 33 mm film approximately five times and contains screw-driven crosshairs for distance measurements. The over-all magnification is determined directly by measuring the image of a ruler included in the experimental setup.

Analysis of this data to derive equation of state points, using a desk calculator, might take several days, but the computer program described in this Appendix does it in a matter of minutes.

The basic equations for this analysis are the Rankine-Hugoniot relations, which relate normal stress σ, density ρ, and particle velocity ahead (u_0) and behind (u) a shock wave advancing at velocity U:

$$\sigma = \sigma_0 + 10\rho_0(U - u_0)(u - u_0) \qquad \text{(C-1)}$$

$$\frac{\rho_0}{\rho} = \frac{(U - u)}{(U - u_0)}$$

(As written here, the units are mm/μsec or km/sec for velocity, g/cc for density, kilobars (kb) for stresses. Subscript "0" refers to variable ahead of the shock and no subscript refers to the variable behind shock.)

Since the state ahead of the shock may be presumed known, these two equations contain four unknown quantities, σ, U, u, ρ, and if any two can be measured the other two may be calculated to give the state behind the shock. The optical lever arm recording method is designed to measure shock velocity U and particle velocity u.[4] Shock velocity is derived from the apparent velocity with which the break-out point of the shock front (discontinuities in traces, Fig. 12) moves across the film, i.e., from the slope of the dotted line in Fig. 12, and particle velocity from the distance the traces are displaced by the shock front.

In the balance of this Appendix the working equations for the analysis sketched above will be derived and the computer program which applies them will be described.

CURVE FITTING

To obtain the apparent velocity of the point of intersection of the shock front and wedge face from the record of Fig. 12, it is necessary to find the slope of a curve represented by a limited number of points (the dotted line). The merits of various schemes for accomplishing this are rather debatable and subject to a good deal of arbitrariness; some investigators sketch a line through the points with a French curve and approximate the tangent with a ruler, some prefer to use "smoothing formulas" such as those found in numerical analysis texts, which amount to replacing the experimental curve by short overlapping sections of polynomials, and some prefer to adjust the coefficients of various formulae to fit the data over a more-or-less wide range.

For this project the latter course was chosen, on the grounds of reproducibility, convenience, and adaptability to machine computation, and we fit (in the least squares sense) the shock arrival times t and positions x by a quadratic, $t = c_1 + c_2 x + c_3 x^2$. We chose to work with t a function of x, rather than vice-versa, because a single curved shock front can and sometimes does break through the surface at two different places at the same time but cannot break out at the same place at two different times; we chose a polynomial for simplicity and convenience, and a quadratic rather than a cubic because the cubic gave no noticeable improvement in most data (Fig. 34) and occasionally injected an inflection point amongst the data, leading to such unphysical results as calculated pressure increasing with greater distance from the explosive. The quadratic is

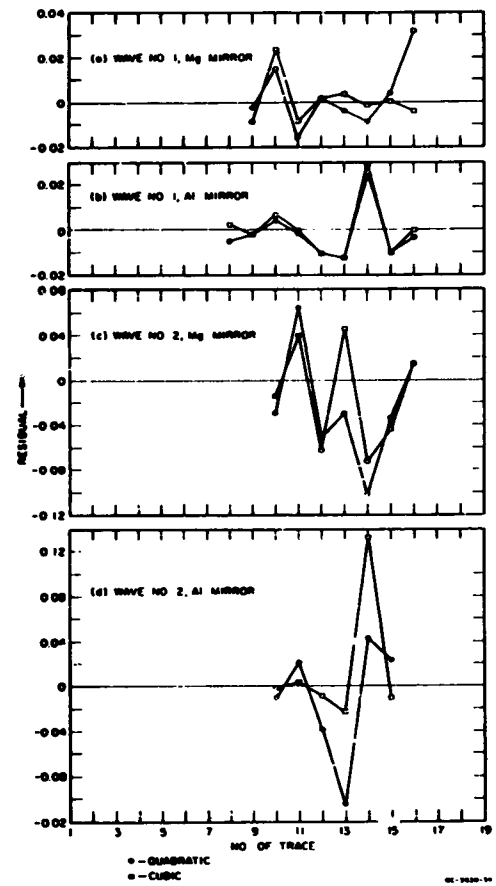

FIG. 34 PLOT OF RESIDUALS OF CUBIC AND QUADRATIC POLYNOMIALS

immune to this particular aberration, having no inflection point. The residuals of the fit are about the size of the errors to be expected in reading the film.

At first, there was a certain amount of worry from what seemed to be systematic bias in the curve fitting; frequently there would occur runs of as many as four or six consecutive points, out of perhaps twelve or sixteen, on the same side of the calculated curve. However, calculation shows that this is rather to be expected than not. For instance, the probability that four random errors will not all have the same sign is $1 - (1/2)^3 = 7/8$, but in a set of 10 points there are $10 - 4 + 1 = 5$ sets of four consecutive points, so the probability that none of these sets will be uniformly of the same sign is $(7/8)^5 = 16807/32768 = 51.3$ percent. The contrary probability, that there will be at least one run of four or more consecutive signs, is thus 48.7 percent. Fig. 35 compares the results of such calculations, assuming a total of 10 points in all cases, with the actually observed frequencies. There seem at first to be rather too many runs of six but this is because several shots had 16 or so points per wave. The striking lack of 5 point-long sequences is unexplained but not believed significant.

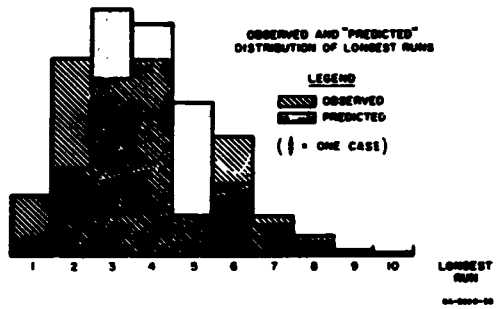

FIG. 35 OBSERVED AND PREDICTED DISTRIBUTION OF LONGEST RUNS

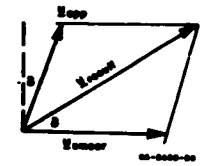

FIG. 36 SMEAR RECORD VELOCITY DIAGRAM

APPARENT VELOCITY

Fig. 36 shows how the motion of the breakout point along the wedge face (U_{app}) and of the image of the wedge face along the film (U_{smear}) combine to give a resulting motion (U_{result}) which corresponds to the tangent of the dotted line in Fig. 12. These two component motions are nominally at right angles, but actually the slit is usually tilted by a small angle δ(~0.5 deg), which can be measured from an image of the stationary slit exposed on the same film before the mirror of the smear camera begins to rotate.

Taking components parallel and perpendicular to U_{smear},

$$U_{result} \sin \phi = U_{app} \cos \delta$$

$$U_{result} \cos \phi = U_{smear} + U_{app} \sin \delta \quad .$$

from which

$$U_{app} = \frac{U_{smear}}{\cot \phi \cos \delta - \sin \delta} \qquad \text{(C-2)}$$

The parameter U_{smear} is evaluated from

$$U_{smear} = \text{screen inches/microsecond} \times \text{object inches/screen inches} \times \text{millimeter/inch} \qquad \text{(C-3)}$$

and $\cot \phi$ from the polynomial fit, $t = c_1 + c_2 x + c_3 x^2$, i.e.,

$$\cot \phi = \frac{dt}{dx} = c_2 + 2c_3 x' \qquad \text{(C-4)}$$

evaluated at the position of the displaced image, x'.

SHOCK VELOCITY

From Fig. 37(a),

$$U = U_0 \sin \alpha \quad , \qquad \theta = \alpha - A \quad , \tag{C-5}$$

where U_0 is the detonation velocity of the explosive. Figure 37(b) shows the shock front and wedge face at two successive instants, for the general case in which the wedge face has been set in motion by a preceding shock front. From this diagram,

$$\frac{U}{U_{app} + u_{f_0} \cot \theta} = \sin \theta \quad .$$

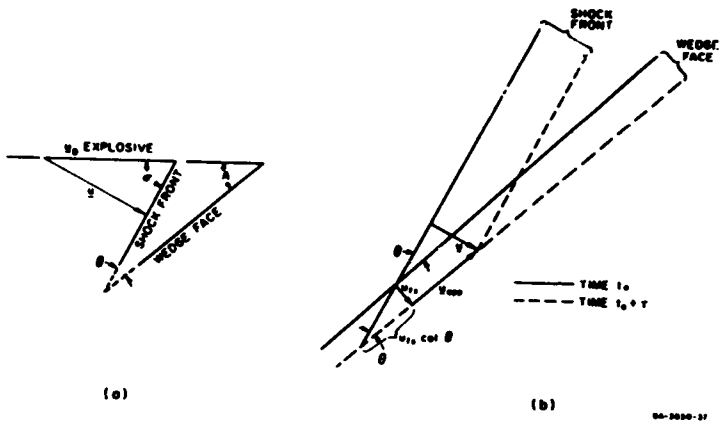

FIG. 37 SHOCK VELOCITY GEOMETRY

Combining this with Eqs (C-5),

$$\alpha = \arctan \frac{u_{f_0} - U_{app} \tan A}{\frac{U_0}{\cos A} + u_{f_0} \tan A - U_{app}} \quad . \tag{C-6}$$

The wedge angle A is measured before the shot is fired. U_0 is found from the time between electric contact of pairs of "pin" switches on the explosive slab, U_{app} is calculated as indicated in the preceding section, and u_{f_0} as in the next. Equations (C-5) and (C-6) are then used to calculate the shock angle α and shock velocity U.

PARTICLE VELOCITY

When a shock wave across which the particle velocity change is $\Delta u (= u - u_0)$ is incident on a free surface at an angle θ, it imparts to the free surface a velocity $\Delta u_{f_0} (= u_{f_0} - u_{f_0 0})$. Referring to Fig. 38(a), Δu_{f_0} is the vector sum of the changes in particle velocity across the incident and reflected shocks, Δu and Δu_r. By the free-surface approximation these are equal, $\Delta u = \Delta u_r$. Thus $\Delta u_{f_0} = 2 \Delta u p \cos \epsilon$. But $2(90° - \theta) + 2\epsilon + \beta = 180°$, so $\epsilon = \theta - \beta/2$ and $2 \cos \epsilon = 2 \cos (\theta - \beta/2) = 2 \cos \theta \sin \beta/2 + 2 \sin \theta \sin \beta/2 = 2 \cos \theta + \beta \sin \theta$, if β is small. Thus we get

$$\Delta u = \frac{\Delta u_{f_0}}{2 \cos \theta + \beta \sin \theta} \quad . \tag{C-7}$$

The change in free-surface velocity is calculated from the angle through which the wedge face is turned, which in turn is calculated from the displacement of the light source image, as follows [Fig. 38(a), (b), Fig. 12]

$$\Delta u_{f_0} = U_{app} \tan \beta \quad ,$$

$$\tan \beta = \frac{y}{2d} \quad , \tag{C-8}$$

$$y = \frac{x' - x}{I_L}$$

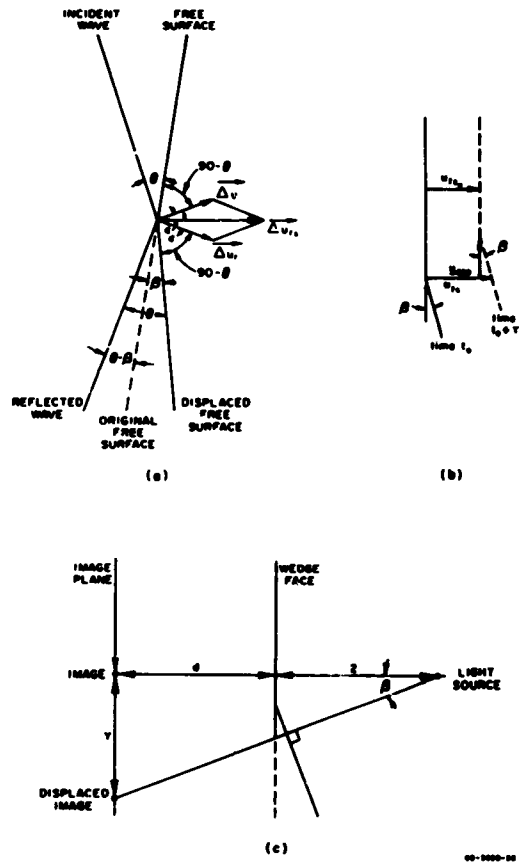

FIG. 38 PARTICLE VELOCITY GEOMETRY

where I_L is the magnification factor from light source to vanguard screen, I_L = screen distance true distance.

IMPEDANCE MATCH

If the method is to yield pressure data, the optical lever arm recording technique requires that the surface of the specimen remain a good reflector after the shock wave hits it. The rocks studied in this project do not meet this requirement, even with the best obtainable polish and a vacuum-deposited metallic reflecting surface. This problem was solved by attaching to the rock surface a 0.5-mm-thick strip of aluminum or magnesium with a highly polished outer surface. When a shock wave which produces a change in the dynamic state of the rock shown as U0 of Fig. 39, for example, strikes the interface, a shock is refracted into the mirror and another is reflected back into the rock. If the mirror does not fly off the surface, continuity at the interface requires that both refracted and reflected shocks reach the same terminal point C, which

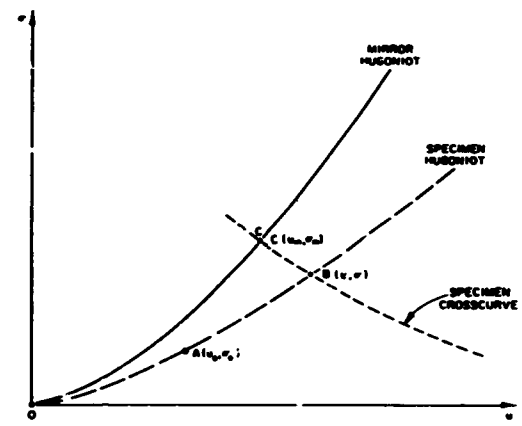

FIG. 39 IMPEDANCE MATCH DIAGRAM

therefore lies at the intersection of the mirror Hugoniot and the specimen cross curve (locus of states attainable by reflected waves) through state B. The final shock OC then propagates to the mirror surface, where it causes deflection of the light-source images and hence can be observed and calculated as outlined above.

(If the rock Hugoniot lies above the mirror Hugoniot, BC will be a rarefaction instead of a shock but the computations are the same.)

The state in the specimen behind the incident shock, B, could therefore be calculated as the intersection of the specimen's Hugoniot through A and its cross curve through C, if the latter two curves were already known. In other words we can calculate the Hugoniot of the rock if we know its Hugoniot and cross curve—but the cross curve is (for nonporous materials) the reflection of the Hugoniot about point B and the section AB of the Hugoniot can be approximated as a straight line whose slope is given by the jump condition, $\sigma = \sigma_0 + 10\rho_0(U - u_0)(u - u_0)$. State B is thus found by the intersection of this equation with $\sigma = \sigma_m - 10\rho_0(U - u_0)(u - u_m)$, i.e., by

$$u = \frac{1}{2}\left(u_0 + u_m + \frac{\sigma_m - \sigma_0}{H}\right) ,$$

$$\sigma = \frac{1}{2}\left[\sigma_0 + \sigma_m - H(u_m - u_0)\right] , \qquad \text{(C-9)}$$

where

$$H = 10\rho_0(U - u_0) .$$

U and u_m are the shock velocity in the specimen and particle velocity of the mirror, respectively, calculated from the film record as outlined in preceding sections, with a small correction to the angle θ between shock front and mirror surface to account for the change in direction of the shock at the specimen-mirror interface. Across the interface Snell's law applies

$$\frac{\sin\theta_m}{U_m} = \frac{\sin\theta}{U} .$$

with θ_m and U_m the shock angle and velocity in the mirror. Since $\sigma_m = 10\rho_m U_m u_m$, this may be written

$$\cos\theta_m = \sqrt{1 - \left(\frac{\sigma_m \sin\theta}{10\rho_m U u_m}\right)^2} . \qquad \text{(C-10)}$$

The pressure in the mirror, σ_m, is obtained from u_m by means of the (known) Murnaghan equation of state of the mirror material,

$$\sigma_m = A_m\left[(\rho_0/\rho_m)^{-\gamma} - 1\right] ,$$

where A_m and γ are known constants. Combining this with Eqs. (C-1) for the mirror material gives

$$\sigma_m\left[1 - \left(1 + \frac{\sigma_m}{A_m}\right)^{-1/\gamma}\right] - 10\rho_m u_m^2 = 0 , \qquad \text{(C-11)}$$

which must be solved for σ_m. This is done by the method of binary chopping, in which an interval in which the root is known to lie is successively halved until the root is located to three decimal places.

The over-all scheme of the impedance-match calculations, to sum up, is as follows: Shock velocity U is found from Eqs. (C-5) and (C-6) (this is the velocity appropriate to the specimen rather than the mirror since the travel time through the mirror is only a small fraction of the total travel time), particle velocity u calculated from Eqs. (C-7) and (C-8) is taken as a first approximation to u_m (*not exact because θ needs to be corrected for refraction*) and an approximate σ_m found from Eq. (C-11). These approximations are improved by use of Eqs. (C-10), (C-7), and (C-11) (the improvement could be iterated but the first cycle change is already small), and the state in the specimen behind the incident shock is calculated from Eq. (C-9).

MULTIPLE-SHOCK RECORDS

The analysis of the preceding section drastically oversimplifies the interactions arising when a multiple-shock system is incident on the rock-mirror interface. It is the purpose of this section to develop more fully the details of the interaction and to show that the simplification is

justified, subject to an easily tested relation among the time delay between the waves, the mirror thickness, and the sound speed in the mirror.

Figure 40(a) shows a two-wave system 0-1, 1-2, propagating through the rock toward the mirror. When the first wave, 0-1, strikes the interface it is reflected as 1-3 and refracted as 0-3 [Fig. 40(b)]. The stress-particle-velocity point behind shock 1-3 must lie *on the reflected rock* Hugoniot through point 1 (Fig. 41) and the state behind 0-3 must lie on the mirror Hugoniot through point 0; since these are the same state (required by continuity) the stress-velocity point is at the intersection of the curves, point 3 in Fig. 41. In Fig. 40(c), shocks 1-3 and 1-2 have collided and interpenetrated (*or reflected from each other*) to produce 3-4 and 2-4. By the same reasoning as above, state 4 in Fig. 41 lies at the intersection of the rock Hugoniot through 3 and the reflected rock Hugoniot through 2. Next the shock 0-3 is reflected from the free surface as a rarefaction 6-3 [Fig. 40(d)]. The velocity indicated for point 6 in Fig. 41 is *observed as a free-surface velocity and one calculates back* successively to points 3 and 1 as indicated in Fig. 41. At time E, [Fig. 40(e)] wave 3-4 passes into the mirror, producing 3-5 and 4-5. Next 3-5 and 3-6 interact in the mirror to produce 5-7 and 6-7 [Fig. 40(f)], 5-7 is reflected and refracted to form 7-8 and 5-8 [Fig. 40(g)], and 6-7 *reflects from the free surface as* 7-9 [Fig. 40(h)]. State 9 is observed at the mirror surface and calculations proceed to states 5 and 2. Shocks 7-8 and 7-9 continue to bounce back and forth in the mirror, crossing and recrossing to produce states 10, 11, 12, etc. Figure 42 shows the full system of shock waves in the time-position coordinate plane.

Figures 40, 41, 42 are drawn for the case where the time separation between the *original shocks, ΔT, is less than the "reverberation time,"* or time for a shock to travel across the mirror and back, τ. The important point is this: although material in the rock near the rock-mirror interface follows the path 0-1-3-4-5 8, material in the mirror near the interface follows 0-3-5-7-8, and material in the mirror near the free surface follows 0-3-6-7-9, the *final observed result* (states 6, 9, 12, etc.) is the same *as if* material in the rock had followed 0-1-2 while that in the mirror followed 0-3-6 and 0-5-9, and these latter paths are those assumed in the preceding derivation of the working equations for impedance-match calculations.

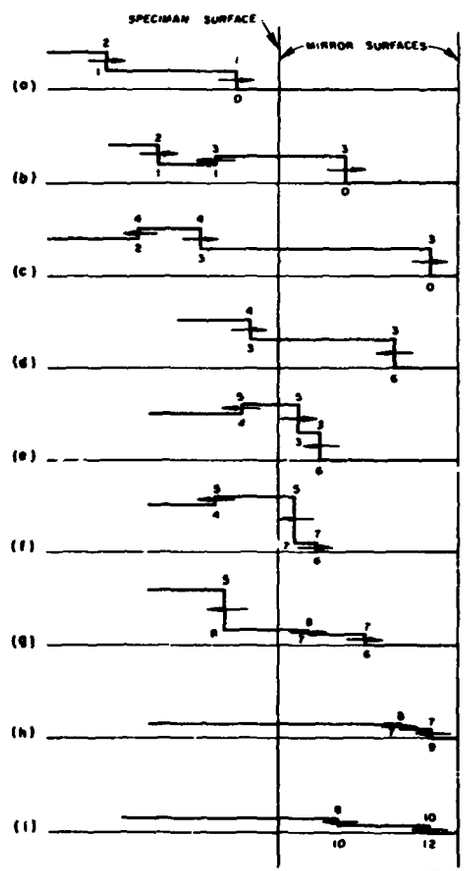

FIG. 40 STRESS PROFILE AT SELECTED TIMES $\Delta T < \tau$

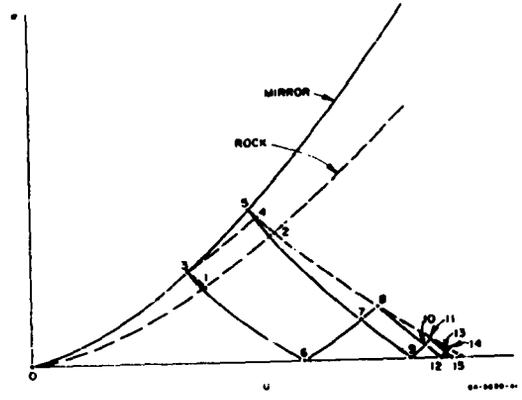

FIG. 41 STRESS-PARTICLE VELOCITY DIAGRAM, $\Delta T <$ [illegible]
(See Figs. 39 and 40)

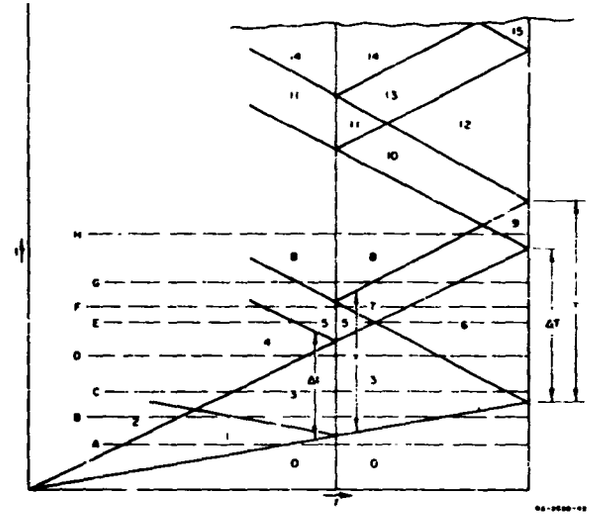

FIG. 42 TIME POSITION DIAGRAM, $\Delta T <$ [illegible]

On the other hand, if the separation of the incoming waves is greater than the reverberation time, $\Delta T > \tau$, this simplification does not apply. Figures 43, 44, 45 drawn for the same set of incident waves as Figs. 40, 41, 42 but a mirror about one-half as thick, show how the reverberation from the first wave arrives at the mirror-rock interface before the incident second shock [compare Fig. 43(c), (d), (e) to Fig. 40(c), (d), (e)], so that analysis according to the above simplified point of view (dotted lines, Fig. 44) would lead to erroneous results. Theoretically state 2 could still be located (for instance, by constructing points 7' and 8' and extrapolating) but in practice it is difficult if not impossible to tell (after the first reverberation) whether a given set of wiggles in the traces on the film represents the arrival of a genuine second (or third) wave, so anything beyond the reverberation time is simply ignored in reading the film.

If the incident shock system contains three waves the interactions are more complicated but the result is the same: any wave that arrives at the mirror surface earlier than the reverberation time of the first shock is analysed from the simplified point of view to give the correct state behind the original wave, anything that arrives later than one reverberation time (= twice mirror thickness divided by sound speed in mirror behind first shock) after the first shock is ignored.

The following three sections present respectively a key to the symbols, a flow chart, Fig. 46, and a listing of the ALGOL program for the Burroughs 220 computer which embodies the preceding analysis.

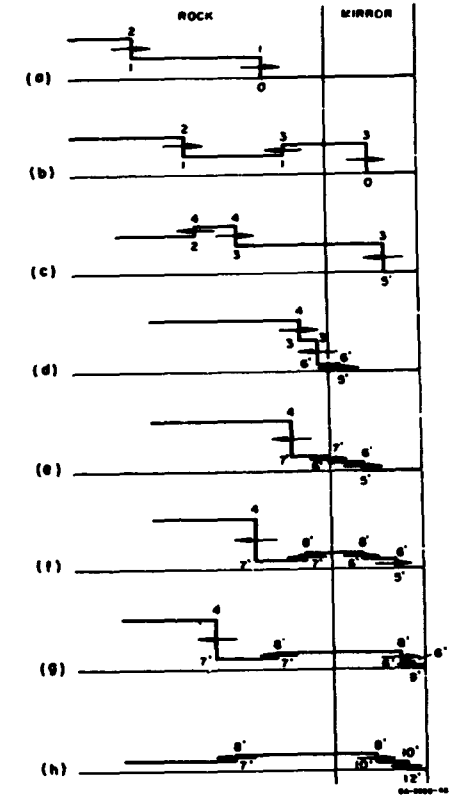

FIG. 43 STRESS PROFILES AT SELECTED TIMES, $\Delta T > \tau$

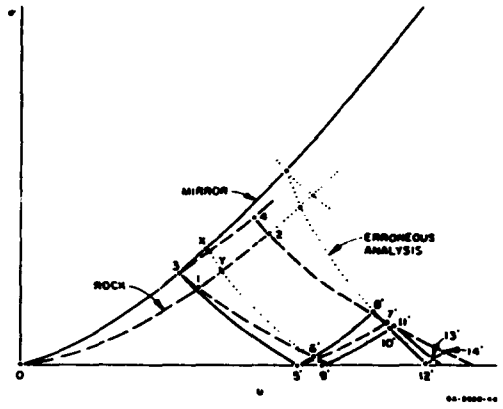

FIG. 44 STRESS-PARTICLE VELOCITY DIAGRAM, $\Delta T > \tau$
(See Figs. 42 and 43)

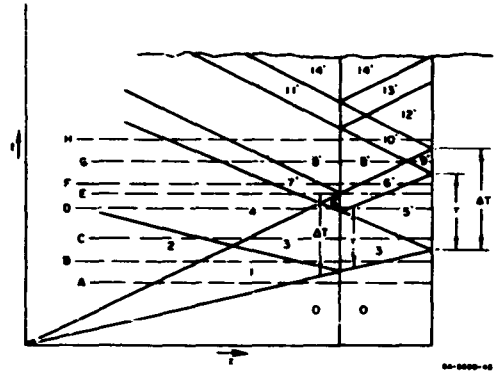

FIG. 45 TIME POSITION DIAGRAM, $\Delta T > \tau$

KEY TO SYMBOLS

SQRT (X) = $\sqrt{x}$. RMMXX = $\sqrt{1 - x^2}$ (double-precision arithmetic)

PCS(N) = 1 if program control switch N is ON
0 if program control switch N is OFF

PALS - curve-fitting routine BISEC - equation-solving routine

Principal variables

NAME IN TEXT	EQ. NO (Where Derived)	QUANTITY	NAME IN PROGRAM	LINE NO. (Where Calculated)
σ	1, 9	Normal stress behind shock wave	SIGMA	81H, 83C
ρ_0/ρ	1	Density ratio across shock	RATIO	84
U_{app}	2	Apparent velocity	UA	69G
U_{camera}	3	Camera-film-viewer parameter	K	52
cot ϕ	4	Slope of first-arrival line	SUM	69E & F
U	5	Shock velocity	US	71
θ	5	Angle between shock and wedge face	THETA	70C
α	6	Angle between shock and explosive	ALPHA	70A & B
Δu	7	Increase in particle velocity across shock	IMP	76A, 80G, 81C
ΔU_{fs}	8	Increase in free-surface velocity	IMFS	76A
β	8	Turning angle of wedge face	BETA	75A
γ	8	Shift in image position		
u	9	Particle velocity behind shock	UP	81A, 83B
H	9	$10\rho_0(U - u_0)$	H	76A & B
sin θ_α cos θ_α	10	sine cosine θ after refraction	SINTHETA COSTHETA	80F & F
	11	Equation to be solved for σ_α	G(P)	16=17

Temporary constants, etc.

NAME LINE NO. (Where Calculated)	TENRO	SD, CD, DR	AH	TENRH	DI, RATE	AVE, T1, T2
	47	48	49	50	51	58, 72B&C, 74A, 87B-D, 90A & B

DENOM, RMS	TANA	DEPTH
63D-G, 64A-D	69D	72A

Loop indices

NAME	J1	J2	J
CONTROLS	54-90D	68-89	20C-D, 26H, 53A, 55C, 58, 59-60, 63F, 64H, 65C, 69E

Limit Numbers & Toggles					
NAME	I	F	N	Q	S
WHERE SET OR RESET	13, 55A	62	63B	61, 70C, 80D	46, 91
Initial values of UP0, R0, P0, ANG, UFS0 set at 53A & B, reset at 75B and 85-87A.					

Inputs	QUANTITIES	LINE NO. WHERE READ IN
	Date, Shot No., Label, $\rho_0 A$, d, x_0=θ_0, I_1, I_2, Rev, M, S,	46
	A_0, γ, ρ_{00}, d, label	50
	I	55A
	x, t, w, x', w'	61

PROGRAM OPTIONS

PCS NO.	ACTION IF *ON*	LINE WHERE INTERROGATED
2	quadratic fit to data	63H
3	cubic fit to data [overrides PCS(2) if both on]	63H
5	stops before processing next wave (used to provide time for resetting other PCS's between cases)	63A
6	suppresses punched-card output	88A
7	Fits XP as a function of X, replaces original values of XP by values of polynomial ("smoothing")	63H

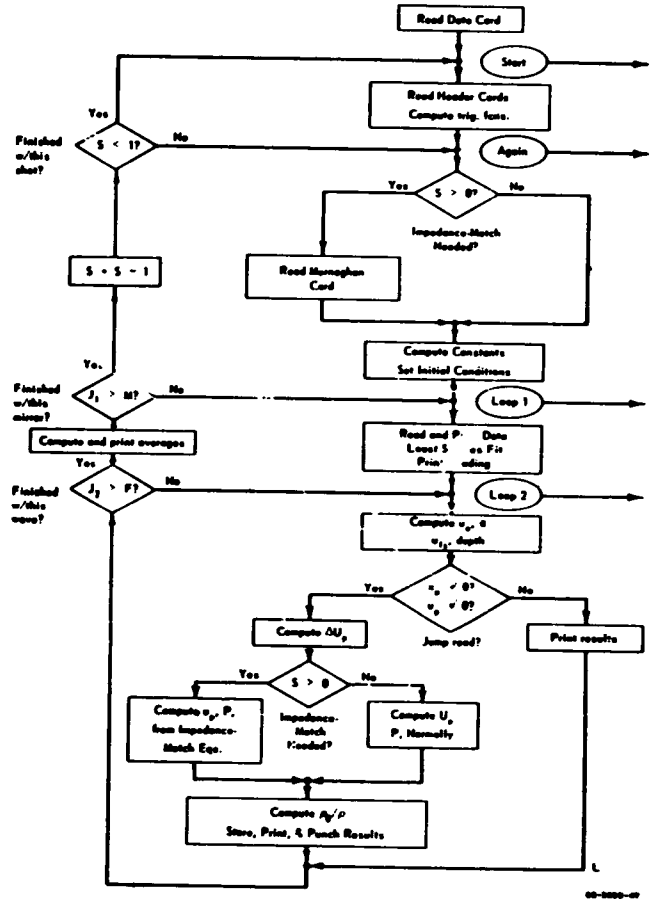

FIG. 46 FLOW CHART

```
      BURROUGHS ALGEBRAIC COMPILER - STANDARD VERSION  7/25/61$
      COMMENT WEDGE PROGRAM. FOR DATA CARD FORMAT SEE CARDS 10-15.          W 01
              FOR THEORY AND USE. SEE POULTER LAB INTERNAL REPORT NO. 010-61  W 02
              RESULTS BOTH PRINTED AND PUNCHED.                             W 03
              COMPILING TIME 3 MIN. RUNNING TIME ABT 1 MIN PER SHOT.        W 04

              BY PW KRASNO PROJ 3630 EXT 3184 6/4/61$                       W 05

      PROCEDURE PALS(M,N,EPS,W(),X(),Y(),Z(,)$ R(),C(),DEG)$                PALS 01
      BEGIN                                                                 PALS 02
      INTEGER  I, J, K, M, N, DEG$                                          PALS 03
      ARRAY  A(22), B(21)$                                                  PALS 04
      SUBROUTINE  SUMS$                                                     PALS 05
        BEGIN  BOX = 0$                                                     PALS 06
        FOR I = (1,1,M)$                                                    PALS 07
          BOX = BOX + Z(N+3,I)*Z(N+3,I)$                                    PALS 08
        IF TGL EQL 0$ GO FRST$                                              PALS 09
        IF BOX GEQ TOT$ (K = K - 1$ GO OUT)$                                PALS 10
      FRST..                                                                PALS 11
        FOR I =  1,1,M)$ IF EPS LSS ABS(Z(N+3,I))$ GO THRU$                 PALS 12
        GO OUT$                                                             PALS 13
      THRU..                                                                PALS 14
        TOT = BOX$ TGL = 1$                                                 PALS 15
        RETURN END$                                                         PALS 16
        K = 0$ TGL = 0$                                                     PALS 17
        FOR J = (1,1,M)$ Z(2,J) = W(J)$                                     PALS 18
        FOR I = (1,1,N)$                                                    PALS 19
        FOR J = (1,1,M)$                                                    PALS 20
```



```
          Z(I+2,J) = X(J)*Z(I+1,J)$                                         PALS 21
          FOR J = (1,1,M)$ Z(N+3,J) = Y(J)*A(J)$                            PALS 22
        IT..                                                                PALS 23
        K = K+1$                                                            PALS 24
          FOR I = (K,1,N+2)$ BEGIN  A(I) = 0$                               PALS 25
          FOR J = (1,1,M)$                                                  PALS 26
        A(I) = Z(K+1,J)*Z(I+1,J) + A(I) ENDS                                PALS 27
          FOR I = (K,1,N+1)$ R(I) = A(I+1)/A(K)$                            PALS 28
          FOR I = (K,1,N+1)$ Z(K,I) = 0(I)$                                 PALS 29
          FOR I = (K+1,N+1)$                                                PALS 30
        FOR J = (1,1,M)$                                                    PALS 31
        Z(I+2,J) = Z(I+2,J) - Z(K,I)*Z(K+1,J)$                              PALS 32
          IF K EQL 1$ ENTER SUMS GO IT)$                                    PALS 33
          FOR I = (1,1,K-1)$                                                PALS 34
          FOR J = (K,1,N+1)$                                                PALS 35
        Z(I,J) = Z(I,J) - Z(I,K-1)*Z(K,J)$                                  PALS 36
          IF K EQL N+1$ GO OUT$                                             PALS 37
          ENTER SUMS GO IT$                                                 PALS 38
      OUT..                                                                 PALS 39
          FOR I = (1,1,K)$ C(I) = Z(I,N+1)$                                 PALS 40
          FOR I = (1,1,M)$ R(I) = Z(N+3,I)$ DEG = K-1$                      PALS 41
          RETURN END PALS)$                                                 PALS 42
```

```
PROCEDURE BISEC (X0,X1,EPP,EPS Y$ F());$                                BISEC  1
BEGIN                                                                   BISEC  2
  COMMENT.  BISECTION ROUTINE TO FIND ROOTS OF ANY EQUATION Y=F(X)$     BISEC  3
  F0 = F(X0)$                                                           BISEC  4
  F1 = F(X1)$                                                           BISEC  5
  IF ABS(F0) LEQ EPP$                                                   BISEC  6
    (Y=X0$ RETURN)$                                                     BISEC  7
  ROOT1.. IF ABS(F1) LEQ EPP$                                           BISEC  8
            (Y=X1)$ RETURN)$                                            BISEC  9
  IF SIGN(F0) EQL SIGN(F1)$                                             BISEC 10
    BEGIN                                                               BISEC 11
      X2 = 3X1 - 2X0$                                                   BISEC 12
      X0 = X1$                                                          BISEC 13
      F0 = F1$                                                          BISEC 14
      X1 = X2$                                                          BISEC 15
      F1 = F(X1)$                                                       BISEC 16
      GO TO ROOT1                                                       BISEC 17
    END$                                                                BISEC 18
  IF SIGN(F0) EQL -SIGN(F1)$                                            BISEC 19
    BEGIN                                                               BISEC 20
      ROOT2.. X2 = 0.5(X0 + X1)$                                        BISEC 21
      F2 = F(X2)$                                                       BISEC 22
      EITHER IF ABS(F2) LEQ EPP$                                        BISEC 23
        GO TO ROOT3$                                                    BISEC 24
      OR IF ABS(X2 -XC) LEQ EPS$                                        BISEC 25
        GO TO ROOT3$                                                    BISEC 26
      OR IF SIGN(F2) EQL SIGN(FC)$                                      BISEC 27
        GO TO ROOT4$                                                    BISEC 28
      OTHERWISE$                                                        BISEC 29
        GO TO ROOT5                                                     BISEC 30
    END$                                                                BISEC 31
  ROOT3.. Y=X2$                                                         BISEC 32
    RETURN$                                                             BISEC 33
  ROOT4.. X0 = X2$                                                      BISEC 34
    F0 = F2$                                                            BISEC 35
    GO TO ROOT2$                                                        BISEC 36
  ROOT5.. X1 = X2$                                                      BISEC 37
    F1 = F2$                                                            BISEC 38
    GO TO ROOT2                                                         BISEC 39
END  BISEC();$                                                          BISEC 40
```



```
INTEGER I, J,... P,  M,... S,  DAYS,...DEG, N, SHOTS                   W 04-7
                    BOOLEAN  OS                                         W 08
ARRAY X(50), Y(50), Z(50), XP(50), YP(50), ROT(50), POT(50), ZT(50,51), W 09A
    R(50), AVE(9), ANG(50), UFS0(50), C(4), XP(50)$                     W 09B

INPUT DATE (DATE1, DATE2, DATE3),                                       W 09C
    HEADR1,SHOT, N1, M2, M3, M4, RHO), A, D,                            W 10
        X5, U0, I5, IL, REV, M, S, DELTA1,                              W 11
        MOON TAM, GAMMA, RHOOM, D, M5, M6),                             W 12
    CONT(1),                                                            W 13
    DATA (X(J), Y(J), Z(J), XP(J), YP(J))$                              W 14-5
```

```
      FUNCTION G(P) = P(1 + (1 + P/AM)*(-1/GAMMA)) - TERM*UP*UMA                  # 16*7


      OUTPUT HDG (SHOT, M1, M2, M3, M4, RHOO, A, D, DATE1, DATE2, DATE3,         # 18
     XO, UD, IS, IL, REV, DELTA, J1, M, I),                                      # 19
     IMPED(AM, GAMMA, RHOOM, D, M5, M6),                                         # 20A
     DEV (RMS),   NUM (J2),                                                      # 20B
     RES  (FOR J = (1,1,F)$ RATE,R(J)),                                          # 20C
     RESX (SQRT(RMS/DENOM),FOR J = (1,1,F)$ R(J) ),                              # 20D
     DATA (J, X(J), T(J), W(J), XP(J), dP(J)),                                   # 21
     OUTA (J2,WP(J2), DEPTH, UA, ALPHA, US),                                     # 22
     OUTB (J2,WP(J2), DEPTH, UA, ALPHA, US,UP,RATIO,SIGMA),                      # 23A
     OUTC (J2,WP(J2), DEPTH, UA, ALPHA, US,UP,RATIO,SIGMA,UPM,PM),               # 23B
     OUTGTUP, US,dP(J2),      99, SHOT, J1, J2, M1, M2, M3, M4,                  # 24A
          M5, M6,                                                                # 24B
     RATIO, SIGMA, WP(J2),  99, SHOT, J1, J2, M1, M2, M3, M4,                    # 25
          M5, M6),                                                               # 26A
     AVER(FOR J = (1,1,9)$AVE(J))$                                               # 26B
FORMAT FRM1(I6, B2, A20, X7.3, * GM/CC=*, X6.1,* DEG, *EDGE=*, X8.3,            # 27
     * INCHES FROM LIGHT=*, B20, A15, /3,                                        # 28
     *  XO=*, X7.3, *  UD=*,  X8.3,  * MM/MS   IS=*, X7.3,                      # 29
          *  IL=*,  X7.3, X8.1, * MS/REV=*, X6.1,* DEG SLIT *                   # 30A
          *TILT=*, W4,                                                           # 30B
     *  WAVE NO.=*, I3, *  OF=*,I3,                                             # 31*2
     * USEABLE TRACES START WITH NO.=*, I3, W4),                                # 33A
     QUADI*    SECOND DEGREE POLYNOMIAL FIT TO ARRIVALS=*, W1,                  # 33B
     CUBE(*    THIRD DEGREL POLYNOMIAL FIT TO ARRIVALS=*, W1,                   # 33C
     FRM2 (*  CONSTANTS USED IN IMPEDANCE MATCH SOLUTION=*,                      # 34
          *  A=*, F15.8, *  GAMMA=*, F15.8, *  RHOO=*, X7.3,                    # 35
```



```
          *  D=*, A7.3,2X4, D1=, A10, X4=,                                      # 36
     FRM3 (I3, 2X8.3, X6.1, X7.3, X6.1, X4),                                    # 37
     FRM4 (=5=, 2(5), X7.3), =1, X3.1, =1, I, 16, 21=, R3, A20.P),              # 38*9
     FRM5 (I3, X8.1, X7.3, X8.=, X6.1, X7.3, X8.3, X7.3, X9.3,                  # 40
          X7.3, X9.3, W4),                                                      # 41
     (ID   (*  J     X       T       A       XP     dP=, W4),                  # 42
     FDEV(*  RMS DEVIATION OF ARRIVALS =*, X5.3, * MS=, W4),                    # 43
     FRES (*     RESIDUALS (MS)=, 12X8.4, W4, (B19, 12X8.4, W11),              # 44A
     FRESX(*   RMS DEV OF 3 MPS (VGO INCHES)=, X8.4, W4,                       # 44B
          *  RESIDUALS =, 12X8.4,  W4, (B12, 12X8.4,  W11),                    # 44C
     MED  (*TRACE WEIGHT DEPTH    UA    ALPHA    US  *,                        # 45A
          *   UP   RATIO PRESSURE   UPM      PM=, W4,                          # 45B
          W14,'=INT (MM/MS) (DEG) (MM/MS)(MM/MS)=,                             # 45C
          B9, *(KB)   (MM/MS)   (KB)=, W1,                                     # 45D
     AGES(W4, =AVERAGES=, X1C.3, X8.3, X6.1, X8.3, X8.3, X7.3,                  # 45E
          X9.3, X7.3, X9.3, W4)$                                                # 45F


     READ($$DATE1$                                                              # 46A
START.. READ ($$HEADR1$                                                         # 46B
     TERMC = TORNOUS    TGL = 0$                                                # 47
     DR = 3.1415927DELTA/180$ SD = SIN(DR1$ CD = ROMXX(SD1$                     # 48
     AR = 3.1415927A/180$                                                       # 49


AGAIN.. IF S GTR 0$(READ($$MORN1$ TERM = 10RNOO%1$                              # 50
     D1='T/ZD,TIL$ RATE = T.332REV/SGO$                                         # 51
```

```
                K = 25.4/RATE.1$                                                    # 52
                FOR J =(1,1,50)$ SUPO(J)=0.0$ RC(J)=1.(SPO(J)=0.98716**-3$          # 53A
                                ANG(J)= ARS UFSO(J)=0.01$                           # 53B
                FOR J1 = (1,1,M)$                                                   # 54
LOOP1..         BEGIN READ(5$CONT)$                                                 # 55A
                IF I EQL 0$ GO AWAYS                                                # 55B
                FOR J = (1,1,I-1)$ W(J) = WP(J) + 0.0$                              # 55C

                WRITE(5$HDG,FRM1)$                                                  # 56
                IF S GTR 0$ WRITE(5$IMPED,FRM2)$                                    # 57
                WRITE(5$H  $ FOR J = (1,1,9)$ AVE(J) = 0$ T1 =T2 =0.0$              # 58

                FOR J = (  ,  ,1)$                                                  W59-60
                    (READ(5$DATC)$ IF 0$ GO DONE$ WRITE(5$DATA,FRM3)$               # 61
                                DONE.. F = J - 1$                                   # 62

                IF PCS(5)$STOP SHOT.1000000 + S.10000 + J)$                         # 63A
                IF PCS(2)$ N = 2$  IF PCS(3)$ N = 3$ IF PCS(7)$ BEGIN               # 63B
                PALS(F,N,0.0,.WP(),X(),XP(),Z(),SR(),C(),DEG)$                      # 63C
                DENOM = RMS = 0.0$                                                  # 63D
                FOR J = (1,1,F)$  IF WP(J) NEQ 0.0$                                 # 63E
                    BEGIN RMS = RMS + R(J)**2.WP(J)**2$                             # 63F
                    DENOM = DENOM + WP(J)**2$                                       # 63G
                    XP(J) = C(1) + X(J)*C(2) + X(J)* C(3)!DEG GEQ 2!                # 63H
                          + X(J)* C(4)!DEG EQL 3!)$ ENDS                            # 63I
                    WRITE(5$RESX,FRES)$  ENDS                                       # 63J
                PALS(F,N,0.0,.W(),X(),T(),Z(),SR(),C(),DEG)$                        # 63K
                DENOM = RMS = 0.0$                                                  # 64A
```



```
                FOR J = (1,1,F)$ ( RMS = RMS + R(J)**2$                             # 64B
                        DENOM = DENOM + W(J)**2 )$                                  # 64C
                RMS = RATE.SQRT(RMS/DENOM)$                                         # 64D
                WRITE(5$HDG,FRM1)$                                                  # 65A
                WRITE(5$DEV,FDEV)$                                                  # 65B
                FOR J = (1,1,F)$ IF  W(J) NEQ 0.0$   IF W(J) NEQ 1.0$               # 65C
                    R(J) = R(J)/W(J)$                                               # 65D
                WRITE(5$RES,FRES)$ IF DEG EQL 2$ WRITE(5$QUAD)$                     # 65E
                    IF DEG EQL 3$ WRITE(5$CUBE)$                                    # 65F
                IF S GTR 0$ WRITE(5$IMPED,FRM2)$                                    # 66
                WRITE(5$MED)$                                                       # 67
                FOR J2 = (1,1,F)$                                                   # 68
LOOP2..             BEGIN                                                           # 69A
                    IF XP(J2) EQL 0.0$ XP(J2) = A(J2)$                              # 69B
                    IF W(J2) EQL 0.0$ BEGIN WRITE(5$NUM,FRM5)$ GO L ENDS            # 69C

                    TANA = TAN(ANG(J2))$                                            # 69D
                    SUM = 0.0$ FOR J = (DEG,-1,1)$ SUM = SUM.XP(J2)                 # 69E
                                                    * J.C(J+1)$                     # 69F
                    UA = K/T1           SUM )CD - SD)$                              # 69G
                    ALPHA = ARCTAN((UFS0(J2) - UA.TANA)/(UD/COS(ANG(J2))            # 70A
                          + UFS0(J2)*TANA - U*T)$                                   # 70B
                    THETA= ALPHA - ANG(J2)$ Q = 0$                                  # 70C
                    US = UD.SIN(ALPHA)$ ALPHA = 180.ALPHA/3.14159275$               # 71
                    DEPTH = TXD = XP(J2)*TS)*TAN(ANG(J2))/TS$                       # 72A
                    AVE(1) = AVE(1) + DEPTHS AVE(2) = AVE(2) + UAS                  # 72B
                    AVE(3) = AVE(3) + ALPHAS T1 = T1 + 1.0$                         # 72C
```

```
                IF XP(J2) EQL 0.0$                                  # 73
                    BEGIN AVE(4) = AVE(4) + USS                     # 74A
                    WRITE(5$OUTA,FRM5$$ GO TO L ENDS                # 74B

BETA =  (X(J2) - XP(J2))DIS DUFS + CA.BETA$                         # 75A
ANG(J2) = ANG(J2) + ARCTAN(BETA)$                                   # 75B
DUP =DUFS/(2COS(THETA) + SIN(THETA).BETA)$                          # 76A
M = TENROOTS - UP0(J2))/RD(J2)$                                     # 76B


EITHER IF S GTR 0$                                                  # 77
    MATCH..     BEGIN UPN = UP0(J2) + DUPS                          # 78
                BISEC(0.P0(J2) + 2M.DUP.5**-6.5**-6$PHASE)$         # 79
                IF NOT OS                                           #80A=B
                    BEGIN                                           # 80C
                        Q = 1$                                      # 80D
                    SINTHETA = PM.SIN(THETA)/US.TENRM.UPRS          # 80E
                    COSTHETA = ROOT(1-SINTHETA)$                    # 80F
                    DUP = DUFS/(2COSTHETA + SINTHETA.BETA)$         # 80G
                        GO TO MATCH                                 # 80H
                    ENDS                                            # 80I
                AVE(8) = AVE(8) + UPMS  AVE(9) = AVE(9) + PMS       # 80J
                UP = 0.5(UP0(J2) + UPN + (PM - P0(J2))/MTS          # 81A
                SIGMA = 0.5(P0(J2) + PM + M.DUP)$                   # 81B
                DUP = UP - UP0(J2)$                                 # 81C
                END MATCHS                                          # 82
OTHERWISES BEGIN                                                    # 83A
```



```
                UP = UP0(J2) + DUPS                                 # 83B
                SIGMA = P0(J2) + MACH ENDS                          # 83C

                RATIO = R0(J2)(1 - DUP/(2.0 - UP0(J2))$             # 84
                R0(J2) = RATIO$                                     # 85
                P0(J2) = SIGMAS (P50(J2) - (P50(J2) +DUFS$          # 86
                UP0(J2) = UPS                                       # 87A
                AVE(4) = AVE(4) + USS    AVE(5) = AVE(5) + UPS      # 87B
                AVE(6) = AVE(6) + RATIOS AVE(7) = AVE(7) + SIGMAS   # 87C
                T2 = T2 + 1.0$                                      # 87D
                IF NOT PCS(6)$  WRITE(5$OUT0,FRM4)$                 # 88A
                EITHER IF S GTR 0$ WRITE(5$OUTC,FRM5)$              # 88B
                OTHERWISES  WRITE(5$OUT3,FRM5)$                     # 88C
    L..         END LOOP2$                                          # 89
                FOR J= 1(1)40$ AVE(J) = AVE(J)/T1$                  # 90A
                FOR J= 15(1)91$ AVE(2) = AVE(J)/T2$                 # 90B
                WRITE(5$AVER,AGES)$                                 # 90C
    AWAY..      END LOOP1$                                          # 90D

            S = S - 1$                                              # 91
            IF S GTR 0$ GO AGAIN$                                   # 92


GO STARTS
FINIS$$
COMPILED PROGRAM ENDS AT 2549
PROGRAM VARIABLES BEGIN AT 3040
```

APPENDIX D

RELATIONSHIPS OF ROCK PARAMETERS

APPENDIX D

RELATIONSHIPS OF ROCK PARAMETERS

Shock wave data from polycrystalline rocks differ from data on single crystals. These differences are the change in peak stress of the first wave and the change in the locus of stress-particle velocity states. This occurs in a pressure range of a few kilobars to about one hundred kilobars.

Differences in shock data are correlated with differences in the composition and texture of the rock.

COMPOSITION AND TEXTURE IN SEDIMENTARY ROCKS

The basis by which the igneous rocks are classified is much different from the basis used in classifying metamorphic rocks. And likewise, the basis for classifying sedimentary rocks is still different. This is made more complicated by the fact that many geologists use variations of the various classifications if it suits their needs. However, the parameters that are used in most all of the classifications are composition and texture. These same parameters control shock wave propagation in rocks. It might be wise to discuss these parameters from both points of view.

Krynine[3] states, "there are altogether ninety-three important derived properties of parameters of sedimentary rocks, but most of these are quite unnecessary for purposes of megascopic identification." Thus, theoretically there are ninety-three different features which can be assigned to the various parameters of a sedimentary classification. However, Pettijohn[4] states, "It is not possible to construct a classification based on all known or knowable properties. A workable classification will take into account two or three and ignore all others. Each choice requires that the (defining) properties be not only genetically significant but that they be the *most* significant."

The parameters that seem to be most significant are those of composition and texture. Most all of the observations and inferences about a rock can be grouped under composition and texture. Thus, these parameters

are perhaps used more than any other two parameters in the classification of a sedimentary rock.

Many genetic features can be inter-related in terms of composition and texture. The parent rock will control the composition of the detrital grains.

The rate of erosion will control the rate of deposition, thus affecting the texture of the sedimentary rocks. During transport of detritus to the deposition site; the shape, size, and roundness of grains will be changed. The effect of density, shape, size, and roundness on sorting grains will be multiplied by the additional sorting from hydraulic features of viscosity, turbulence, fluid velocity during the time of deposition. Features such as the depth of water at the deposition site, temperature, salinity, acidity, oxidation-reduction potential, and it's position with respect to the deposition interface, freedom of circulation, muddiness of water, and the nature of organic life all affect the texture of the sediment that is being deposited. Even after deposition, composition and texture are effected by diagenetic changes that take place in the sediment.

Composition and texture in sedimentary rocks is genetically significant but different measures of composition and texture are necessary in a chemical rock in comparison to a clastic rock. For example, application of the Udden-Wentworth grade scale to a clastic rock has genetic meaning but application of this scale to a precipitated rock does not. Instead, textures and grade sizes of chemical rocks, such as igneous textures and grade sizes, must be applied if there is to be any genetic interpretation. The application of the Udden-Wentworth grade scale to rocks that have been diagenetically changed or that have both clastic and chemical constituents has little genetic meaning. But neither will it be valid to apply the chemical rock texture and grain size to these "hybrids." Instead a combination of the two methods must be used to gain genetic meaning.

Dapples, Krumbein, and Sloss[16] give four different constituents of which all sediments are composed. These are:

"1. Detrital particles which have been carried to the site of deposition and under the prevailing energy state of the transporting medium settles downward to the depositional interface

2. Inorganic salt precipitates from solution at or above the depositional interface and is incorporated as an integral part

3. Inorganic salts precipitated on the existing grains or crystals, or in the interstitial spaces

4. Material produced by organic activity."

Many sedimentary rocks are either endogenetic or exogenetic. That is, exogenetic grains are the clastic grains that are carried to the deposition site whereas endogenetic material is formed at the site of deposition. Extreme examples of endogenetic and exogenetic rocks are a chemically precipitated limestone and a well sorted sandstone, respectively.

Most sedimentary rocks are composed of mixtures of the endogenetic and exogenetic constituents, and thus show varying characteristics of each. These are termed "hybrid" by Pettijohn.[17] "Superimposed on the textures due to mechanical and chemical sedimentation and commonly obscuring them may be those textures induced by recrystallization and replacement (diagenesis)."[17]

In trying to systematically describe the composition and textures of sedimentary rocks, many classifications have been constructed. The sandstones have been the first and easiest to classify. Texture and composition will indicate the maturity of the clastic rock as well as the source area. Composition and texture will also indicate the nature of the transporting medium before burial. Maturity, source, and transporting medium are three of the most important genetic interpretations that can be made in rock analysis.

Pettijohn[14] used the three parameters of maturity, source, and "fluidity index" as the basis of sandstone classification. The source rock parameter is measured by the ratio of feldspar to other rock fragments. The maturity index is measured by the ratio of feldspar to quartz fragments. And "fluidity index" is measured by the ratio of detrital grains to matrix.

From the three parameters of sandstone classification four groups of clastics can be derived: graywackes, lithic sandstones, arkosic sandstones, and orthoquartzites. These groups are indicative of different tectonic environments and give maximum possible information about the genesis of the sandstone that can be obtained.

Other clastic sedimentary rocks such as purely clastic limestones and conglomerates can also be described in terms of maturity and fluidity factor (and also source area in the case of conglomerate). Composition and texture will be the method of indicating these parameters.

Chemical sediments cannot be indicative of maturity and transporting medium since their composition and texture was formed *in situ*. Instead, a chemical sediment will have its composition and texture interpreted in terms of salinity, acidity, redox potential and other chemical properties of the precipitating medium and later diagenetic changes.

The argillaceous sediments contain chemical, biochemical, and clastic elements. These sediments are a hybrid class having characteristics of both chemical and clastic sediments. Moreover, the clay particles included in the clastic element are also affected by chemical changes. Pettijohn[14] states, "A satisfactory classification, yet to be worked out, must contain elements of both classifications" (chemical and clastic).

Some writers have tried to group clastic, chemical and argillaceous rocks into different suites that indicate tectonic environment. These suites are basically the graywacke, arkose, and orthoquartzite group of sandstones but expanded to include chemical and argillaceous rocks. The concept of suites should be useful but since sandstones have been the only group that has been successfully classified into suites, other chemical and argillaceous rocks will have to be grouped into suites before the concept becomes completely useful.

EFFECT OF COMPOSITION AND TEXTURE ON SHOCK DATA

Thus, we see that composition and texture of a rock is interpreted by the geologist to obtain information about the source of the rocks, its history and environment as it was being transported and effects during and following deposition. These same parameters of composition and texture determine the shock wave data for each rock.

Composition: Composition is the most important. Composition determines the velocity of the shock wave including flow, phase changes, and velocity of the elastic precursor. The over-all features of shock propagation are characteristic for each composition.

Texture: The shock effect of texture, *i.e.*, grain size, shape, sorting, cement, etc., produce variations on the shock effect from composition. The effect from texture can be quite strong on some of the data. Thus, far, the parameter of texture can be primarily considered in terms of porosity. Porosity is dependent upon many textural features[9,20,21] and it is necessary to determine which are most important.

Two types of porosity in sedimentary rocks are possible. Both may exist in the rock to some degree of importance but they will be discussed separately. Two types of porosity may be termed primary porosity and secondary porosity.

Primary porosity is a characteristic of the rock that is determined at the time when the sediment is deposited. A quartz sandstone with no cement would be a typical example. But in general, pore space in a sediment may be reduced either by filling pores with a cement or by compacting the sediment to a more lithified state. Compaction is most important in consolidating muds and clays and not so for sand-sized particles.

The primary porosity of any clastic rock is a combination of the following parameters: packing, sorting, particle shape, particle size, cement, compaction.

If the clastic rock were composed of only spheres of a uniform size, the porosity would be 47.6 percent if the spheres were cubically packed and 25.9 percent if the spheres were rhombohedrally packed. The size of the grains is unimportant. From this, it follows that the porosity may range between the two values if packing is not completely uniform. If the sorting of grains is good, *i.e.*, grains are the same size, porosity will range between the above two values depending upon the packing. If sorting is poor, porosity may be much less than the above values because smaller grains will fill the spaces between larger grains. The particle shape can influence porosity because deviation in shape from a sphere will distort the packing and thereby affect porosity. Grain size is usually not significant in changing porosity but it may greatly affect it if the grains are very small. A small grain size usually means that the grain is very irregular in shape and thereby causes a very irregular packing. Some muds have a pore space of 60 to 90 percent, and diatomaceous earths can easily have porosities of 75 percent. Cement can reduce porosity as can compaction.

Compaction efforts, if primarily controlled by grain size, can be separated into compaction of unconsolidated sediments and compaction of lithified sediments. Compaction of unconsolidated sediments is not of interest to us but it consists mainly of pore reduction and squeezing fluids out of the sediment. Sandstones are generally only compacted about 10 percent or so but muds are compacted up to 30 or 40 percent.

Compaction of lithified sediments consists mainly of squeezing finer grained material into pores or in deforming grains plastically. A general rule is that larger grains are less easily compressed. Compaction in sandstones is quite often typified by an increase in the point contacts between grains.

"Some of the diagenetic processes in carbonate rocks continue after the rock has become lithified, and these contribute to secondary porosity. Compaction, cementation, solution, recrystallization, and dolomitization are all common in diagentic as well as post-diagenetic changes. The porosity that results from these processes, when it can be determined, may be said to be secondary, whereas that which merely modifies primary depositional characteristics may be said to be primary."[20]

RELATION OF ROCKS STUDIED TO COMPOSITION AND TEXTURE

The rocks, as much as is possible, are selected because they have the fewest parameters to consider.

The sandstones and quartzites are composed of pure quartz grains. Little or no matrix is present. The grains are well sorted, rounded, and large enough so that the original porosities should lie between 47 to 26 percent. Cement is present. The preferred orientation of grains is small. From the parameters controlling porosity (packing, sorting, particle size, particle shape, cement, compaction), the only ones pertinent are original packing and cement. It might be that other parameters affect some of the shock properties, such as grain size, but these have not been noticed.

The marble and limestone are not as simple. The marble has been recrystallized and the porosity is secondary. The limestone had a higher original porosity but there has been cementation and some solution. The marble has a high degree of preferred alignment of grains. The parameters affecting shock properties are porosity, and mineral alignment. Again grain size may affect rise times of shock waves but it is not certain at this time. Parameters related to porosity are uncertain.

REFERENCES

1. Rice, M. H., J. M. Walsh and R. G. McQueen, "Compression of Solids by Strong Shock Waves," Solid State Physics, ed by F. Seitz and D. Turnbull, Acad Press, Inc., 6, New York (1958).
2. Walsh, J. M., M. H. Rice, and R. G. McQueen, "Shock Wave Compression of 27 Metals - Equations of States of Metals," Phys Rev 108, 196.
3. Fowles, G. R., "The Development of an Explosive Electric Transducer, Part I, Equation of State of Quartz," Final Report on P.O No. 18-1966-A for Sandia Corp, Livermore, California, (1961).
4. Fowles, G. R., "Shock Wave Compression of Hardened and Annealed 2024 Aluminum," Jour App Phys 32, 8, 1475-1487 (1961).
5. Katz, S., D. G. Doran, and D. R. Curran, "Hugoniot Equation of State of Aluminum and Steel," 32, 8, 1475-1487, (1961).
6. Fowles, G. R., "Shock Wave Compression of Quartz," Poulter Laboratories Tech Report 003-61, October 26, 1961.
7. Rocherle, Jerry, "Shock Wave Compression of Quartz," Jour of App Phys 33, 3, 922-937, March 1962.
8. Adadurov, G. A., D. N. Baloshov, A. N. Dremin, "A Study of the Volumetric Compressibility of Marble at High Pressure," Bull Acad Sci. USSR ((Geophysics), 5, 463-466, May 1961.
9. Turner, F. J., D. T. Griggs, and H. Heard, "Experimental Deformation of Calcite Crystals," Bull Geol Soc of Amer, 65, 883-934, (1954).
10. Griggs, D., and J. Handin, ed, "Rock Deformation," Geol Soc of Amer, Memoir 79, March 1, 1960.
11. Folk, R., and C. E. Weaver, "A Study of the Texture and Composition of Chert," Amer Jour of Sci, 250, 498-510, July 1952.
12. Moore, H. J., "Personal Communication," Geologist, U S.G.S., Menlo Park, California, December 1961.
13. Billings, M., F. J. Turner, and C. M. Gilbert, "Petrography," W. H. Freeman and Company, San Francisco, (1955).
14. Pettijohn, F. J., "Sedimentary Rocks, sec ed Harper & Brothers, New York, (1957).
15. Birch, F., "The Velocity of Compressional Waves in Rocks to 10 Kilobars, Part 1," Jour of Geoph Res 65, 1083-1102, (1960).
16. Birch, F., "The velocity of Compressional Waves in Rocks to 10 Kilobars, Part 2," Jour of Geoph Res, 66, 2199-2224, July 1961.
17. Pettijohn F. J., R. R. Schrock, and Krynine, "Symposium on Classification of Sedimentary Rocks," Jour of Geol, 56, (1948).
18. Dapples, E. C., W. C. Krumbein, and L. L. Sloss, "The Organization of Sedimentary Rocks," Jour of Sed Pet, 20, 3-20, (1950).
19. Athy, L. F., "Compaction and its Effect in Local Structures, Symposium," Problems of Petroleum Geology," A.A.P.G., (1934).
20. Leverson, A. I., "Geology of Petroleum," W. H. Freeman and Co., San Francisco, (1956).
21. Nevin, C. M., "Porosity, Permeability, Compaction (Foreword), Symposium, Problems of Petroleum Geology," A.A.P.G. (1934).

STANFORD RESEARCH INSTITUTE

MENLO PARK
CALIFORNIA

Regional Offices and Laboratories

Southern California Laboratories
820 Mission Street
South Pasadena, California

Washington Office
808 17th Street, N.W.
Washington 6, D.C.

New York Office
270 Park Avenue, Room 1770
New York 17, New York

Detroit Office
The Stevens Building
1025 East Maple Road
Birmingham, Michigan

European Office
Pelikanstrasse 37
Zurich 1, Switzerland

Representatives

Honolulu, Hawaii
Pineapple Factors Building
195 South King Street
Honolulu, Hawaii

London, Ontario, Canada
85 Rockwood Park
London 14, Ontario, Canada

London, England
15 Abbotsbury Close
London W. 14, England

Milan, Italy
Via Mandanese Mollam 4C
Milano, Italy

Tokyo, Japan
Ikoi Building
22, 2-chome, Uchisaiwai-cho, Chiyoda-ku
Tokyo, Japan

END